# TITANIUM OXIDATION:

# KINETICS AND $TiO_2$ GROWTH EFFECTS

by

DANIEL JOSEPH ROSE

B.A.Sc., University of British Columbia, 1960
M.A.Sc., University of British Columbia, 1962

A THESIS SUBMITTED IN PARTIAL FULFILMENT OF

THE REQUIREMENTS FOR THE DEGREE OF

DOCTOR OF PHILOSOPHY

in the Department

of

METALLURGY

We accept this thesis as conforming to the
required standard

THE UNIVERSITY OF BRITISH COLUMBIA

January, 1966

In presenting this thesis in partial fulfilment of the requirements for an advanced degree at the University of British Columbia, I agree that the Library shall make it freely available for reference and study. I further agree that permission for extensive copying of this thesis for scholarly purposes may be granted by the Head of my Department or by his representatives. It is understood that copying or publication of this thesis for financial gain shall not be allowed without my written permission.

Department of Metallurgy

The University of British Columbia,
Vancouver 8, Canada

Date February 22, 1966

The University of British Columbia

FACULTY OF GRADUATE STUDIES

PROGRAMME OF THE

FINAL ORAL EXAMINATION

FOR THE DEGREE OF

DOCTOR OF PHILOSOPHY

of

DANIEL JOSEPH ROSE

B.A.Sc., The University of British Columbia, 1960
M.A.Sc., The University of British Columbia, 1962

IN ROOM 210, METALLURGY BUILDING
MONDAY, FEBRUARY 21, 1966, AT 2:30 P.M.

COMMITTEE IN CHARGE

Chairman: C. A. Brockley

W. M. Armstrong
E. Peters
K. L. Pinder
E. Teghtsoonian
D. Tromans
J. Trotter

External Examiner: W. W. Smeltzer
Department of Metallurgy
McMaster University

Research Supervisor: W. M. Armstrong

# TITANIUM OXIDATION: KINETICS AND $TiO_2$ GROWTH EFFECTS

## ABSTRACT

Titanium oxidation was studied between 400 and 800°C with oxygen partial pressures over the range 760 to $10^{-5}$ mm Hg and times up to 20,000 minutes. Oxidation rates were measured with a Cahn electrobalance after sophisticated metal preparation and experimental procedures. Growth effects in the oxide film were thoroughly examined at time intervals by removing specimens for metallographic observation. Films were stripped from these specimens for transmission electron microscope examination. The morphology development was then related to the rate curves.

In all cases the rate curves were complex functions of temperature, pressure, specimen preparation, and oxidation procedure. In spite of the numerous rate transitions with time, reproducibility under a specific set of conditions was excellent.

As the oxide grows from a thin film to a thick scale, an intermediate period of peculiar network formation, most pronounced at 500°C, is observed. The networks consist of thousands of small crystallites, approximately 100 to 5000 Angstroms in size, and arranged in random and oriented patterns of accelerated and suppressed growth areas. Two different types of whisker formation were observed in addition to the network phenomena.

The complex rate data associated with periods of network growth do not conform to any of the simple rate laws reported by previous investigators. Since the network structures violated all of the assumptions associated with current transport theories regarding planar homogeneous films, it was concluded that these theories were inadequate to describe the growth kinetics. Surface diffusion is probably the main growth mechanism during network formation although orientation and epitaxial effects may have some influence.

## GRADUATE STUDIES

**Field of Study: Metallurgy**

| | |
|---|---|
| Metallurgical Thermodynamics | C. S. Samis |
| Metallurgical Kinetics | E. Peters |
| Hydrometallurgy | E. Peters |
| Metallurgy of the Rarer Metals | E. Peters |
| Nuclear Metallurgy | W. M. Armstrong |
| Structure of Metals | E. Teghtsoonian |
| Topics in Physical Metallurgy | E. Teghtsoonian |
| Properties of Ceramic Materials | A. C. D. Chaklader |
| Electron Microscopy | D. Tromans |

**Related Fields of Study:**

| | |
|---|---|
| Quantum Mechanics | J. Grindlay |
| Quantum Theory of Solids | R. Barrie |
| Statistical Mechanics | R. F. Snyder |
| Surface Chemistry | J. Halpern |

## PUBLICATIONS

W. M. Armstrong, A. C. D. Chaklader and D. J. Rose,

Interface Reactions Between Metals and Ceramics, Part III: MgO-Fe Alloy System, Trans. AIME, 227, 1109 (1963).

ABSTRACT

Titanium oxidation was studied between 400 and 800°C with oxygen partial pressures over the range 760 to $10^{-5}$ mm Hg and times up to 20,000 minutes. Oxidation rates were measured with a Cahn electrobalance after sophisticated metal preparation and experimental procedures. Growth effects in the oxide film were thoroughly examined at time intervals by removing specimens for metallographic observation. Films were stripped from these specimens for transmission electron microscope examination. The morphology development was then related to the rate curves.

In all cases the rate curves were complex functions of temperature, pressure, specimen preparation, and oxidation procedure. In spite of the numerous rate transitions with time, reproducibility under a specific set of conditions was excellent.

As the oxide grows from a thin film to a thick scale, an intermediate period of peculiar network formation, most pronounced at 500°C, is observed. The networks consist of thousands of small crystallites, approximately 100 to 5000 Angstroms in size, and arranged in random and oriented patterns of accelerated and suppressed growth areas. Two different types of whisker formation were observed in addition to the network phenomena.

The complex rate data associated with periods of network growth do not conform to any of the simple rate laws reported by previous investigators. Since the network structures violated all of the assumptions associated with current transport theories regarding planar homogeneous films, it was concluded that these theories were inadequate to describe the growth kinetics. Surface diffusion is probably the main growth mechanism during network formation although orientation and epitaxial effects may have some influence.

## ACKNOWLEDGEMENTS

The author gratefully acknowleges the encouragement and advice offered by Dean W. M. Armstrong during his supervision of this work. Particular thanks are extended to Mrs. A. M. Armstrong, whose prodigious efforts in attempting quantitative interpretation of the kinetic data helped the author to become convinced that no interpretation by the usual techniques was possible. Gratitude is expressed for the electron microscope assistance of Dr. D. Tromans, Mr. A. Lacis, and the pole figure analysis of Mr. G. C. Wootton.

Finally, the author is most indebted to the National Research Council whose financial assistance throughout the program made this work possible.

TABLE OF CONTENTS

# LIST OF FIGURES

# LIST OF TABLES

# TITANIUM OXIDATION:

# KINETICS AND $TiO_2$ GROWTH EFFECTS

## I. INTRODUCTION

### A. General

Although the oxidation of titanium has been extensively studied during the past decade, resulting in some one hundred publications, the inconsistency of kinetic data indicates that even today the process is inadequately understood. In addition to kinetic anomalies, the degree of participation by oxygen ions and titanium ions in the diffusion process has not been positively established at all temperatures. This confusion arises from a multitude of inter-related factors, some of which will be discussed briefly.

Previous titanium oxidation studies fall into two categories: rate studies or scale structure studies. Although early investigators recognized the need for combining these approaches they were unsuccessful in their attempts. Interpretation of results was commonly based entirely upon kinetic data or structural data alone. Recently a few comprehensive works[1,2] including not only kinetic but metallographic, X-ray diffraction, electron microscopy and microhardness studies have appeared in the literature and thrown new light upon the complexity of the process.

One of the objects of these investigations has been a quantitative measure of the oxidation rate by some conventional technique such as thermogravimetry, pressure drop measurement, or interferometry, and subsequent explanation of the rate curve according to one of the classical

transport theories proposed by Wagner, Mott-Cabrera, Uhlig, Hauffe and others. Of course, inherent in this approach is the assumption that the results of these studies can be explained by a simplified classical theory or modification thereof. A growing volume of evidence indicates that in reality the oxide growth morphology is so far removed from the models upon which the theories are constructed[3] that in some cases there is no justification for even attempting to apply classical theories. This problem has been recognized by some experimenters and sophisticated studies on specially prepared single crystals of copper[4], nickel[5], and iron[6] have provided more complete information on the growth processes. Unfortunately most of this work has been confined to morphological investigations and, with the exception of copper[7], very little quantitative kinetic data of this calibre is yet available.

The inconsistencies observed, not only within one titanium oxidation study, but between works by different authors, generally arise from the normal experimental factors that limit reproducibility in all heterogeneous gas-metal reaction studies: metal purity, gas purity, surface preparation, procedure, operating conditions, and measurements.

However the failure to apply a satisfactory theoretical explanation to kinetic results after inconsistencies are minimized is usually due to some oxide growth pattern that is radically different from theoretical models. Whereas much attention has been directed to minimizing inconsistencies arising from experimental technique in the past decade, conformity with theoretical conditions is just beginning to arouse attention, largely as a result of electron microscope studies.

B. Transport Theory Assumptions

The following theoretical conditions are normally required for

application of one of the classical transport theories:

(1) oxide thickness uniform over the entire surface,

(2) oxide free of preferred growth locations (i.e. surface or interface irregularities such as steps, jogs, pits, etc.),

(3) oxide free of line and bulk defects (dislocations, pores, etc.),

(4) point defects uniformly distributed in any one plane through the oxide parallel to the surface,

(5) a continuous planar monatomic oxide-metal interface,

(6) in most diffusion models, lattice diffusion only and negligible contribution from low resistance paths (grain boundaries, etc.).

In many experimental situations the slight deviation from these conditions can be considered negligible and the oxidation data can be satisfactorily interpreted in terms of transport of oxygen ions or metal ions through the oxide layer in accord with the theories[8]. However thin film electron microscopy has revealed that in some instances, particularly those of titanium[9] and zirconium[10], none of these conditions are fulfilled and the deviations may no longer be neglected.

Condition (1) is rarely applicable to the oxidation of any polycrystalline metal[11]. Optical interference studies have shown that in most cases the oxide growth rate on different metal grains varies according to the epitaxial relationships present and the anisotropy of diffusion in the film[7]. The surface of an oxidizing polycrystalline metal may be as irregular as that shown in Figure 1. Further complication arises from the possibility of having many oxide crystals of different orientation and growth rate on one metal grain as indicated (grain A). The shape of the oxide crystals may differ from one another. Superimposed upon these difficulties is the possible existence of substructure in each oxide crystal.

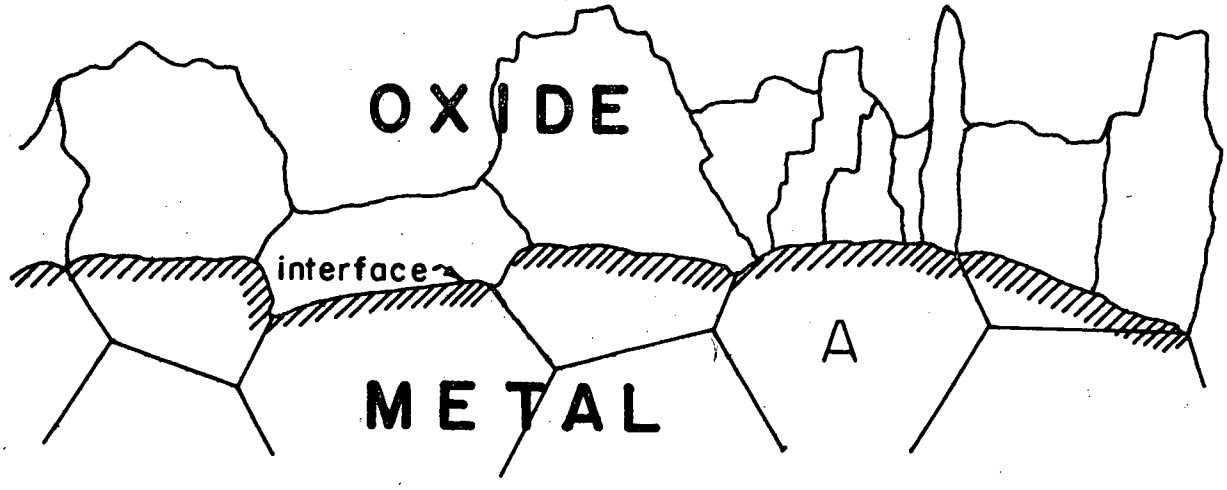


Figure 1. Schematic representation of irregular oxide growth on fully annealed metal

Differences in oxide thickness at various points on a single metal grain may arise from nucleation and growth, network formation, mound formation, whisker growth, cracking, blistering, pore formation, etc. The large amount of electron microscope work now being published suggests that the presence of such irregularities is normal behaviour rather than exceptional[3].

Most rate measurement methods detect the total weight gain, total volume of oxygen absorbed, or total optical interference of the specimen. With several crystal faces in various stages and modes of oxide growth, the best kinetic data are merely a statistical average of a complex process.

These complex growth patterns have recently been labelled by the growth morphologists as "heterogeneous oxidation" although the kinetic implications of a possible "homogeneous oxidation", i.e. uniform growth, are rather confusing. Perhaps "heteromorphic" growth would describe the irregularities more adequately.

C. Titanium Oxidation Rates

A review of the many publications on titanium oxidation reveals that all of the conventional rate laws have been observed at one temperature or another. Some authors claim several different rate laws are obeyed at one temperature during different time intervals. Perhaps the greatest confusion arises in the temperature range from 400 to 800°C. In this region there is considerable disagreement among the rate laws observed as shown in Table I. The most intriguing feature of this region is the observation of a cubic rate law that even today defies a satisfactory theoretical explanation[8]. Most attempts to clarify this relation have been based upon transport theories and the possibility of an explanation centred

TABLE I.

Observed Rate Laws

| Author | Ref. | Year | 100 200 300 400 500 600 700 800 900°C |
|---|---|---|---|
| Gulbransen | 12 | 1949 | parabolic |
| Alexander | 13 | 1950 | logarithmic |
| Kieffer | 14 | 1950 | paralinear |
| Hass | 15 | 1957 | log, inv. |
| Davies | 16 | 1951 | paralinear |
| Waber | 17 | 1952 | cubic |
| Pfeiffer | 18 | 1952 | parabolic |
| Waber | 19 | 1953 | logar. cubic |
| Richardson | 20 | 1954 | parabolic |
| Jenkins | 21 | 1955 | paralinear |
| Kofstad | 2 | 1958 | logar. cubic parabolic paralinear |
| Wallwork | 22 | 1959 | paralinear |
| Hurlen | 1 | 1960 | log. cubic parabolic |
| Stringer | 23 | 1960 | parabolic |
| Lainer | 24 | 1961 | cubic-parabolic |
| Revyakin | 25 | 1962 | parabolic |
| Menard | 26 | 1962 | paralinear |

SUMMARY

| | | | | |
|---|---|---|---|---|
| Short times..... | logarithmic | logarithmic | cubic | parabolic #1 |
| Long times..... | logarithmic | cubic | parabolic | linear, parabolic #2 |

around geometrical effects arising from the complicated growth morphology has been ignored.

D. The Cubic Rate Law

Cubic rate laws at intermediate temperatures for p-type oxides such as copper and nickel oxide have been explained by Cabrera and Mott[54] in terms of space charge considerations. Their theory claims that the transport of lattice defects, through which oxidation proceeds, is motivated by the presence of an electric field resulting from the concentration of negative charge associated with chemisorption of oxygen at the surface.

In order to satisfy the thermodynamic requirements for chemical potential equilibrium between species in a space charge layer, the concentration of ion lattice defects differs from the concentration of electron defects. In n-type oxides containing free electrons and cation interstitials (or anion vacancies), free electrons from the bulk are withdrawn to the surface because of the high electron affinity of the gaseous oxygen. This depletion leaves a small concentration of free electrons and cation interstitials (or anion vacancies) scattered sparsely throughout the bulk and the overall result is a weak space-charge layer. On the other hand, in p-type oxides where positive electron holes and cation vacancies (or anion interstitials) are present, electrons can only be removed from the surface region for chemisorption because each removed electron generates an additional positive hole. This enhances the accumulation of positive charge in the region below the surface and creates an enriched space charge layer of high field strength. The vacancy density in this region is proportional to the surface density of the chemisorbed oxygen ions, which in turn, is inversely proportional to the

layer thickness[8], hence

$$n_{\square} = \frac{k_1}{X} \qquad \ldots.(1)$$

where $n_{\square}$ = vacancy concentration
$X$ = space-charge layer thickness
$k_1$ = constant

Introducing the mobility concepts proposed by Engel-Hauffe-Ilschner[27] as a refinement to the Mott-Cabrera theory, the cation vacancy flow in a p-type oxide can be represented by

$$j_{\square} = -u_{\square} n_{\square} \frac{V}{X} \qquad \ldots.(2)$$

where $u_{\square}$ = mobility of vacancies
$V$ = potential difference caused by the space charge effect

Further growth of the oxide is proportional to this vacancy flow so that

$$\frac{dX}{dt} = k_2 u_{\square} n_{\square} \frac{V}{X} \qquad \ldots.(3)$$

and substituting relation (1) into (3)

$$\frac{dX}{dt} = k_3 u_{\square} \frac{V}{X^2} \qquad \ldots.(4)$$

which yields a cubic rate law upon integration. Relation (1) holds only for p-type oxides with enriched space charge layers. If titanium oxide were p-type this theory could possibly explain the observed kinetic data.

## E. Rutile Structure Anomalies

Although the phase diagram for the titanium-oxygen system[28] (Appendix A) indicates that TiO, $Ti_2O_3$, and the anatase form of $TiO_2$ are all stable from room temperature up to approximately 800°C, the rutile modification of $TiO_2$ is the only form detected by X-ray and electron diffraction measurements in a large number of oxidation studies in this temperature range[7,8]. Above 800°C small quantities of TiO and $Ti_2O_3$ begin to appear between the metal and rutile phase[29]. The exclusive formation of rutile at intermediate temperatures simplifies phase analyses in oxidation

studies but the kinetics are confused by the uncertainty in the diffusion mechanism within this oxide.

Rutile has been definitely established as a metal-excess n-conducting oxide. Ehrlich[30] reported that rutile exists over a range of stoichiometry from $TiO_{1.90}$ to $TiO_{2.00}$. Andersson et al[31] later discovered that $TiO_{1.96}$ was the lower limit of stoichiometry. A recent thesis by Graves[32] involving thermogravimetric equilibration again revises the lower limit to 1.99. Although all of these authors agree that $TiO_{2.00}$ is the upper limit, the degree of contribution to the substoichiometry by anion vacancies and/or cation interstitials has been questioned.

If anion vacancies are operative during diffusion, the oxide will form at the oxide-metal interface and any markers used for Kirkendall shift measurements should remain on the surface. On the contrary, if cation interstitials are participating, the oxide will form at the oxide-gas interface and markers should become imbedded. Most experimental work supports the existence of oxygen ion vacancies at low and intermediate temperatures.

Radioactive silver marker experiments by Davies and Birchenall[16], and platinum marker studies by Kofstad and coworkers[33], Jenkins[34], Wallwork and Jenkins[22], Arkharov and Blankova[35], and Lainer and Bai[36] all resulted in the markers remaining on the surface. Jenkins[34] also observed that scratches on the metal surface prior to oxidation, were present on the scale surface after oxidation, suggesting growth at the metal-oxide interface. Incorporation of foreign metal ions (Ta, Nb, Sb, and W) of valence greater than four into the rutile lattice has resulted in a colour transition to dark grey-blue which Hauffe[8] interprets as the formation of F-centres, i.e. an oxygen ion vacancy and a trapped electron.

Hurlen[37] has recently presented some significant facts that suggest the existence of cation interstitials. He summarizes the possible defect equilibria in rutile as follows:

anion vacancy type: $\text{Nil} \rightleftharpoons O_{\square}^{++} + 2e^- + \frac{1}{2}O_2(g)$ ....(5a)

$\text{Nil} \rightleftharpoons O_{\square}^{++}e^- + e^- + \frac{1}{2}O_2(g)$ ....(6a)

$\text{Nil} \rightleftharpoons O_{\square}^{++}2e^- + \frac{1}{2}O_2(g)$ ....(7a)

cation interstitial: $TiO_2 \rightleftharpoons Ti_i^{n+} + ne^- + O_2(g)$ ....(8a)

where Nil = stoichiometric crystal
$\square$ = vacancy
i = interstitial

Assuming the defect formation to be reversible according to the Schottky-Frenkel theory, thermodynamic equilibria for equations (5a) to (8a) can be written according to the mass action law:

$$(O_{\square}^{++})(e^-)^2 p_{O_2}^{\frac{1}{2}} = \text{constant} \quad ....(5b)$$

$$(O_{\square}^{++}e^-)(e^-)p_{O_2}^{\frac{1}{2}} = \text{constant} \quad ....(6b)$$

$$(O_{\square}^{++}2e^-)p_{O_2}^{\frac{1}{2}} = \text{constant} \quad ....(7b)$$

$$(Ti_i^{n+})(e^-)^n p_{O_2} = \text{constant} \quad ....(8b)$$

Hence the electrical conductivity (q) resulting from the free electrons should vary with pressure according to the following relations:

$$q \propto p^{-1/6} \quad ....(5c)$$

$$q \propto p^{-1/4} \quad ....(6c)$$

$$q \propto p^{-1/n+1} \quad ....(8c)$$

Hurlen then suggests that the dependence of $\frac{-1}{4.5}$ to $\frac{-1}{5}$ observed by Hauffe et al[38] in the temperature range from 800 to 1000°C is the result of interstitial three and four-valent titanium ions. The recent work of Graves, who also observed a $\frac{-1}{5}$ dependence seems to confirm this finding.

From structural considerations Hurlen shows that the rutile lattice contains a large number of interstitial octahedral positions

surrounded by oxygen ions and arranged in chains that are exceptionally suitable for reception of titanium ions. He also claims that the blue colouring attributed to F-centres may be caused by the formation of a trivalent interstitial titanium ion.

In the absence of titanium interstitial cations, the incorporation of foreign cations of lower valence, presumably by substitution into titanium ion lattice sites, would be expected to consume free electrons and lower the electrical conductivity. In the case of small additions of gallium, aluminum, and nickel, Hauffe[39] observed almost no effect and chromium appeared to increase the conductivity. Hurlen resolves this observed increase in terms of a small fraction of chromium in interstitial positions, still greater evidence for the existence of titanium cation interstitials.

With regard to oxidation studies, he points out that whiskers have frequently been observed on top of rutile films and this configuration is difficult to imagine in terms of growth at the underlying oxide-metal interface in accord with the anion vacancy theory.

In summary, Hurlen suggests that all of this confusion may result from a combined defect system which is not accounted for in the Wagner-Hauffe theory.

A growing volume of recent work establishes with certainty the predominant existence of anion vacancies below 800°C. The results of incorporating foreign metal cations into the $TiO_2$ lattice during both conductivity and oxidation studies have conformed to predictions based upon the presence of anion vacancies[8]. The radioactive oxygen mobility studies in rutile by Haul and Dumbgen[40] have positively established the existence of oxygen ion vacancies and provided information about the

diffusion of oxygen in rutile between 710 and 1300°C. The diffusion coefficient for the a and b directions in the tetragonal crystal is 1.6 times greater than in the c direction. At 900°C, the diffusion coefficient is pressure-independent over the pressure range $10^{-3}$ to 725 mm. They conclude that oxygen diffusion is the principal mechanism in rutile but they do not exclude the possibility of a minor contribution from cation interstitials.

Marker experiments by Kofstad and coworkers[33] indicate that below 900°C oxygen ion vacancies are operative. However above this temperature Kofstad began to observe markers imbedded in the scale and suggested that a growing contribution of cation interstitial movement was making its presence felt. Imbedded markers obtained at higher temperatures by Lainer and Bai[36] confirm this hypothesis.

F. Solubility of Oxygen in Titanium

In addition to the controversy over the defect structure in rutile, the extremely high solubility of oxygen in the metal seems to complicate the oxidation behaviour. Titanium can dissolve up to 33 atomic percent of oxygen in interstitial lattice positions[30]. Until 1958 it was thought that this dissolution had a negligible effect on the oxidation behaviour below 800°C. This assumption originated from the observation that under high vacuum conditions, thin oxide films would form on titanium at temperatures below 800°C, whereas these same films could be redissolved in the metal at temperatures above 800°C[2]. Dissolved oxygen can be detected in the metal by an increase in hardness or change in lattice reflection intensities and d-spacings during X-ray diffraction. The work in both of these areas by Hurlen[1] shows that after six hours at 700°C, the oxygen content reaches a steady level of approximately 15 atomic percent; at 650°C, two days were required to reach this concentration. At 500°C after two days the

dissolution was still negligible.

Kofstad and Hauffe[41] first suggested that the cubic rate law observed at intermediate temperatures in n-type oxides ($TiO_2$ and $ZrO_2$) may be a result of oxygen solution in the metal. Smith[42] has recently presented a theoretical interpretation of this phenomenon based upon the competition between diffusion of oxygen in the oxide and in the metal. He suggests that the cubic region observed is merely a quasi-cubic transition period between two parabolic regions, one of which is governed by diffusion of oxygen in the oxide, and the other by diffusion of oxygen in the metal. The time of transition decreases with increasing temperature until eventually the cubic relation disappears and a simple parabolic rate is observed.

Kofstad et al[2] presaturated some samples with oxygen and discovered that they oxidized parabolically at temperatures down to 300°C whereas the unsaturated titanium oxidized cubically. They concluded that the cubic relation is associated with an oxygen build-up in the metal. When saturation is achieved, a parabolic law is obeyed. Normally the solution of oxygen in the metal would also yield a parabolic law but some evidence has been presented that interstitial oxygen diffusion in titanium may be concentration dependent[42] and this could transform the parabolic law into a cubic relation.

One of the difficulties in accepting this explanation lies in the experimental evidence that dissolution of oxygen in titanium is almost negligible below 600°C and yet the cubic law is observed in the region from 300 to 600°C. In view of the large activation energies for oxygen diffusion in titanium (62 Kcal/mole[23] and 51 Kcal/mole[33]), it is especially difficult to imagine oxygen entering the titanium at 300°C.

The theory also implies that the oxide thickness is stationary during the cubic period. The film forms initially because the amount of

oxygen diffusing through the film per second exceeds that dissolving in the metal. As the film thickens, the oxygen flux through the film decreases until a critical thickness is reached where the amount of oxygen passing through the film equals that dissolving in the metal. Since the latter oxygen must originate at the metal-oxide interface the film thickness remains constant until the metal reaches saturation. This situation is not consistent with the results of interference studies. Furthermore Hurlen observed a pressure dependence of the cubic oxidation region at 500°C which is not accounted for by the theory.

G. Oxide Growth Morphology

In addition to rutile defect anomalies and oxygen solution in the metal, the third major factor that may influence the observed kinetic relations is the exceptionally complicated growth morphology of the oxide in the intermediate temperature range. The replica electron microscope work of Kofstad et al[2] and Hurlen[1] have provided preliminary information on this problem. A recent transmission electron microscope study by Markali[9] on titanium oxidized at 500°C revealed extremely small crystals. He estimated a grain boundary region comprising ten percent of the total area. In view of this, oxide growth would probably proceed by grain boundary diffusion and hence any comparison with the Wagner model is unjustifiable. A phenomenological theory developed by Smeltzer and coworkers[43] that accounts for the contribution of grain boundary diffusion would probably be more suitable in explaining titanium oxidation under these conditions.

A more complete transmission electron microscope study, as yet unpublished by Douglass and Van Landuyt[44], reveals that a complicated oxide nucleation and growth phenomenon takes place at intermediate temperatures. The nuclei grow out of a thin primary film and eventually coalesce to form a network which then builds up as a secondary overgrowth. This effect was

most pronounced at 450 to 550°C.

## H. Object and Scope of the Present Work

A more extensive study of pressure effects at intermediate temperatures was suggested by Kofstad et al[2] in an effort to elucidate the cubic kinetic relationship observed. Hurlen[1] and Markali[9] indicated that the complicated growth morphology during oxidation may have some influence on the kinetic data and this requires further investigation. In addition, the preliminary literature review indicated that kinetic results may have been affected by specimen preparation and procedure. In view of the many inconsistencies in the kinetic data obtained at 500°C, and the suggestion by Hurlen that this may be related to geometrical effects associated with a variation in the area undergoing oxidation, further work at this temperature was justified.

As a result of these considerations, a proposal was made to investigate the oxidation of titanium using an automatic recording vacuum ultramicrobalance combined with related electron microscope and optical observations to clarify the kinetic anomalies existing in the temperature vicinity of 500°C. A wide range of operating pressures from $10^{-5}$ to 760 mm Hg of oxygen was studied in the hope of shedding new light on the cubic rate law. Attention to specimen preparation and procedure as related to the kinetic data was also considered. At the time the author was undertaking this study, an original manuscript of a very recent electron microscope investigation of titanium oxidation was made available through the kindness of Dr. D. L. Douglass and the relation of his observed nucleation phenomena to the kinetic data was also undertaken.

# II. EXPERIMENTAL

## A. Apparatus

### 1. Microbalance

In four different kinetic studies of titanium oxidation at 500°C in the past seven years, four alternate methods have been used. Menard[26] used reflected plane polarized light (1962), Lainer and Tsypin[24] employed interferometry (1961). Hurlen[1] performed his work on a quartz-beam microbalance of the Gulbransen[45] type (1960) and Kofstad and coworkers[2] used a volumetric technique (1958) to measure oxygen absorbed. Unfortunately the optical methods are of no use when the film reaches a critical thickness which prevents light penetration. The volumetric technique is exceptionally difficult to control under high vacuum. Hence it was decided that a microbalance would be most suitable in the pressure range from $10^{-5}$ to 760 mm.

The quartz-beam microbalance developed by Gulbransen is very sensitive but requires careful handling and the intermittent collection of data demands the presence of an operator at all times. Unobserved zero point shifts between readings often result from mechanical shock, etc., and the final plot contains a large scatter of experimental points.

In 1960 Cahn[46] developed the first rugged, automatic recording ultramicrobalance (model RG) with a sensitivity comparable to the Gulbransen type. When these became commercially available in 1962, Gulbransen himself purchased one and acknowledged their versatility. The Department of Metallurgy acquired an RG Electrobalance in 1963 for use in this study.

The instrument is a null-type balance and operates according to the schematic diagram in Figure 2. Any slight motion of the beam resulting from a sample weight change causes the flag, which is attached to the right end of the beam and located between the lamp and phototube, to allow more light to

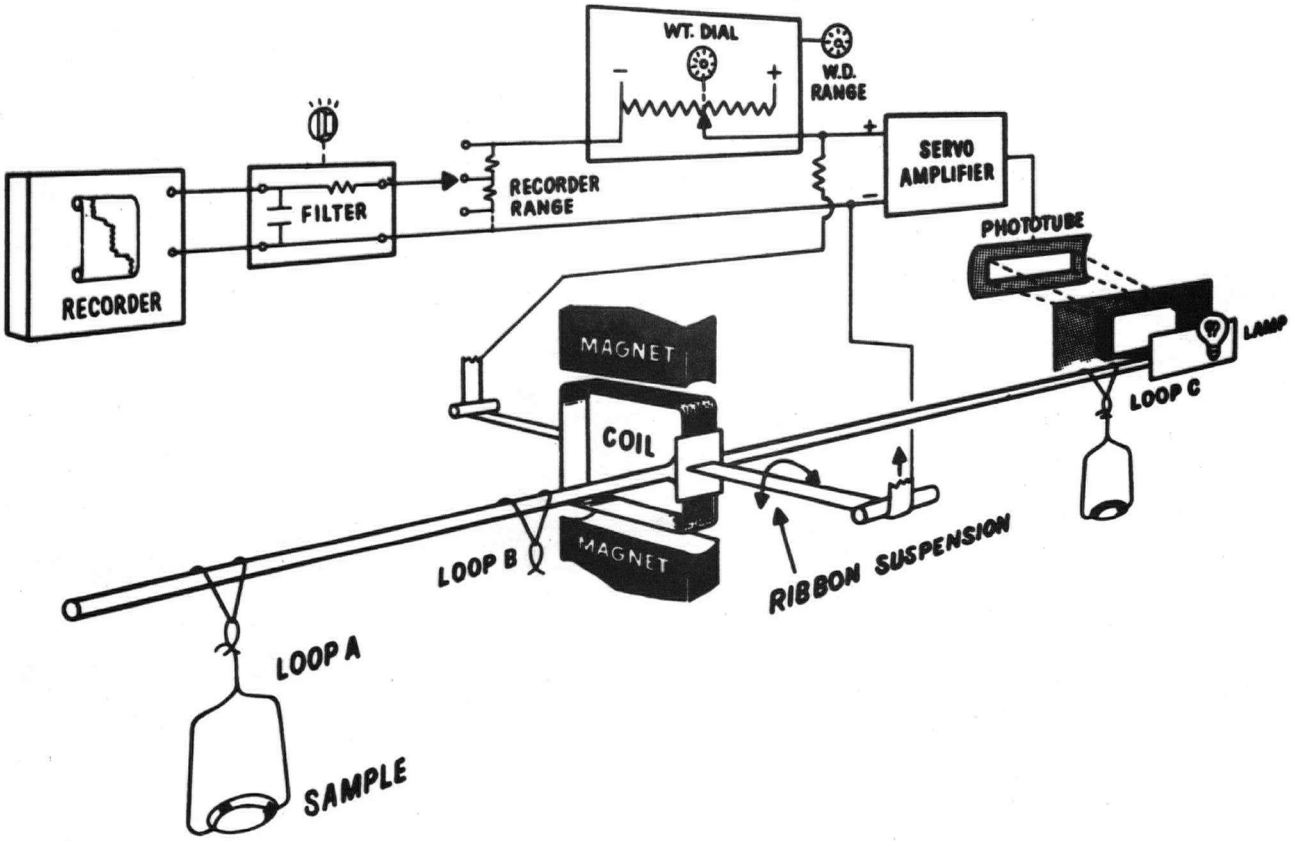


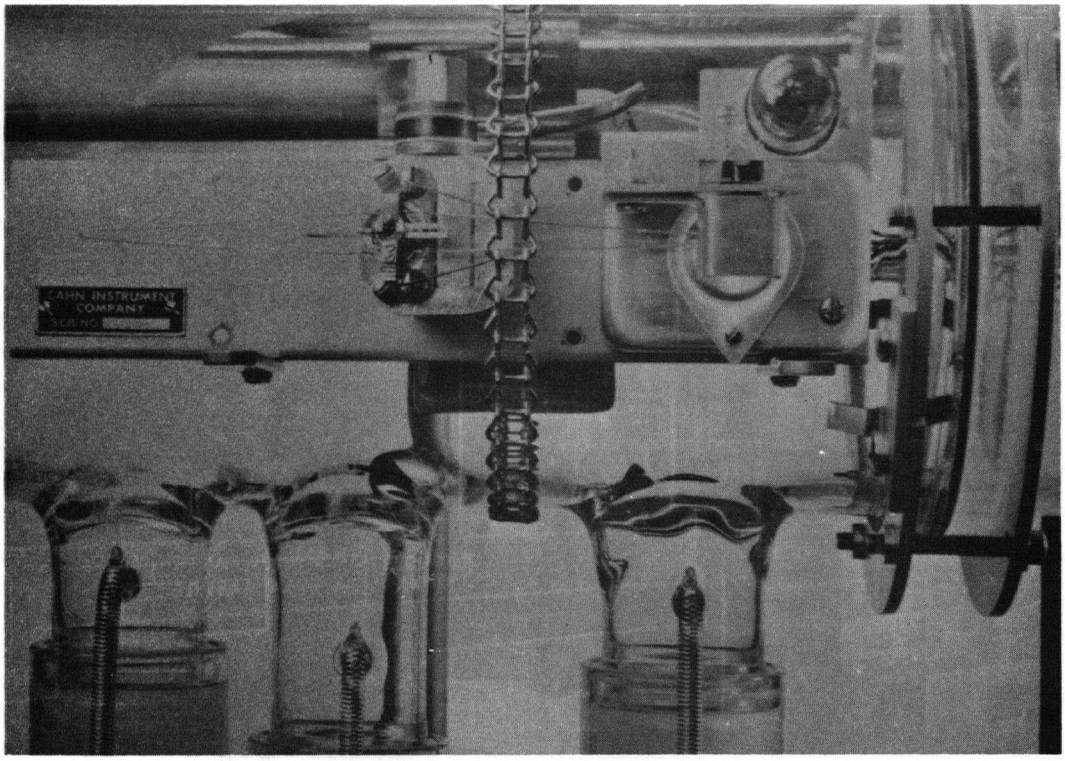


Figure 2. Cahn RG Electrobalance

reach the photocell. The increased photocell current is detected by a servoamplifier which restores the beam to its zero position by applying current to the beam coil located between the magnet poles. Since the restoring current is directly proportional to the weight change, the current can be measured and calibrated with reference to known weights. This is readily achieved by measuring the voltage changes across precision resistors, amplifying this voltage, and feeding it into a chart recorder (in this work a Sargent SR recorder) as shown. Introduction of a filter at the output allows variable damping where vibration is a problem. The most rapid response is 0.01 seconds, which by comparison with quartz beam balances, is the equivalent of taking readings every 1/100 of a second and recording these on a graph. The elastic ribbon suspension virtually eliminates friction effects associated with pivotal balances. Damage to this suspension is unlikely with normal handling because the beam deflects into stops when overloaded. A high gain feedback eliminates drift effects in circuit components with aging. All components are premium grade, all supply voltages are regulated, all rectifiers and regulators are solid-state. Table II lists the operating characteristics of the Cahn RG Electrobalance.

Balance operation was disturbed by electrical, temperature, and illumination effects in the early experiments. However these problems were minimized by controlling the ambient room temperature, reducing solar illumination below the photocell operating level, and removing inductive furnace-switching devices from the balance circuit. After these precautions had been taken, the balance performed according to specifications.

2. Vacuum system

Hurlen[1] has performed the only recent kinetic study of titanium oxidation under vacuum conditions at 500°C. His oxygen pressures varied from

TABLE II.

Operating Characteristics of Cahn RG Electrobalance

1. Precision: the smallest weight change that can be reliably detected. This depends on:

   (a) Load - precision is $10^{-6}$ of load, or $2 \times 10^{-7}$g. maximum
   (b) Weight Change - precision is $10^{-4}$ of weight change

   Whichever of these two factors is larger determines the maximum precision.

2. Sensitivity: the weight change equal to 0.5% on a one millivolt recorder:

   $1 \times 10^{-7}$ g.

3. Accuracy: agreement of the balance reading with the true sample weight as established by reference to National Bureau of Standards calibration weights. This is determined by the linearity of the weight-reading potentiometer, which for the balance, is 0.01% of the mass dial range.
   Maximum accuracy is $1 \times 10^{-7}$ g.

4. Standard deviation: on removing and replacing test weight,

   $3 \times 10^{-7}$ g.

5. Drift: 0.02% of the mass dial range in eight hours, or

   $2 \times 10^{-7}$ g.

6. Maximum load: 2.5 g.

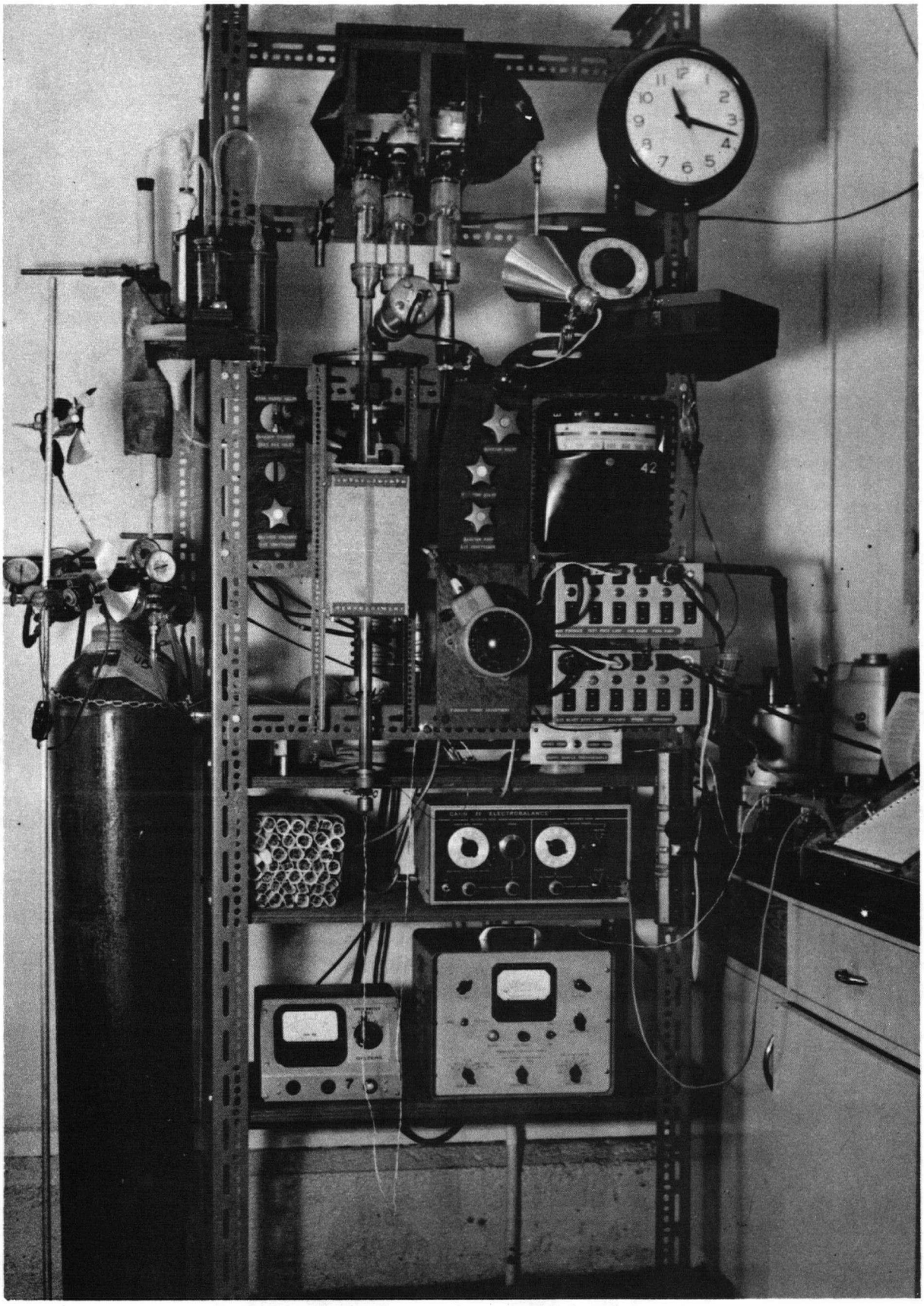

Figure 3. Apparatus assembly

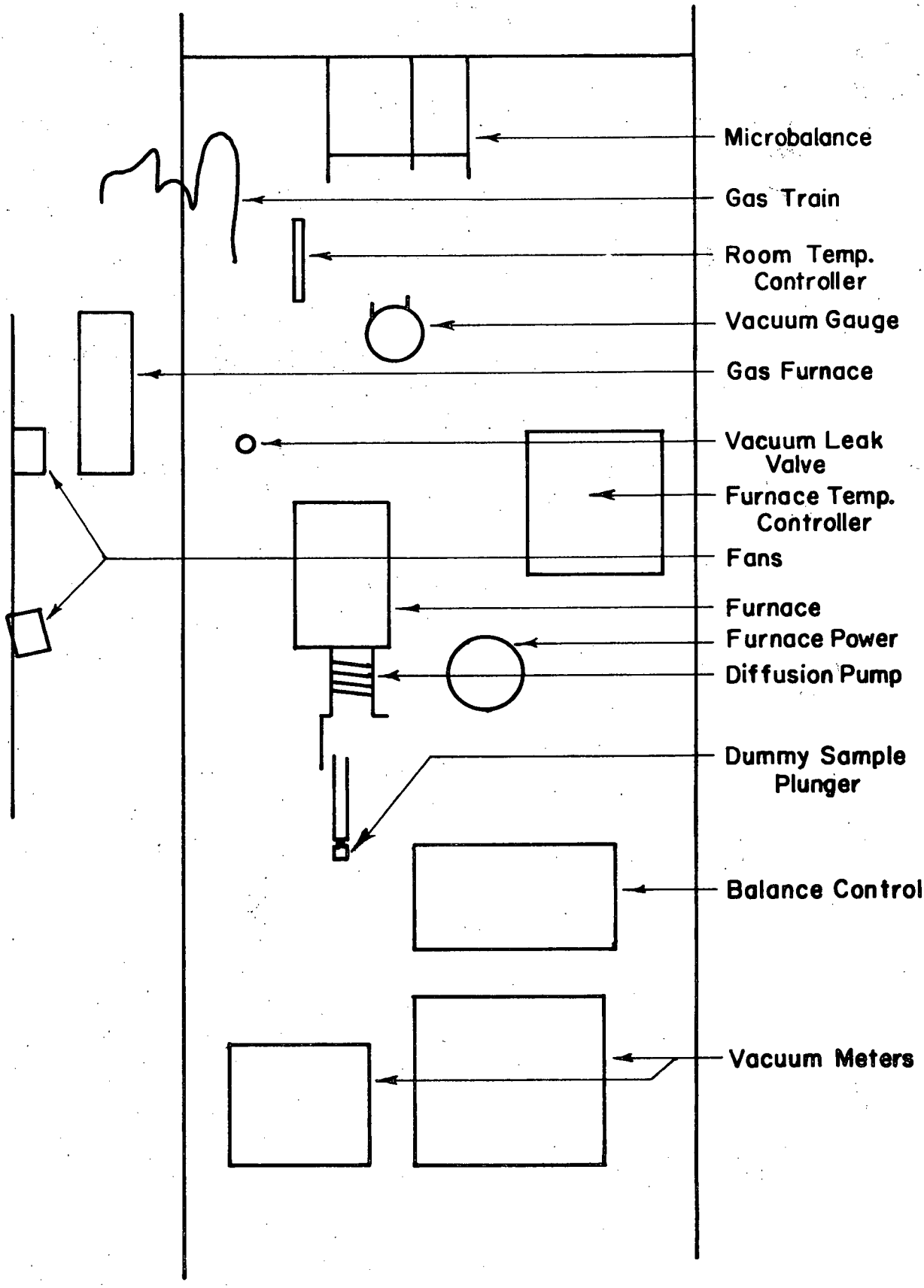


Figure 4. Component identification chart for Figure 3.

$10^{-2}$ to 760 mm. The interesting effects that he began to observe at the lower pressures prompted the author to design a vacuum system which would operate down to $10^{-6}$ mm. It was hoped that nucleation effects, which are quite pressure sensitive[7], could be observed under high vacuum.

The microbalance bottle was therefore connected through a baffle valve and liquid nitrogen trap to an Edwards mercury diffusion pump of 70 liter/second capacity. This was backed through an appropriate roughing valve system by a Balzers mechanical pump. A Millaflow micrometering valve was incorporated for controlled leaks at high vacuum. The total evacuated volume was approximately four liters. Ultimate vacuum of the system was $1.4 \times 10^{-6}$ mm. The sealed system would maintain a static pressure of one millimeter for 24 hours. Vacuum measurements were taken with four different gauges in overlapping pressure regions (McLeod Gauge, NRC thermocouple gauge, NRC ion gauge, and Balzer cold cathode gauge) so that a better estimate of the true oxygen pressure could be obtained. Experiments between one and 760 mm were conducted in a static system, while experiments between $10^{-3}$ and $10^{-5}$ utilized a dynamic system.

A photograph of the assembled apparatus and a component identification chart appears in Figures 3 and 4.

3. Furnace

A furnace constructed around the specimen hangdown tube consisted of a 7/8 inch I.D. mullite tube wound with chromel ribbon and insulated with two bricks. Power consumption was 500 watts. The advantage of such a small unit is the low heat capacity which allows very rapid warm-up (10 minutes to 500°C) and cool-down periods (one hour from 500°C, fanned). The disadvantage is the large temperature gradients present in the hot zone. The effect of these gradients were recorded with two thermocouples spot-welded to

different points on a dummy sample. Steady state thermal profiles throughout the furnace were plotted at temperature intervals of 100° from 400° to 800°C at both atmospheric pressure and high vacuum. The location of the thermal centre of the furnace was established for each set of operating conditions and the maximum gradient across the sample was determined to be 2°C. A Wheelco controller was connected to a slide wire resistor and variable potentiometer so that a small differential voltage could be applied to the furnace for maximum control at any operating temperature. This system yielded a temperature fluctuation of 3°C at the highest temperature. The furnace temperature was monitored and controlled by two thermocouples spot-welded to a platinum dummy sample which could be positioned within the furnace by means of a plunger at the lower end of the furnace tube. Normally the dummy sample, of identical dimensions to a test specimen, was located beside the test specimen in the hot zone.

A remote-controlled lowering system was designed as shown in Figure 5 in order to allow specimen introduction after the furnace temperature and pressure had stabilized at the operating level. The specimen was held above the furnace in the position shown during warmup. Any heating of the specimen by convection or radiation prior to oxidation was prevented by the molybdenum thermal shield mounted on an iron slug and suspended by an external magnet, B. This region was cooled by a fan. When magnet B was removed, the slug and shield fell through the hot zone to the plunger cap below. Then by raising magnet A, the hook at X became disengaged and the specimen was lowered into position with magnet A until the hook engaged at Y. The magnet and slug were lowered further until they rested on the furnace top at C.

Oxygen of 99.7% purity was passed through a furnace containing packed alumina chips at 800°C for conversion of residual CO to $CO_2$, then

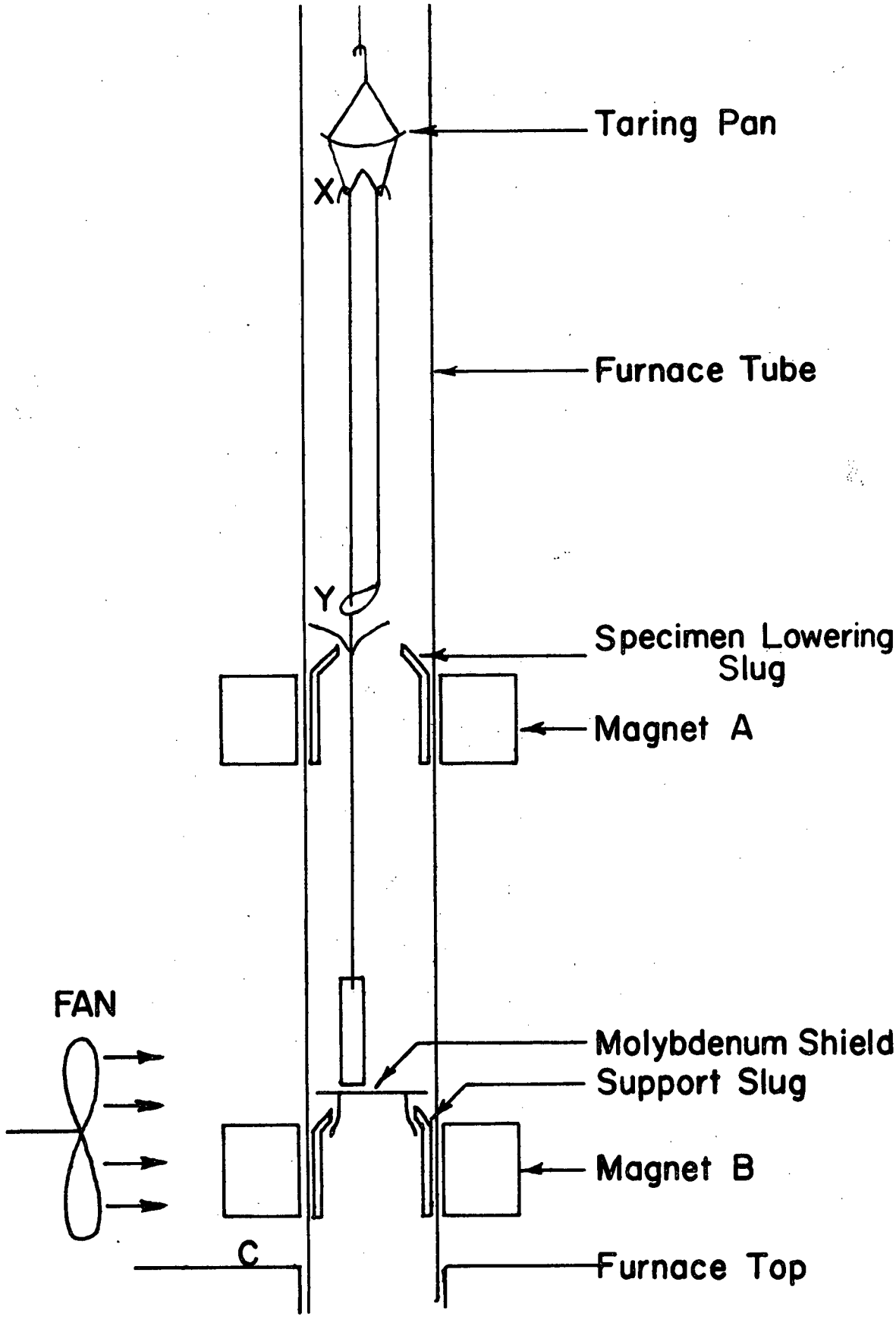


Figure 5. Remote-controlled lowering system

through a column of silica gel for water removal and a molecular sieve (Linde 4A) for $CO_2$ removal before bubbling out of a low vapor pressure oil trap (di-nonyl pthalate) into the room. A tee was located prior to the trap so that a small amount of oxygen could be tapped off into the evacuated system through the Millaflow leak valve.

## B. Materials

### 1. Titanium

Preliminary experiments to establish proper techniques were conducted with Ti65-A, a commercial purity (nominally 99%) sheet supplied by Titanium Metals Corporation of America. Final work was carried out on EP Grade A titanium supplied by Chicago Research and Development Corporation. Resistivity tests on this material by Oak Ridge National Laboratory[47] yielded a resistivity ratio $\frac{R_{300^oK}}{R_{4.2^oK}}$ of 74 compared to the best iodide titanium value yet reported of 44. They concluded that the EP titanium was of exceptional purity. This material is produced by a special fused-chloride salt process developed by the suppliers. The hardness of selected crystals of this material, which is believed to be the purest titanium ever made, is less than Brinell 50 and the oxygen content is below 0.001%. The normal polycrystalline deposit has a hardness of approximately BHN 80 and an oxygen content of 0.01%. Unfortunately this material is very susceptible to oxygen pickup during subsequent fabrication and the hardness increases. Fabrication of the material used in this study by the supplier consisted of arc-melting 200 grams of EP titanium into a button and hot forging the button. This was followed by hot-rolling, cold-rolling, annealing, and cold-rolling to 0.020" sheet. Oxygen content of the final sheet was 0.03%. A spectrographic analysis of metallic impurities appears in Appendix B together with the purity of several materials used by other authors.

2. Preparation

Samples 5 mm by 20 mm were sheared from the sheet and holes 0.020" in diameter were drilled near one end for microbalance suspension. Groups of 20 were then mounted on a polished steel block with jewelers wax. The imbedded specimens were mechanically polished on successive emery papers from #2 grit through to #3/0 grit. All specimens were turned over and remounted on the block for the same procedure. Following this, the specimens were removed and residual wax was dissolved by ultrasonic cleaning in three successive methanol rinses. Specimen edges were finished on #1/0 emery. Individual samples were then suspended on a platinum wire passed through the hole and immersed in an acid solution (25% HF, 75% $HNO_3$) heated to 150°F for three seconds. Transfer to an ultrasonically-vibrated boiling anhydrous methanol rinse was executed in less than one second by placing the plastic beaker of acid and three glass beakers of methanol side by side in the heated ultrasonic cleaning tank. It was imperative that this acid-methanol transfer take place almost instantly otherwise residual staining by the acid on the titanium surface produced non-uniform oxidation. After two further methanol rinses, each sample was quickly dried with an air blast and all were placed in a furnace which was evacuated to $3 \times 10^{-6}$ mm. The samples were annealed for one hour at 850°C, during which thermal facets formed on the surface. Facets were removed and the specimen thinned to approximately 0.007" by a five to seven second immersion in the same warm chemical polish that was used before the anneal. All polishing was performed in a fume hood because of the noxious brown fumes produced. The agitated methanol rinse in triplicate was again followed by air blast drying. Final dimensions of the specimen were measured with microcalipers and within five minutes of the air blast treatment, the specimen was under vacuum in the apparatus. It was found necessary to use plastic tweezers in all handling as most metal types scratched the very soft titanium surface.

The weight of each specimen before oxidation was approximately 100 milligrams.

Preliminary difficulties in surface preparation caused rather spurious results in the first few experiments. Residual staining from the polish solution prevented uniform oxidation and the specimens frequently appeared mottled with large patches of different interference colors. Once the chemical polishing technique had been perfected, exceptionally uniform interference colours, analogous to those of anodically oxidized metal, were observed over the entire surface.

3. Preliminary Tests

Microhardness tests on the as-received sheet, which had undergone a 66% reduction in area by cold-rolling, yielded an average value of BHN 180. On the as-annealed surfaces, an average of BHN 166 was measured. Following the final chemical polish, the hardness dropped to BHN 110. This decrease in hardness with removal of the surface layers indicates that oxygen enrichment of the sample surface must have taken place during the one hour anneal. In spite of the high vacuum the titanium was probably gettering residual oxygen in the system during this period.

Titanium recrystallizes at 490°C (with 50% cold work) so that a large variation in grain size is possible by varying the temperatures and times involved. The annealing treatment used in this work produced an average grain size of approximately 500 to 600 grains/mm$^2$. A few specimens were annealed at 550°C for three hours in order to investigate:

(a) whether faceting occurs during recrystallization or grain growth at this temperature,

(b) whether this annealing treatment or grain size (17,000 grains/mm$^2$) affected the kinetic results.

No facets were formed at 550°C after three hours. One of these specimens was then lightly etched and reheated to 850°C for three hours under high vacuum. Grain growth and faceting occurred as shown in Figure 6.

Pole figure analysis of the annealed sheet indicated the presence of an annealing texture which conformed to that reported in the literature[48]; approximately 70% of the basal plane poles are aligned in the rolling direction and 30% in the transverse direction.

Carbon replicas of the final polished surface were prepared and gold-shadowed at an angle of 15° with the surface to emphasize any topographical irregularities. In the electron microscope these replicas revealed a very smooth surface even at the highest magnifications (Figure 7a). Hence in all area calculations the surface roughness factor was assumed to be approximately unity (i.e. real area was equal to measured area).

It should be mentioned at this point that an insufficiently heated polishing solution, a slight excess of HF above the ratio stated, or a delayed rinse all caused a small degree of pitting as shown in Figure 7b.

Thin film specimens of EP titanium were prepared for transmission electron microscope studies using the chemical polishing technique described earlier. Annealed specimens contained small, highly oriented particles of a second phase (Figure 8a) which did not yield an electron diffraction pattern strong enough for identification. However one line of d-spacing equal to 2.96 Angstroms was detected.

An attempt was made to determine the origin of these particles. Samples of the as-received cold-worked sheet were chemically thinned by

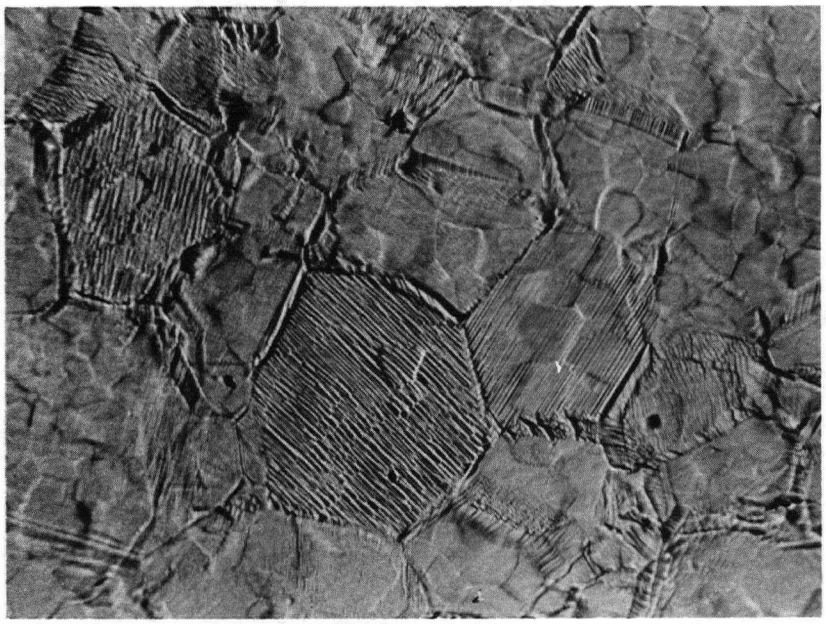

Figure 6. Thermal facets on annealed EP titanium

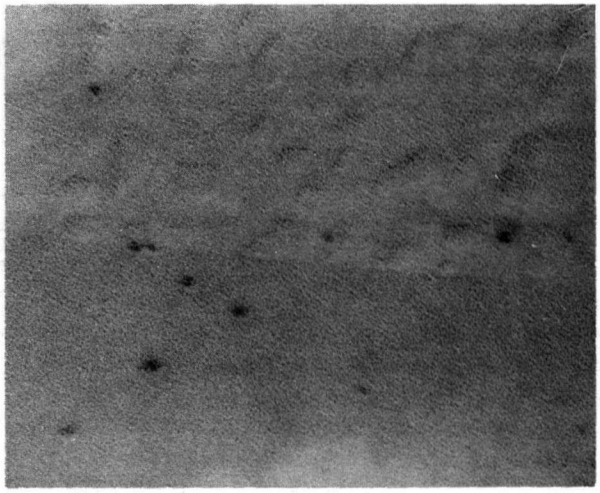

[a] typical surface before oxidation
X70,000

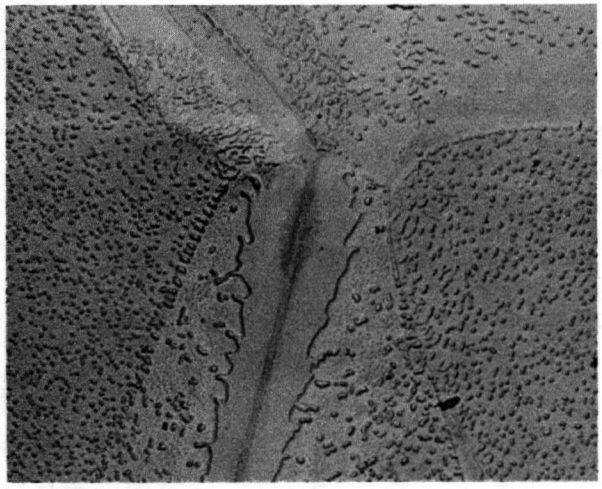

[b] pitted surface resulting from incorrect polish
X14,000

Figure 7. Gold-shadowed carbon replicas of polished EP titanium surfaces

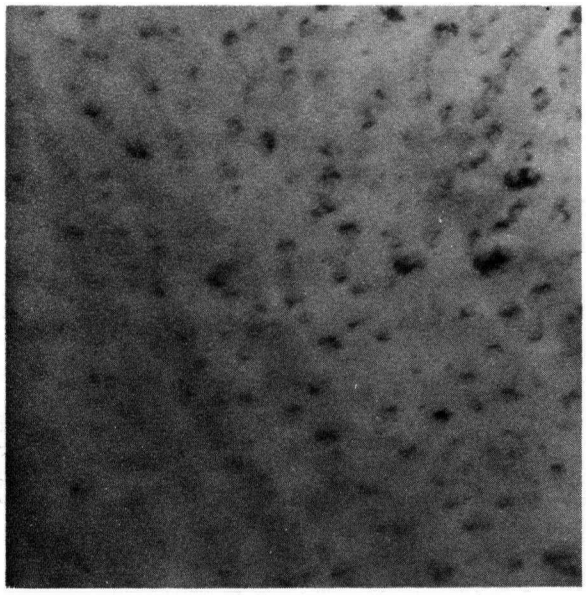

[a] annealed X32,000

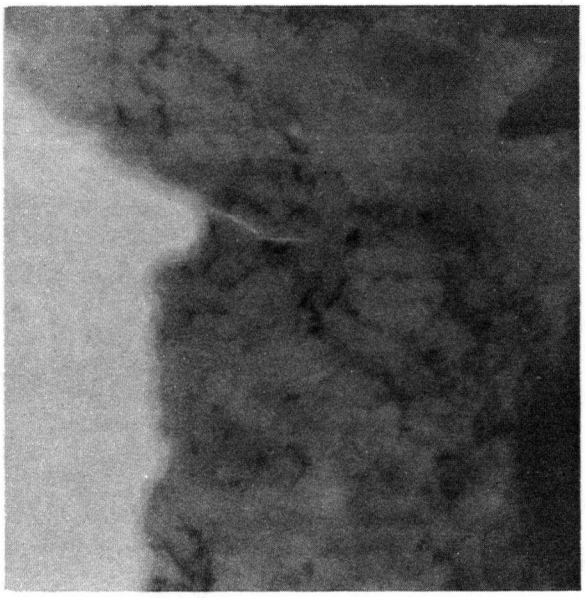

[b] cold-worked X43,000

Figure 8. Transmission electron micrographs of chemically-thinned EP titanium films

the same technique and revealed no particles as shown in Figure 8b. It was therefore concluded that these particles had formed during annealing and were probably some lower oxide of titanium.

Single crystal growth was attempted by two methods reported in the literature[49]. The starting material for both was a fine-grain annealed sheet. In one case thermal cycling through the $\alpha$-$\beta$ transition temperature of 880°C causes growth; in the other, tensile straining followed by annealing causes recrystallization, hopefully at a limited number of sites, with resultant single crystal formation.

In the first experiment, annealed and polished titanium samples were placed in a titanium tube which was wrapped in molybdenum foil along with titanium turnings. The package was sealed in a vycor tube under a vacuum of 200 microns and was placed in a vacuum annealing furnace at $10^{-6}$ mm. The temperature was held at 1200°C for four hours and decreased to 850°C for three days. This cycle was repeated three times. After removal, most of the titanium had vaporized and reacted with the vycor forming a black deposit. The remaining titanium was so heavily faceted that it was unsuitable for oxidation work in spite of the large crystals which had formed in a few of the samples. Attempts by others of this method using an argon atmosphere to prevent faceting yielded no large crystals[50].

In the second experiment, annealed and polished specimens were deformed $\frac{1}{2}$%, 1%, $1\frac{1}{2}$%, 2%, and $2\frac{1}{2}$% in tension. These were then sealed in similar containers to those above under argon in a vycor tube and placed in a vacuum annealing furnace. The temperature was raised to 850°C and held for one week. Although large crystals formed in some of the samples, all were polycrystalline and most contained over 20 crystals. Similar failures in this technique have been attributed to the formation of numerous

deformation twins at small strains and these provide several nucleation sites for recrystallization. Further attempts at single crystal growth were abandoned.

## C. Procedure

### 1. Kinetic Experiments

The metal preparation in previous titanium oxidation experiments has differed markedly as shown in Appendix C. Some investigators have oxidized as-annealed specimens. An oxygen-enriched surface region may have formed during the anneal and this would affect subsequent oxidation. Kofstad et al[2] have shown that the kinetic behaviour varies with initial oxygen content of the metal. Other authors have oxidized mechanically polished surfaces on both annealed and cold-worked sheet. The strain energy contributed by the metal may influence the oxidation kinetics, or the distorted metal may be unfavorable for epitaxial relationships suitable for rapid oxide growth.

Frequently the specimen has been placed in the furnace at room temperature and held under vacuum (as poor as $10^{-4}$ mm) while the temperature was raised to the operating level. Oxygen was then admitted to a fixed pressure and after stabilization, the first measurements were taken. This entire procedure consumed between 10 and 60 minutes and it was assumed that negligible oxidation had occurred prior to the first measurement. This assumption is probably in error. Arntz and Chernow[51] have recently deposited titanium vapor on a halide substrate under a vacuum of $5 \times 10^{-9}$ mm while monitoring the electron diffraction pattern of the film. It was found that by leaking in oxygen to a pressure of $2 \times 10^{-5}$ mm the 500 Angstrom metal film could be partially converted to oxide at temperatures below 500°C. This suggests that oxidation causing a significant change in the kinetic data may have been overlooked during the warmup period in previous work.

It was therefore decided that specimen preparation and start-up procedures should be investigated more fully. The following variations in specimen preparation were adopted:

PREPARATION NUMBER:

1. Cold worked metal (66%), mechanically polished to one micron diamond paste and degreased.
2. Annealed metal (850°C, one hour, $10^{-6}$ mm), mechanically polished to one micron and degreased.
3. Cold-worked metal, chemically polished as described.

4a. Annealed metal (550°C, three hours, $10^{-6}$ mm, 17,000 grains/$mm^2$) chemically polished as described.

4b. Annealed metal (850°C, one hour, $10^{-6}$ mm, 500 grains/$mm^2$) chemically polished as described.

5. As-annealed metal (850°C, one hour, $10^{-6}$ mm), no subsequent polish.

Most of the samples were prepared according to 4b, which eliminated cold-work effects, surface oxygen enrichment, faceting effects, and surface roughness.

Two different procedures were used following the chemical polish and air blast drying:

PROCEDURE A:

(a) specimen was placed on chromel suspension wire in elevated position 2" above the furnace top as shown in Figure 5,

(b) balance was tared,

(c) lowering slug and thermal shield slug were positioned in the furnace tube and the system sealed,

(d) system was evacuated to $10^{-6}$ mm,

(e) furnace was raised to temperature,

(f) oxygen was bled into the system until the desired pressure was established,

(g) the thermal shield was dropped through the hot zone,

(h) specimen was lowered into the oxidation position and weight gain was recorded,

(i) the test was terminated by furnace cooling the samples to room temperature over a $1\frac{1}{2}$ hour period under the same oxygen pressure as in the experiment.

PROCEDURE B:

(a) the specimen was placed on the suspension wire in the lowered position (i.e. in the furnace centre),

(b) balance was tared,

(c) system was evacuated to $10^{-6}$ mm,

(d) weight recording was initiated,

(e) furnace was raised to temperature,

(f) oxygen was bled into the system to the desired pressure,

(g) termination by the same procedure as in A(i).

Procedure A was adopted in most experiments to permit measurement of the total oxidation. Procedure B, similar to that used by Hurlen[1], provided for comparison with his results.

In several experiments the initial weight in air was recorded immediately after taring. The system was then evacuated and the oxidation experiment continued according to procedure A. After furnace cooling, the system was opened to the air and the final weight recorded. The difference between initial and final weight in air was compared with the weight gain recorded during oxidation. In all cases this difference was between three and eleven micrograms greater than the recorded weight increase resulting from oxidation. The discrepancy probably results from zero point shift in the balance caused by shocks or thermal effects.

Specimen heating rates were measured by spot-welding a thermo-

couple to the sample and recording the time to reach operating temperature after the specimen was lowered from the elevated state into the furnace under a vacuum of $10^{-5}$ mm. The lowering operation required three seconds. Sample temperatures after one minute were as follows:

| | | | | | | | |
|---|---|---|---|---|---|---|---|
| Furnace temperature, °C | 200 | 300 | 400 | 500 | 600 | 700 | 800 |
| Sample temperature, °C | 130 | 293 | 395 | 497 | 600 | 700 | 800 |

The necessity of using a thermal shield between the elevated specimen and hot zone was also confirmed. One half hour after the furnace had reached operating temperature of 500°C, the temperature rise of the elevated specimen with the shield in place was 15° above ambient at $5 \times 10^{-5}$ mm. At 760 mm the rise was only 9°C, probably because of more efficient heat removal through convection and conduction by the external fan. When the shield was dropped, the increase above ambient was 35°C at 760 mm. This value increased to 75°C at $5 \times 10^{-5}$ mm.

A platinum dummy sample identical in dimensions with the titanium specimens was used in an experiment conducted according to Procedure A. The operating conditions were 500°C and $10^{-4}$ mm of oxygen. No weight loss was observed during furnace warm-up. After the specimen was lowered a total weight gain of 2.5 micrograms was observed in the first minute. The weight was then constant within ± 0.5 micrograms for the next 130 minutes.

2. Electron Microscopy

Samples were sheared into two pieces; one half for optical metallographic examination and the other for electron microscope studies which were performed on a HITACHI HU-11A. Oxide films were initially stripped from the metal using a 0.5% solution of HF in water. When a platinum wire was attached to the sample and immersed, a small electrochemical cell developed which allowed dissolution of the metal and simultaneous formation

of hydrogen bubbles on the platinum wire. In this case the film could be stripped in five minutes. However bubble evolution and anodic point attack tended to break up the film.

Douglass[52] then suggested the use of a 10% bromine, 90% ethyl acetate mixture heated to 70°C. This combination produced large flakes of oxide which were excellent for transmission studies. The very large pieces always curled into a tight roll indicating that high residual stresses must be present in the film.

Selected area electron diffraction patterns were obtained so that identification and orientation could be established.

In order to emphasize the surface topography of the oxide, the specimens were frequently shadowed with gold at an angle of 30° to the surface before stripping. Both $TiO_2$ and gold were removed together and examined.

3. Metallography

A portion of each specimen was examined using reflected light in a Reichert microscope. In addition to black and white photographs, colour photographs were taken with blue filtered light and Kodacolor II film. The complex interference color patterns on the surface assisted in resolving the relative thickness of the oxide layer.

# III. RESULTS

## A. Kinetics

Microbalance oxidation studies have always involved problems of reproducibility. These are caused by variation in the oxidation behaviour of specific samples and also by operating performance of the balance. After specimen preparation and procedure had been perfected and balance operation stabilized, smooth curves showing few irregularities were recorded. A typical oxidation trace for a one day experiment appears in Figure 9. In this case the weight range was switched in three sequences: 100 micrograms full scale on the first portion, 200 on the second, and 2000 on the last segment. The oscillations at the beginning of the test are a disturbance by the remote-controlled specimen-lowering system which develops a pendulum motion after the suspension is engaged.

In order to compress the kinetic data obtained on a ten-foot strip of recorder chart over a period of days without losing the precision achieved, all curves were transferred to a log-log plot for presentation in this thesis. Figure 10 shows such a plot of three experiments performed under identical oxidation conditions (500°C, 1 mm of $O_2$). In this case the samples were polished according to preparation 4b and oxidized according to procedure B. The scatter in the results expressed as $(\Delta W/W_{min})_t$ averages approximately ten percent.

Figure 11 shows the effect of using procedure A and B with identical sample preparation (4b) and oxidation conditions (500°C, 1 mm). The oxidation behaviour of specimens prepared by different methods and oxidized by procedure B under identical conditions (500°C, 1 mm) is shown in Figure 12. The titanium in experiment 7, 9, and 11 was annealed and chemically polished (preparation 4b) while that in experiment 118 was oxidized in the as-annealed condition (preparation 5). Since the preparation and procedure

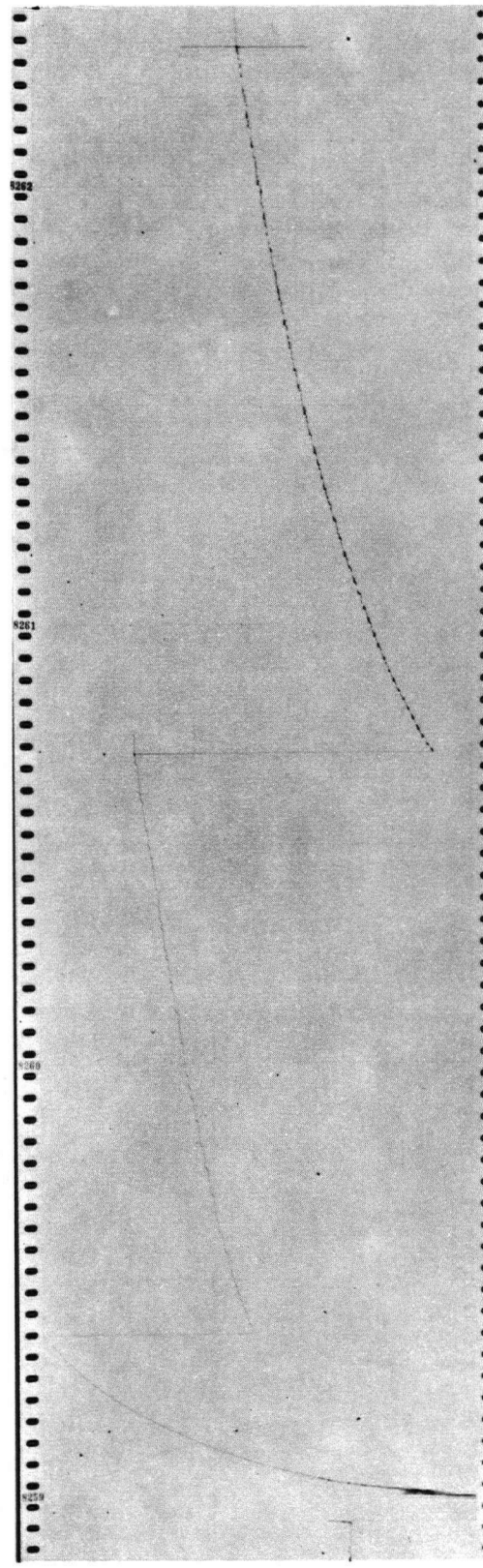

Figure 9. Typical weight-gain trace for a 24-hour oxidation experiment

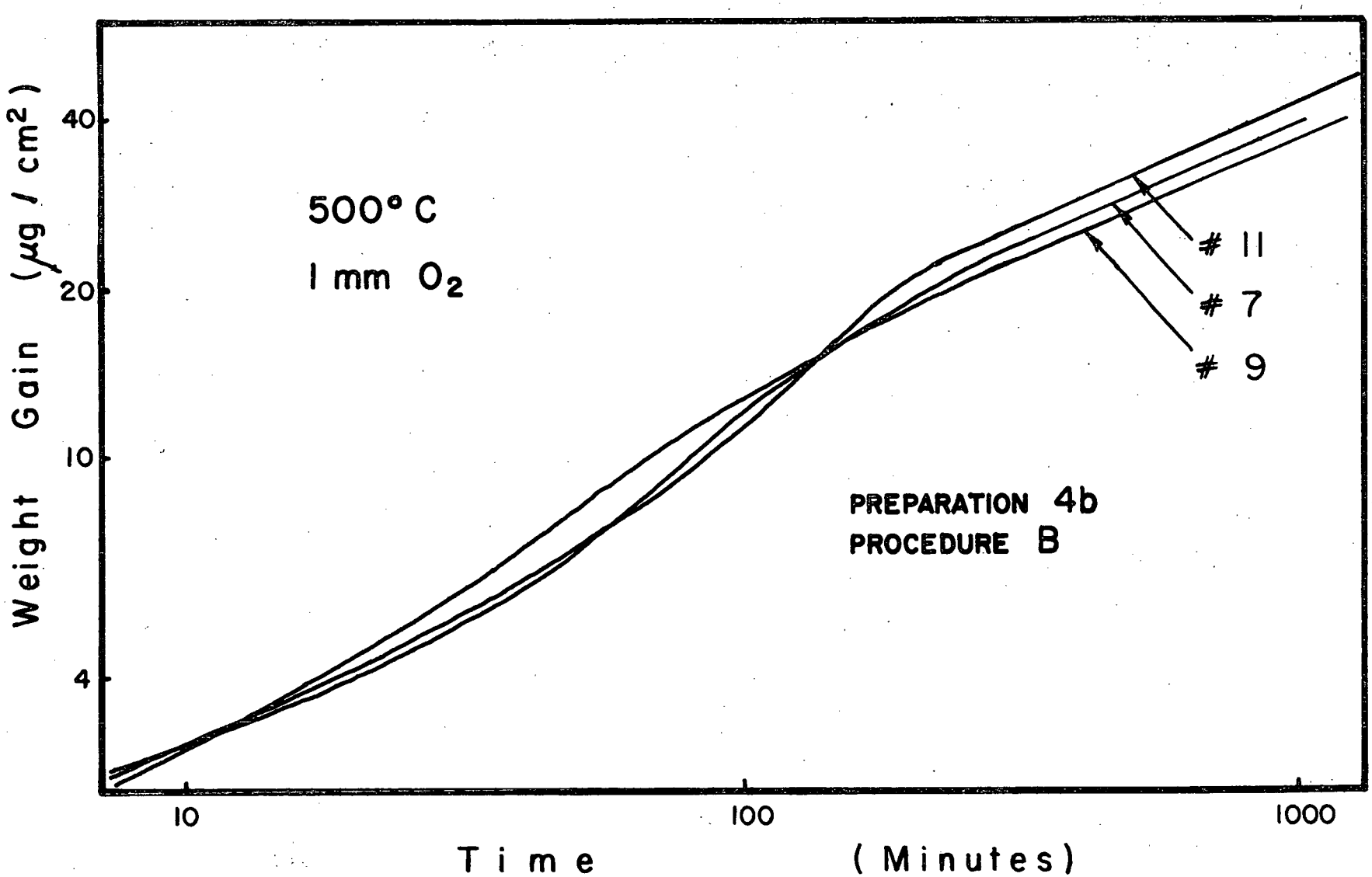


Figure 10. Reproducibility experiments

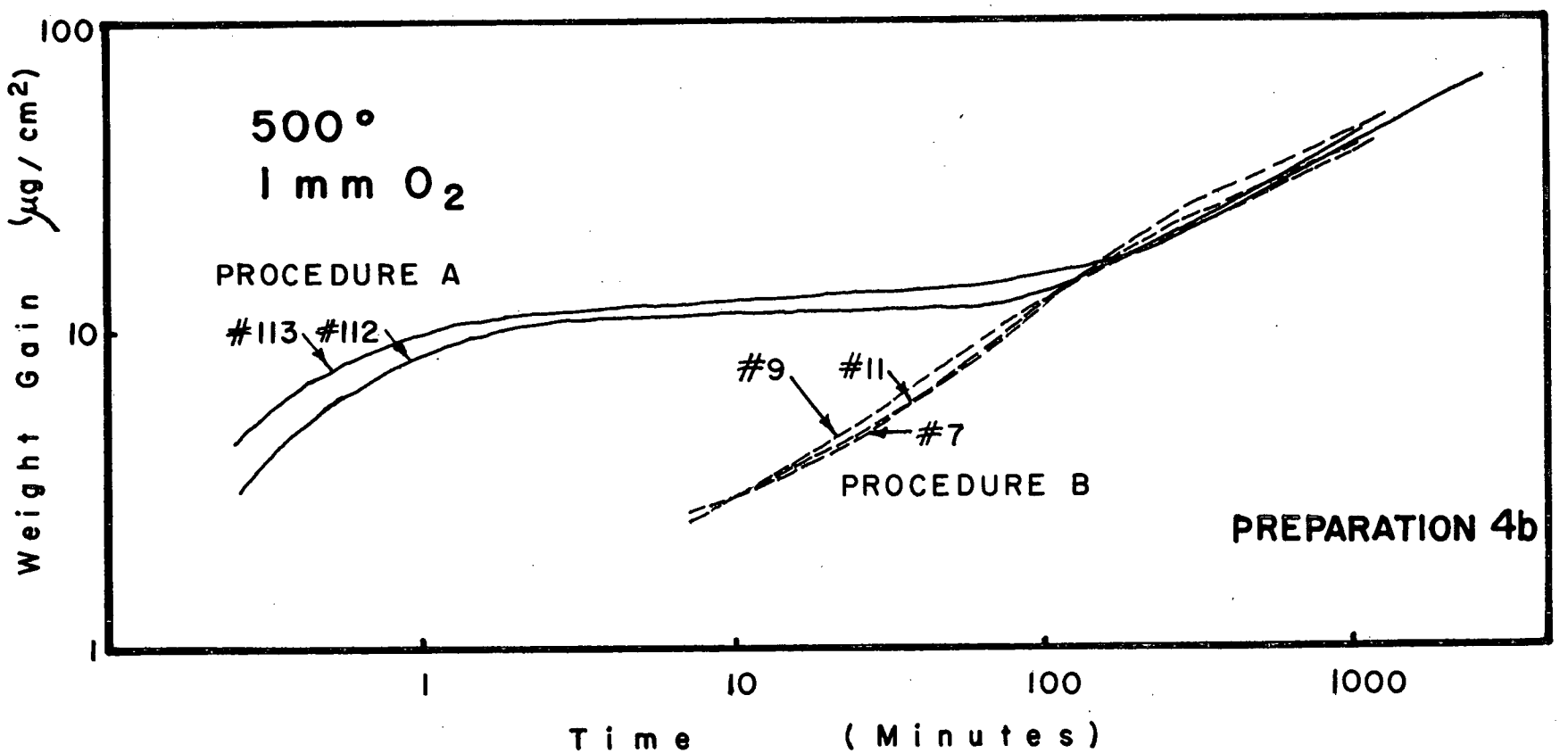


Figure 11. Effect of procedure on kinetic data

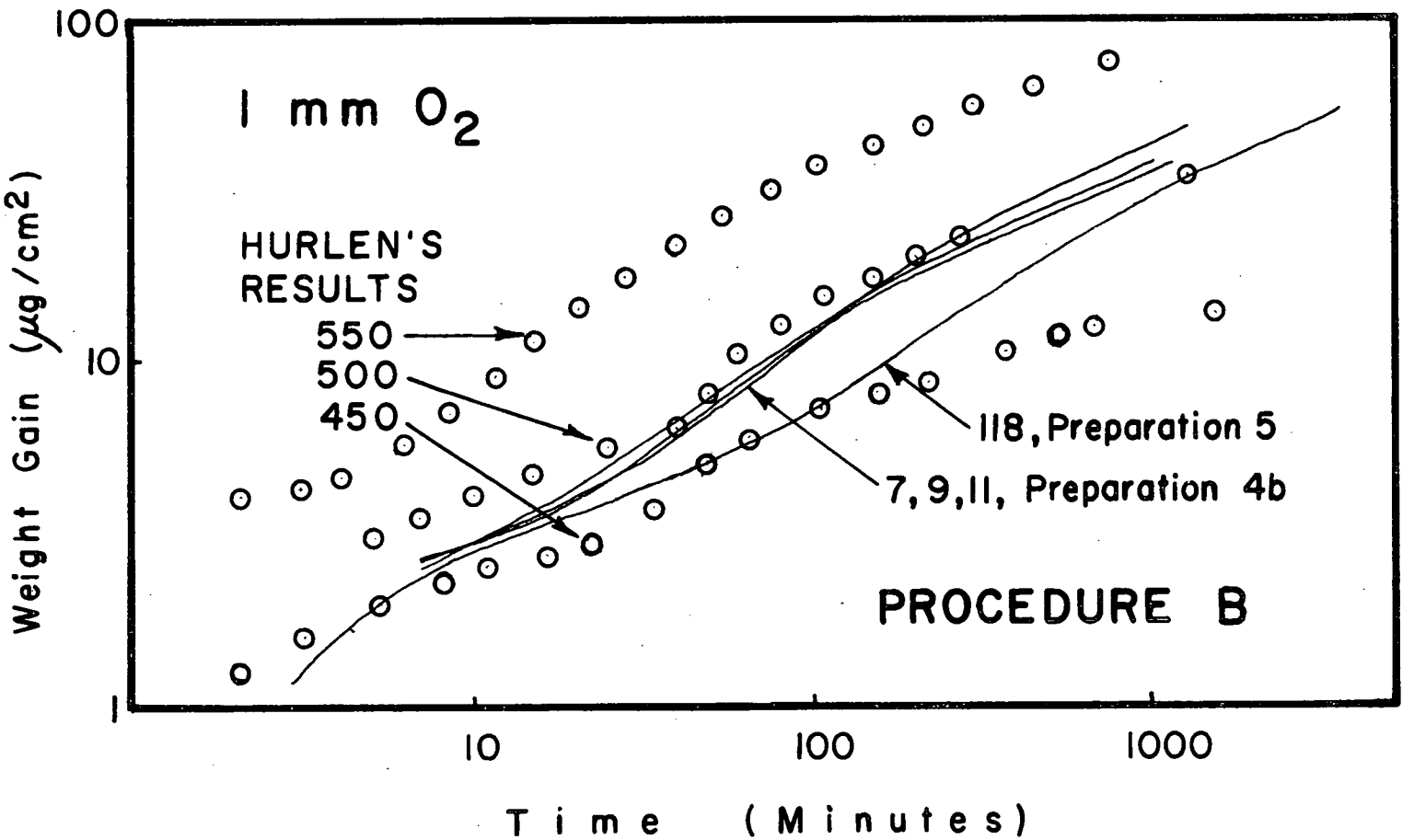


Figure 12. Comparison of 500°C kinetic data with Hurlen's[1] results

of experiment 118 is similar to Hurlen's[1] under identical conditions, his results are also included for comparison. The effect of other preparations was examined using the same procedure (A) and oxidation conditions (500°C, 10 mm $O_2$) as shown in Figure 13.

With the adoption of preparation 4b and procedure A as the most suitable for elimination of deformation stresses, surface roughness, annealing effects, and prior oxidation, further tests were conducted to determine the pressure dependence of oxidation. Experiments at 500°C were performed in duplicate so that the variation with pressure could be positively established within the reproducible limits of technique. These results are presented in two groups of data. The low vacuum kinetics ($>$ 1 mm $O_2$) were obtained in a static system (Figure 14) while the high vacuum ($<$ 1 mm $O_2$) data were measured in a dynamic system (Figure 15). Kinetic curves for oxidation at five different pressures at 600°C are presented in Figure 16.

The effect of temperature on the kinetic data is shown in Figure 17 for oxidation at 760 mm and 10 mm of oxygen pressure.

B. Metallography

The relation of oxide growth morphology to the kinetic data was established by removing specimens at fixed time intervals (10, 100, 1200, and 4000 minutes) and observing the oxide formation. Table III summarizes the specimens examined by optical and electron microscope techniques for this work. In special instances where reproduction of the interference colours is necessary to appreciate the oxide thickness variation, colour photomicrographs were taken as indicated.

Figure 18 shows the effect of different oxygen pressures on the surface appearance of the oxide after ten minutes of oxidation at 500°C.

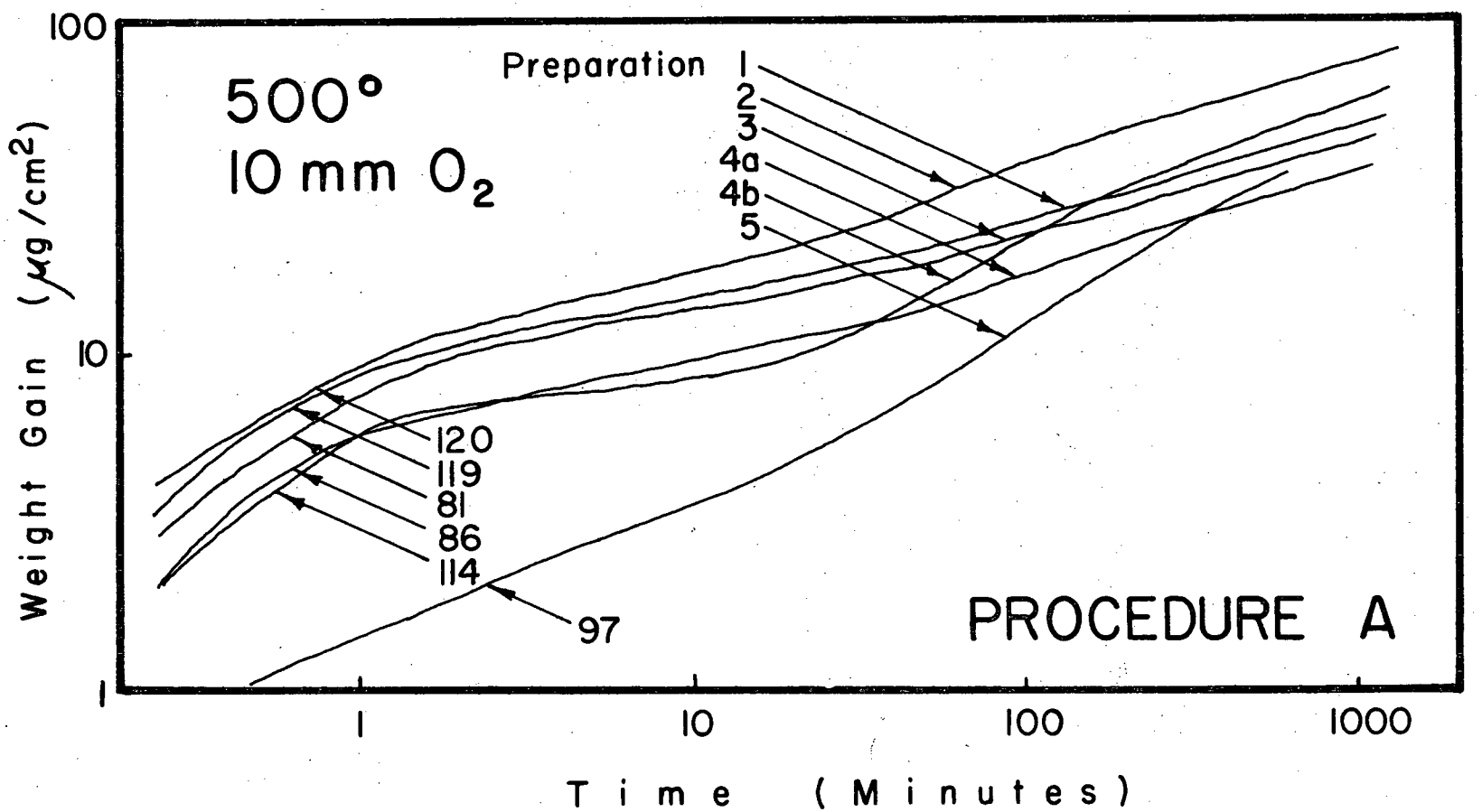


Figure 13. Effect of preparation on kinetic data

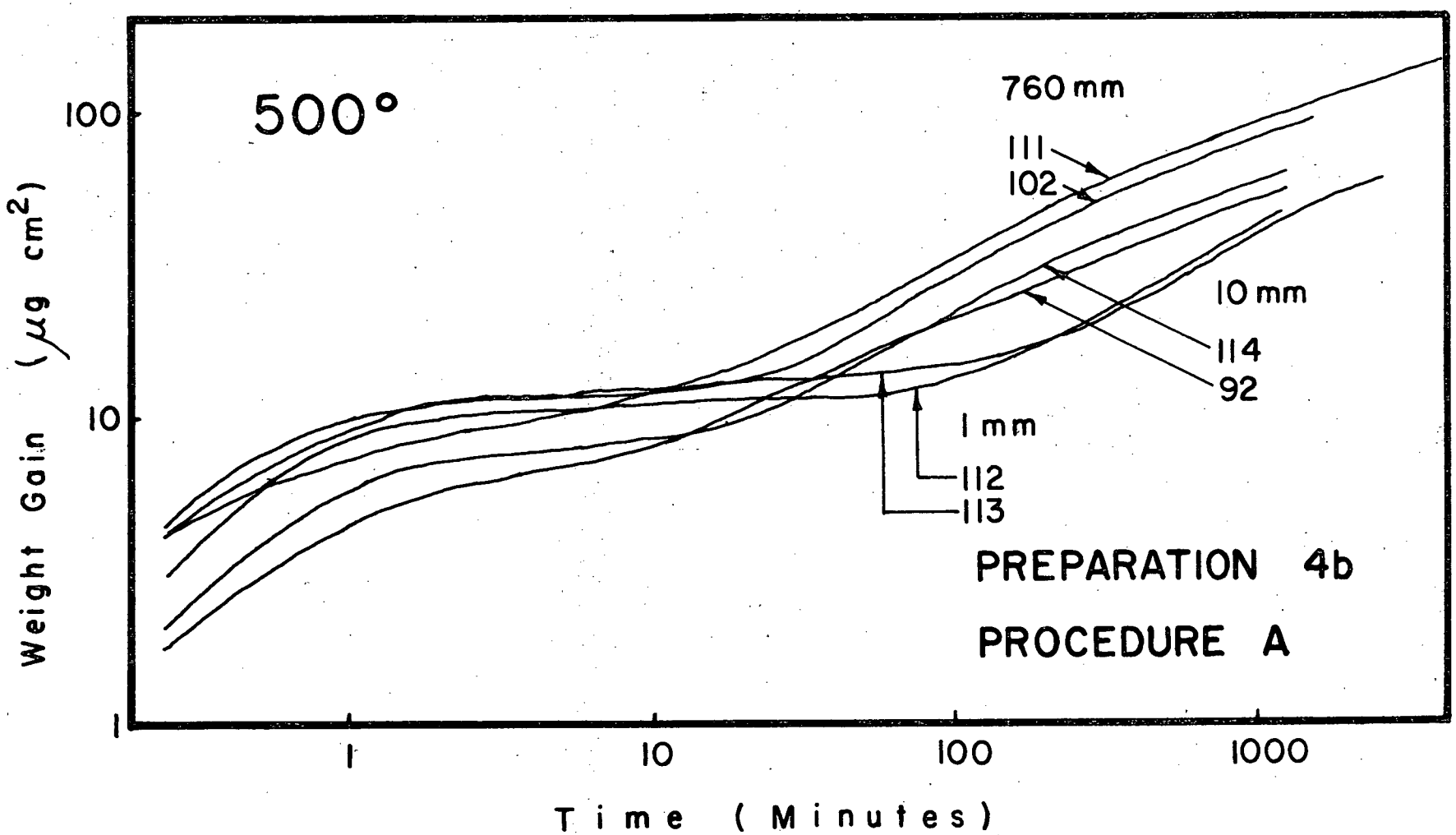


Figure 14. Effect of pressure [at low vacuum] on 500°C kinetic data

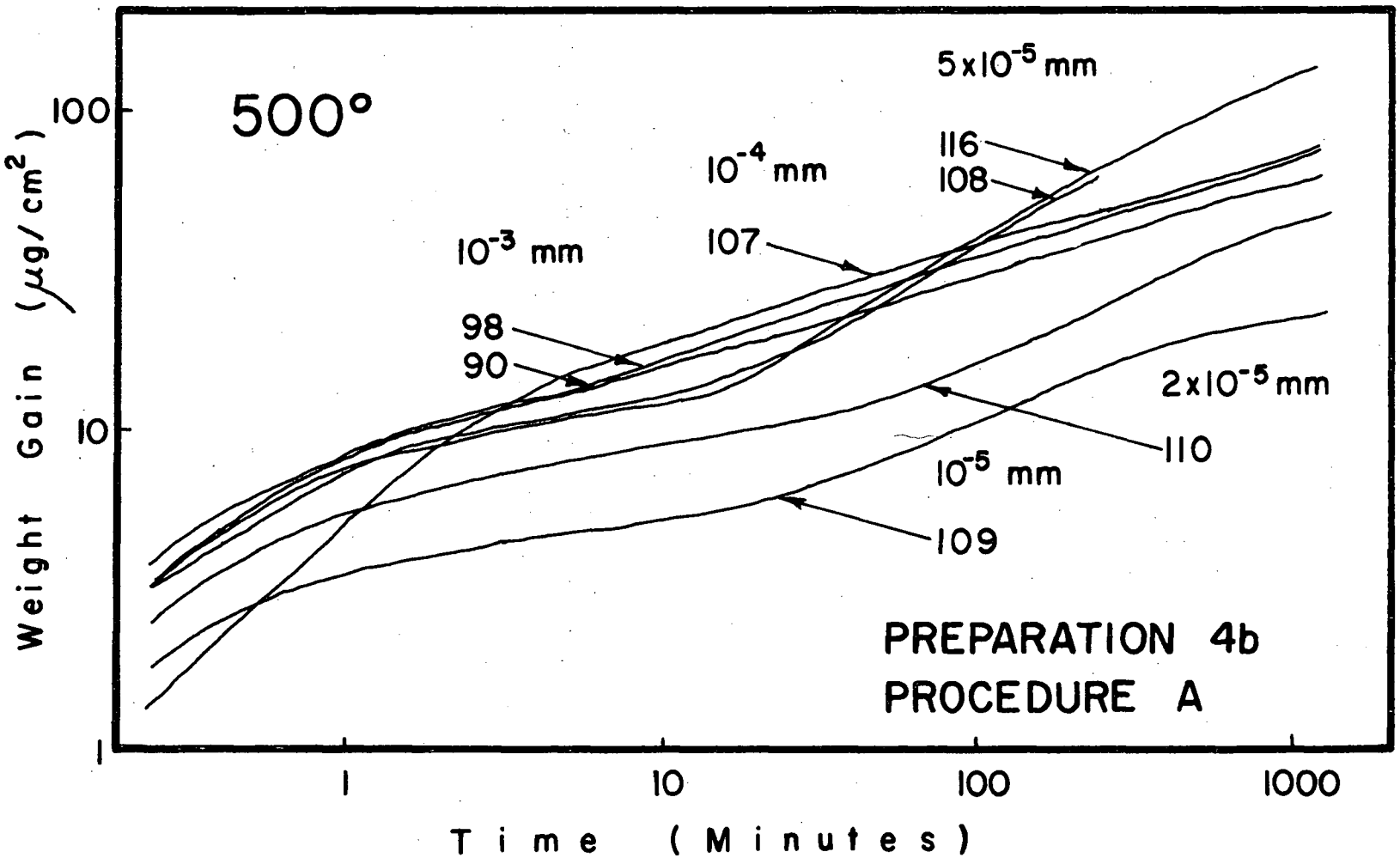


Figure 15. Effect of pressure [at high vacuum] on 500°C kinetic data

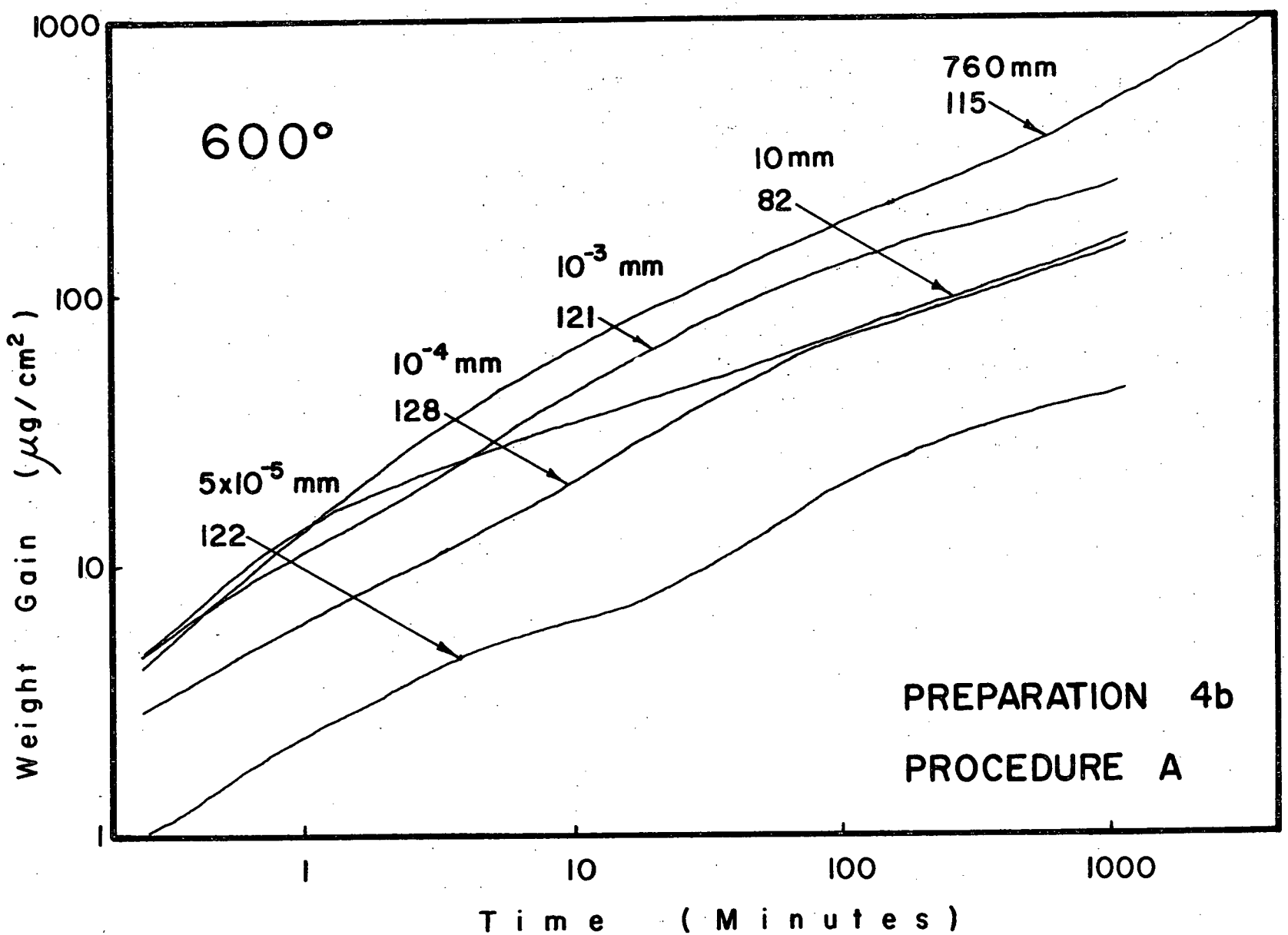


Figure 16. Effect of pressure on 600°C kinetic data

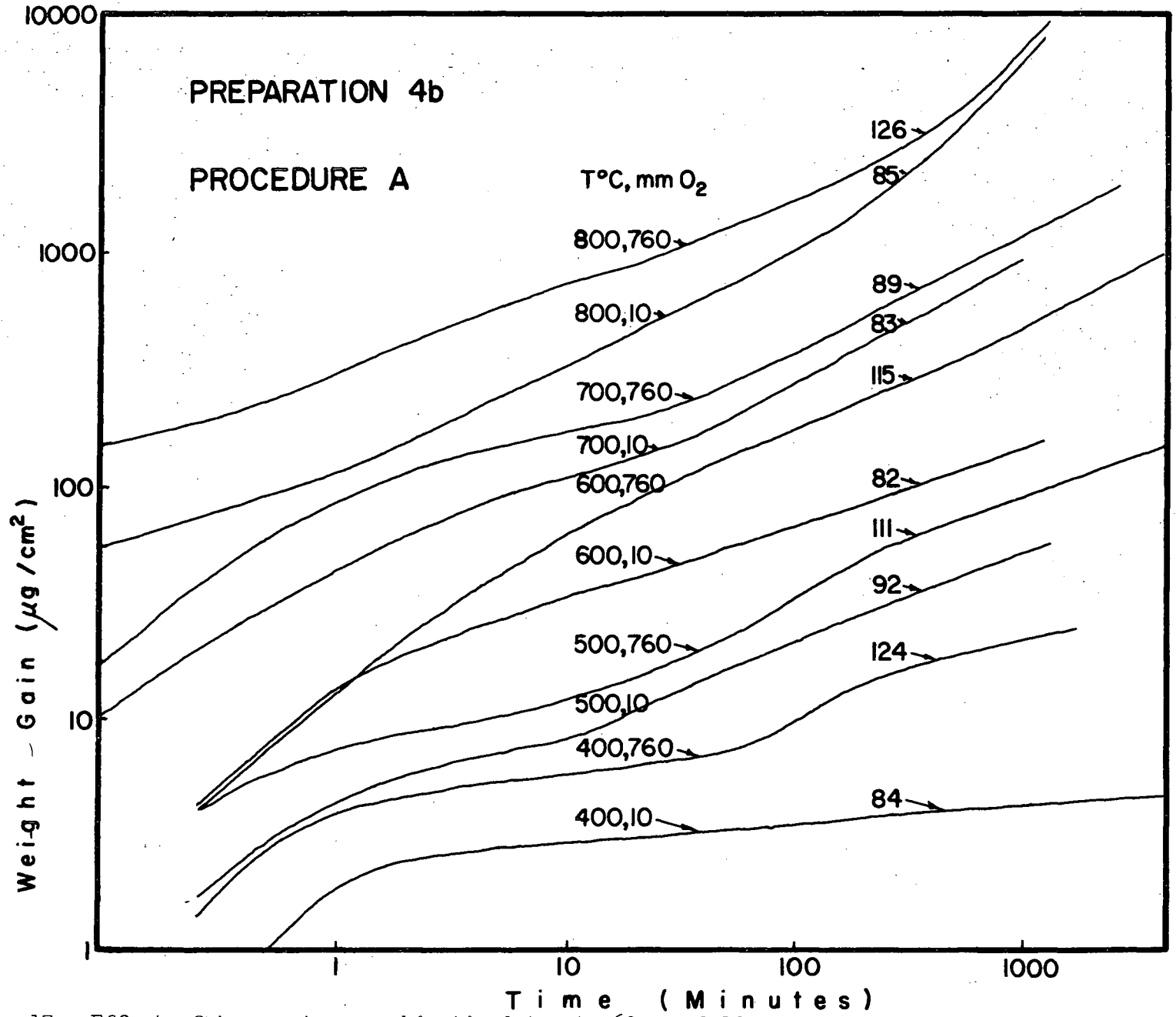


Figure 17. Effect of temperature on kinetic data at 760mm and 10mm

TABLE III.

Specimens Examined for Growth Morphology

| Temp. °C | (time, minutes) 5 | 10 | 100 | 1200 | 4000 |
|---|---|---|---|---|---|
| 800 | | | | #126-760 mm | |
| 600 | | | | # 88-760 mm<br>82- 10 mm<br>121-$10^{-3}$mm<br>128-$10^{-4}$mm<br>122-5x$10^{-5}$mm | #115-760 mm |
| 500 | #99-760 mm* | #129-760 mm<br>93- 10 mm*<br>127- 1 mm<br>103-$10^{-2}$mm<br>95-$10^{-3}$mm*<br>96-$10^{-4}$mm<br>94-5x$10^{-5}$mm* | #123-760 mm<br>125-760 mm | # 87-760 mm*<br>114- 10 mm*<br>112- 1 mm<br>98-$10^{-3}$mm*<br>107-$10^{-4}$mm<br>116-5x$10^{-5}$mm*<br>109-$10^{-5}$mm<br>80-$10^{-5}$mm, as-annealed | #111-760 mm |
| 400 | | | | #124-760 mm (1700 minutes) | # 84- 10mm (20,000 min) |

Notation:

* electron microscope examination
colour photomicrographs

all others, black and white photomicrographs

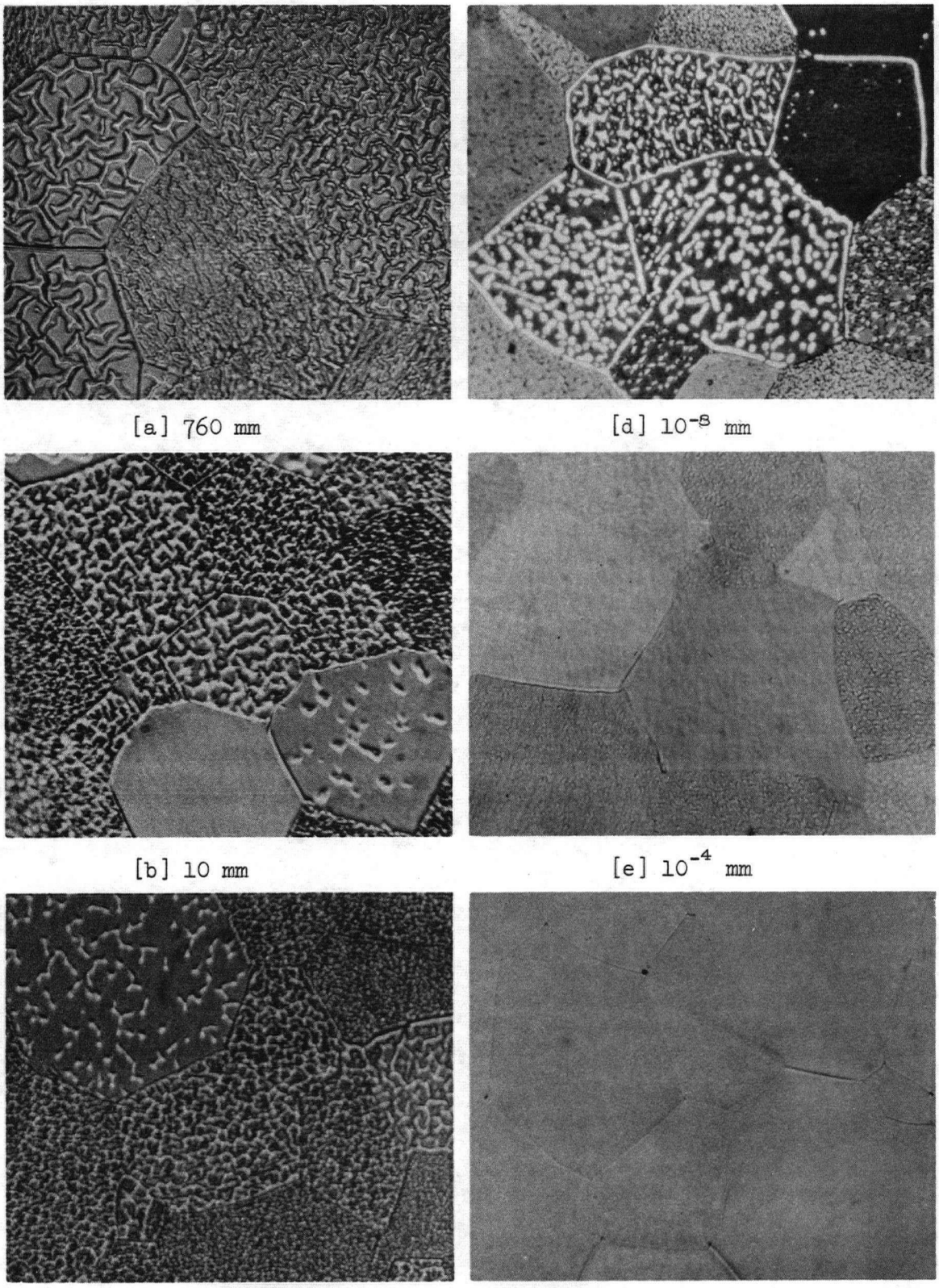

[a] 760 mm

[d] $10^{-8}$ mm

[b] 10 mm

[e] $10^{-4}$ mm

[c] 1 mm

[f] $5x10^{-5}$ mm

Figure 18. Effect of pressure on oxide morphology after 10 min., 500°C [X650]

A transition in these structures occurs with time as shown in Figure 19, which represents 1200 minutes of oxidation under the same conditions. The effect of temperature on growth morphology can be observed by comparing the sequence of structures for 1200 minutes of oxidation at 600°C under different pressures (Figure 20) with those at 500°C (Figure 19). Figures 22a and 22b show the oxide structure after 1200 minutes under 760 mm at 800° and 400°C respectively. The similar structures in Figures 22c and 22d result from vastly different oxidation conditions: 500°C, $10^{-5}$ mm, 1200 minutes and 400°C, 10 mm, 20,000 minutes.

Figure 23 shows the effects of oxidation anisotropy in colour. Figures 23b and 23d are enlarged (x800) views of Figures 23a and 23c (x200) respectively. Figure 23e (x200) illustrates the interference colours of the film formed at 500°C, $10^{-5}$ mm after 1200 minutes oxidation while Figure 23f (x800) shows a similar film after 1200 minutes at 600°C, $5 \times 10^{-5}$ mm of oxygen. Figure 24 contains colour photomicrographs of oxide networks in various stages of growth and development. Figures 24a to 24d are oxides formed after 100 minutes at 500°C, 760 mm, while 24e and 24f represent 1200 minutes oxidation at 500°C, 1 mm. Figure 25 shows oxide films formed under low oxygen partial pressures at 500°C. Figures 25a to 25d represent 1200 minutes at $10^{-3}$, $10^{-4}$, $5 \times 10^{-5}$, and $10^{-5}$ mm of oxygen respectively. Figure 25e illustrates regions of suppressed oxide growth after ten minutes at $10^{-3}$ mm while Figure 25f shows the film formed on an as-annealed specimen oxidized for 1200 minutes at $10^{-5}$.

## C. Electron Microscopy

Since a large amount of pertinent information was obtained from electron microscope examination of each specimen, the results will be presented individually for each specimen, rather than collectively as were the optical observations. With reference to Table III, the specimens indicated

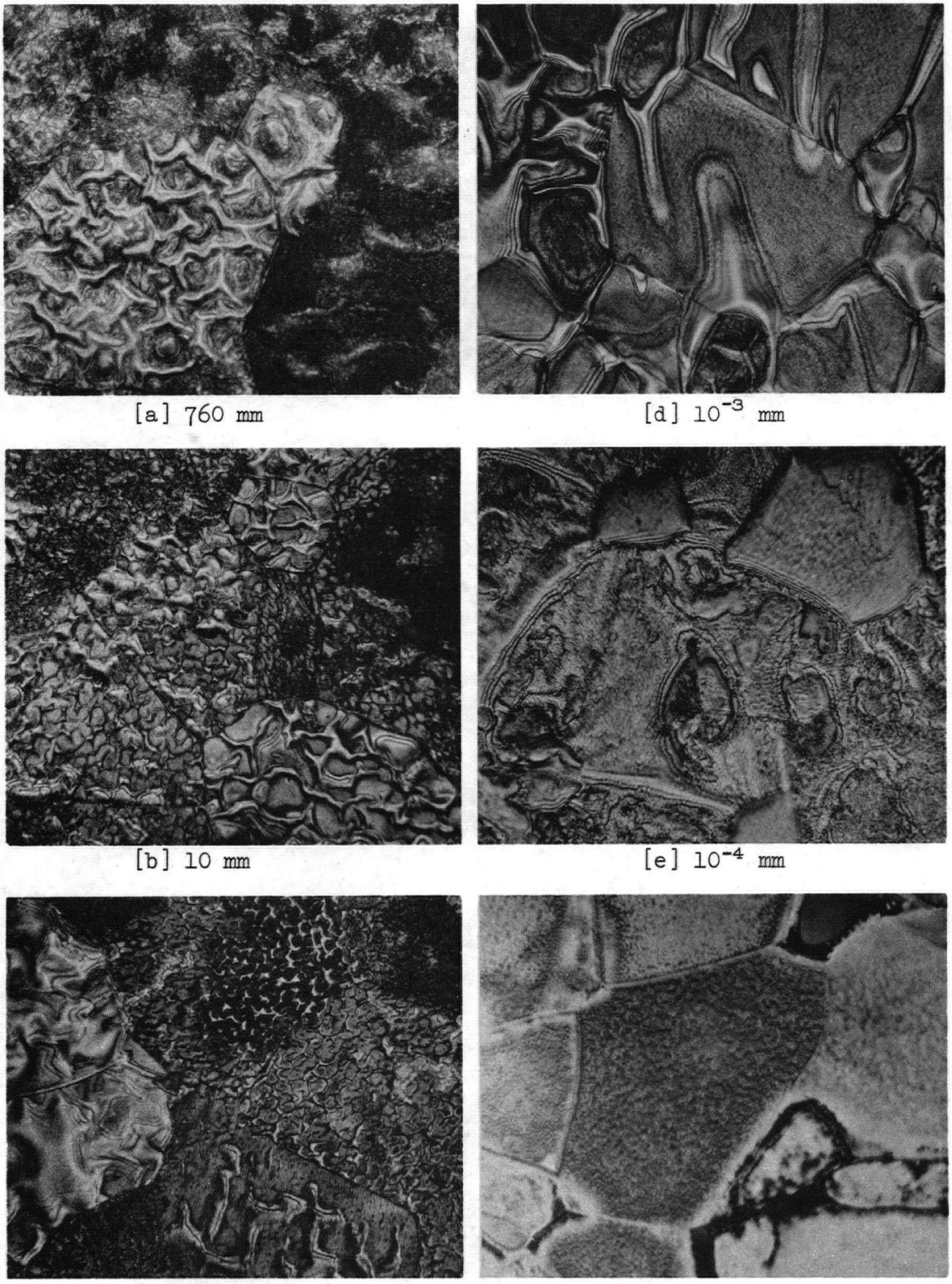

[a] 760 mm

[d] $10^{-3}$ mm

[b] 10 mm

[e] $10^{-4}$ mm

[c] 1 mm

[f] $5 \times 10^{-5}$ mm

Figure 19. Morphological transition of structures in Figure 18 after 1200 minutes under identical oxidation conditions [all X 650]

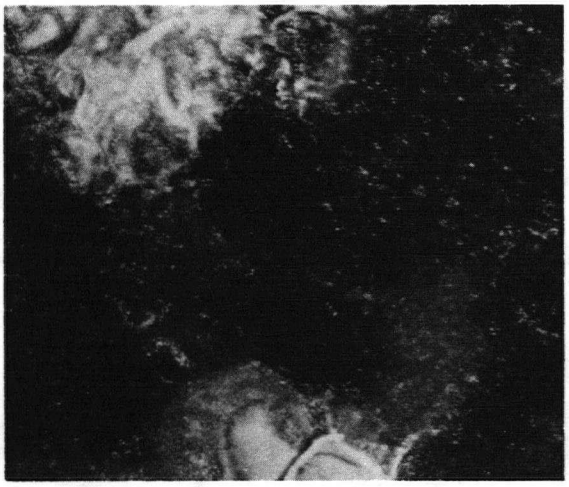

[a] 760 mm

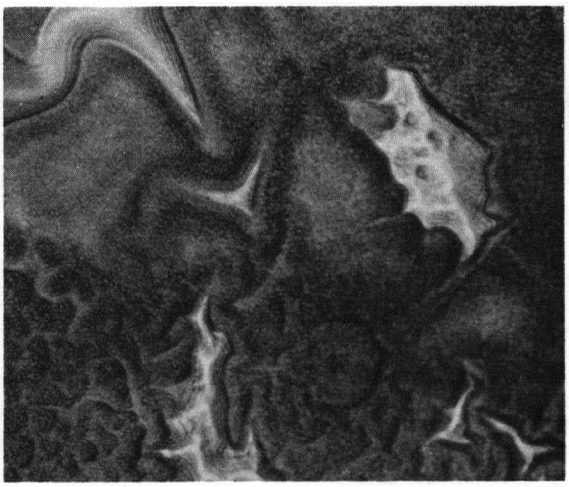

[c] $10^{-3}$ mm

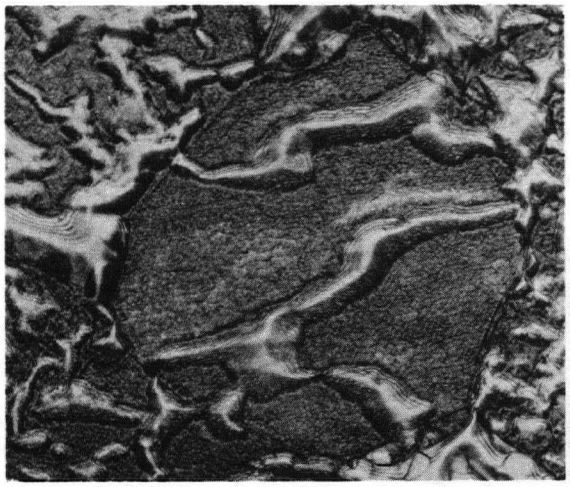

[b] 10 mm

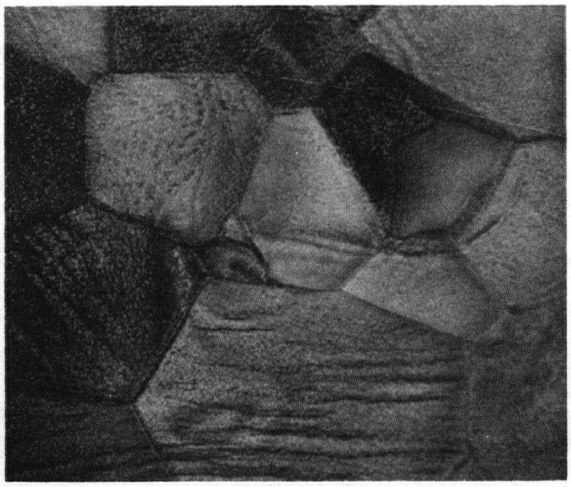

[d] $10^{-4}$ mm

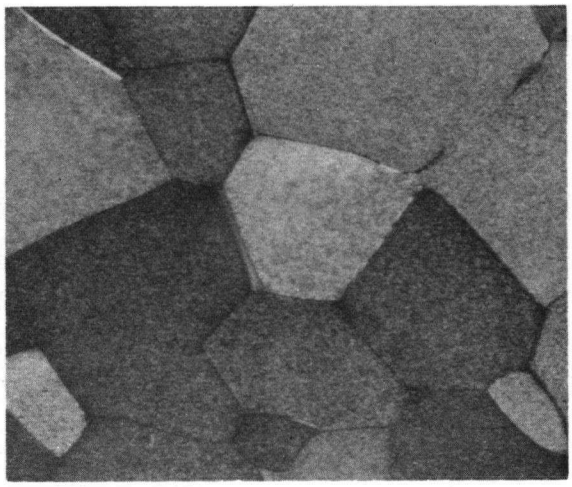

[e] $5 \times 10^{-5}$ mm

Figure 20. Morphology of specimens oxidized under identical pressures for same time [1200 min.] as in Figure 19, but at 600°C [all X650]

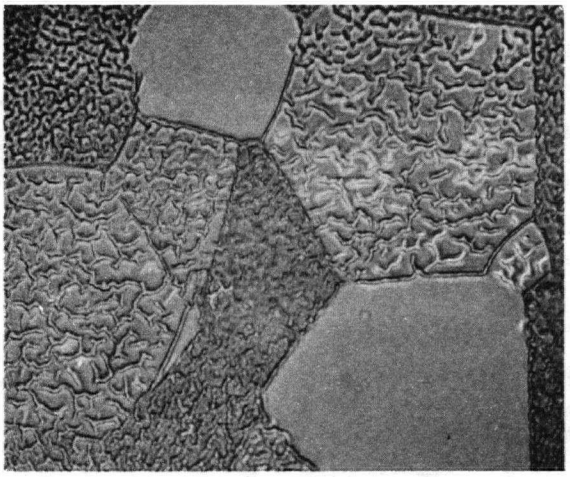

[a] 5 min.

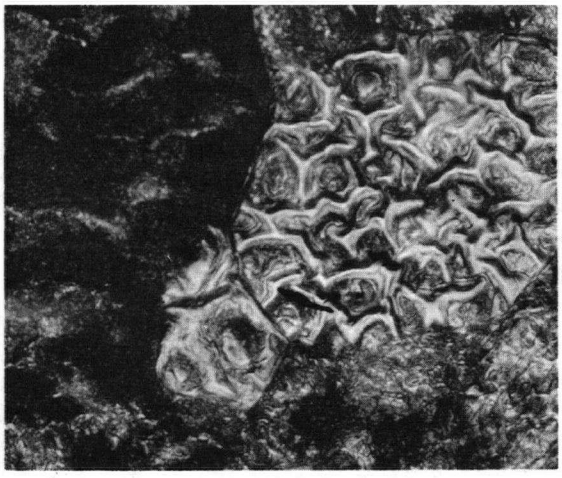

[d] 1200 min.

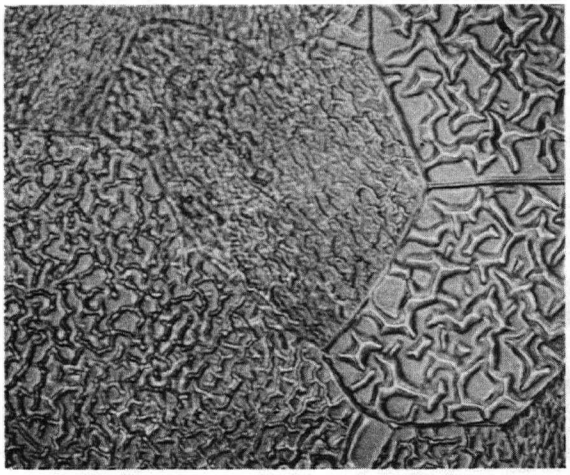

[b] 10 min.

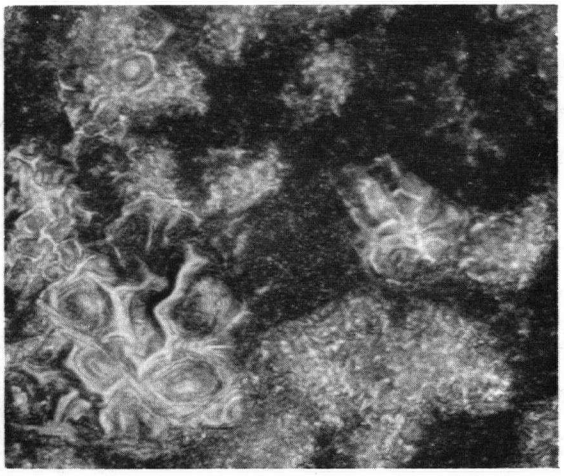

[e] 4000 min., 500°C

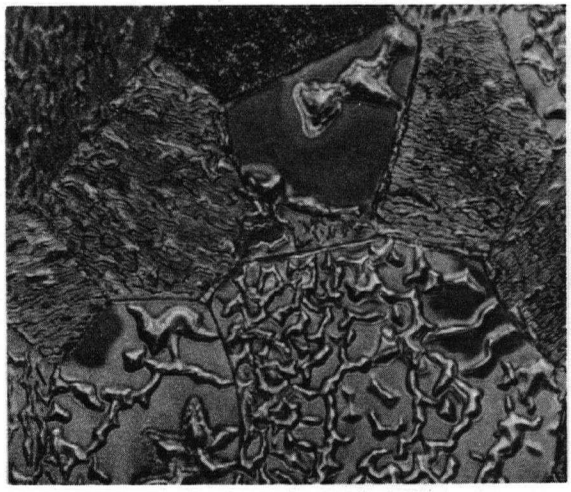

[c] 100 min.

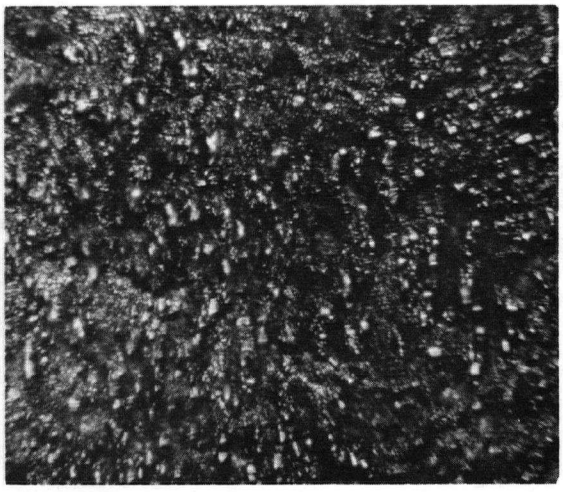

[f] 4000 min., 600°C

Figure 21. Network growth sequence at 500°C, 760 mm (all X650)

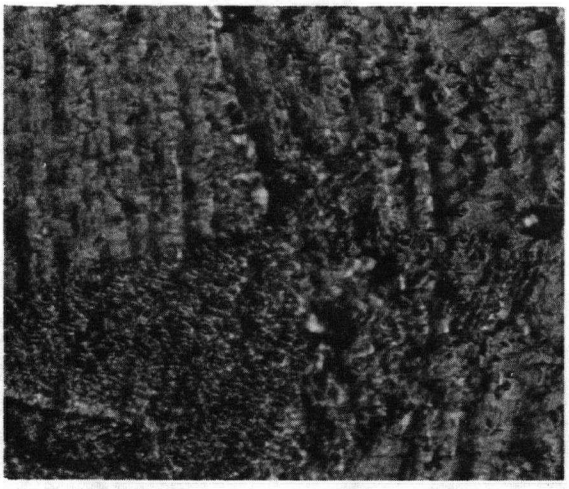

[a]800°C, 760 mm, 1200 min.

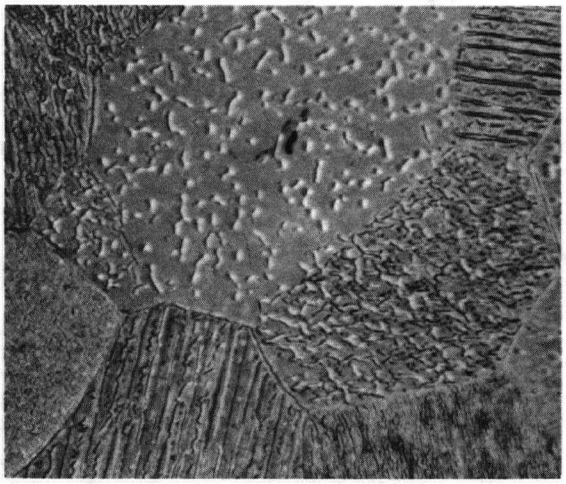

[b]400°C, 760 mm, 1700 min.

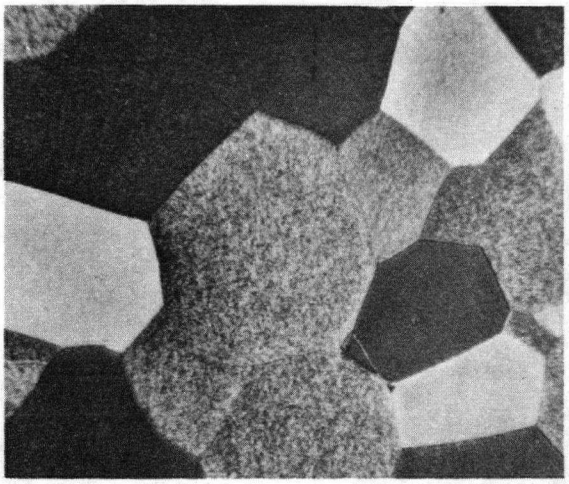

[c]500°C, $10^{-5}$ mm, 1200 min.

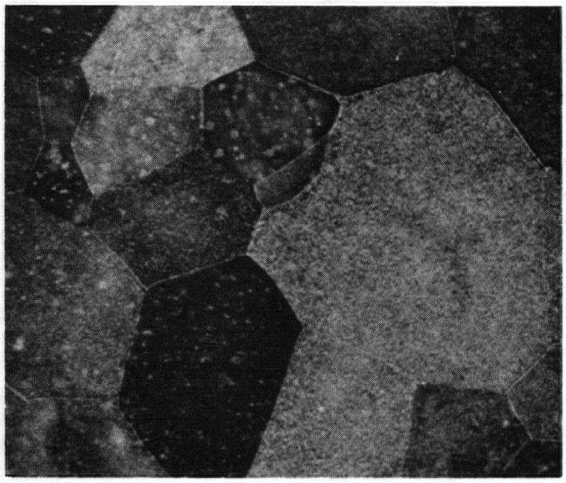

[d]400°C, 10 mm, 20,000 min.

Figure 22. Miscellaneous oxide structures (all X650)

[a] 500°C, $10^{-2}$ mm, 10 min. X200

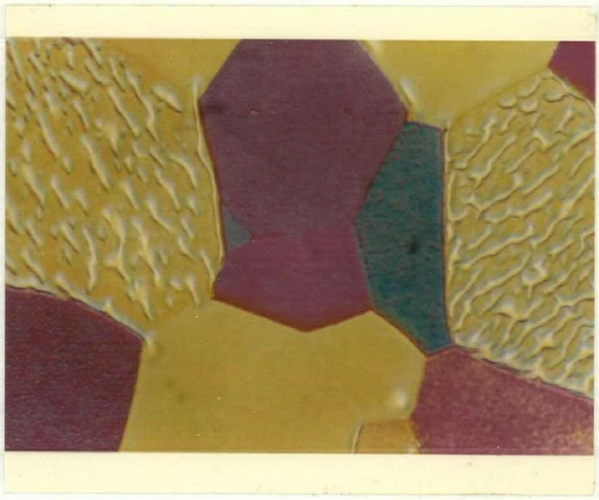

[b] same as [a], X800

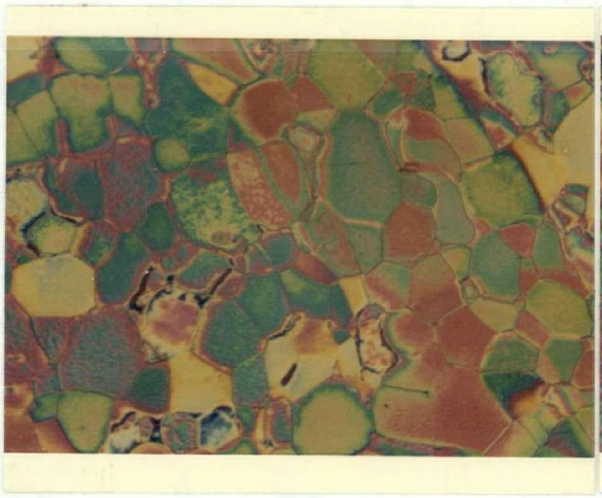

[c] 500°C, $5x10^{-5}$ mm, 1200 min. X200

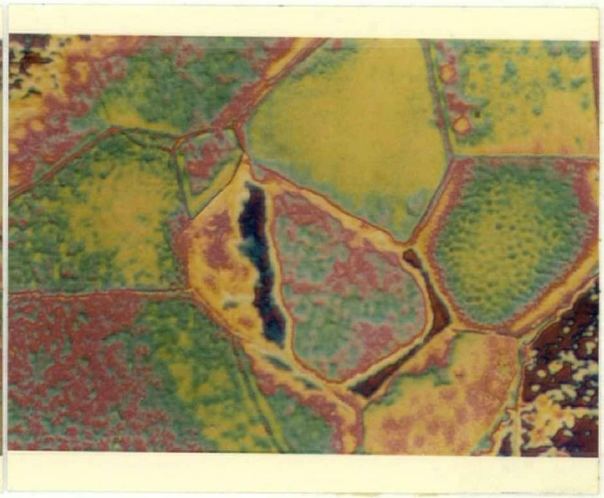

[d] same as [c], X800

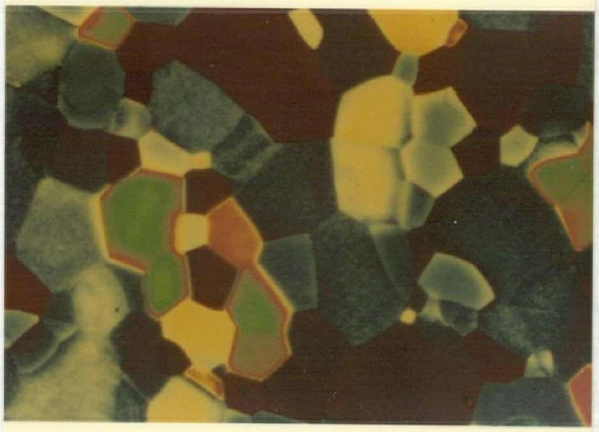

[e] 500°C, $10^{-5}$ mm, 1200 min. X200

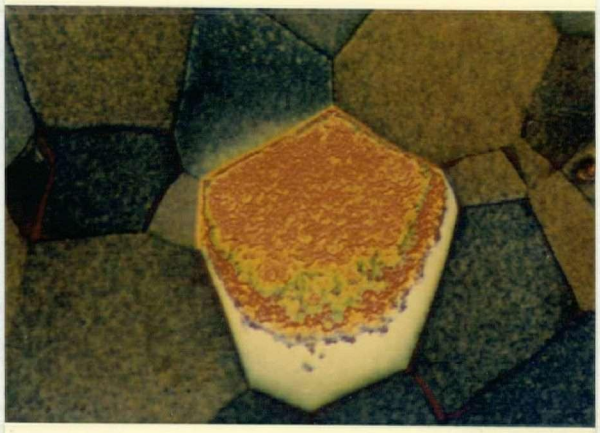

[f] 600°C, $5x10^{-5}$ mm, 1200 min. X800

Figure 23. Colour photomicrographs showing oxidation anisotropy

[a] 500°C, 760 mm, 100 min. X800

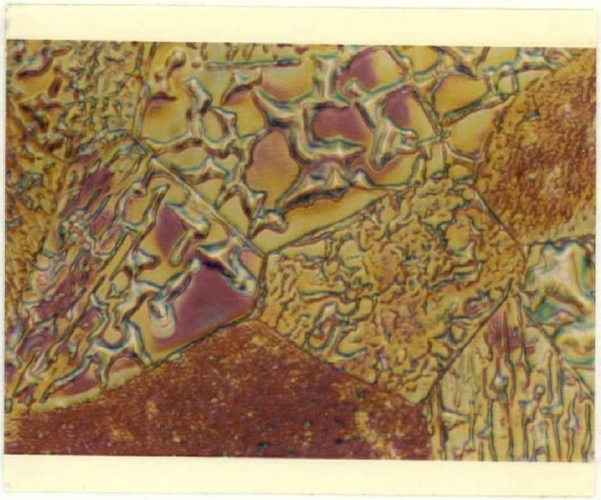

[b] same as [a], different area

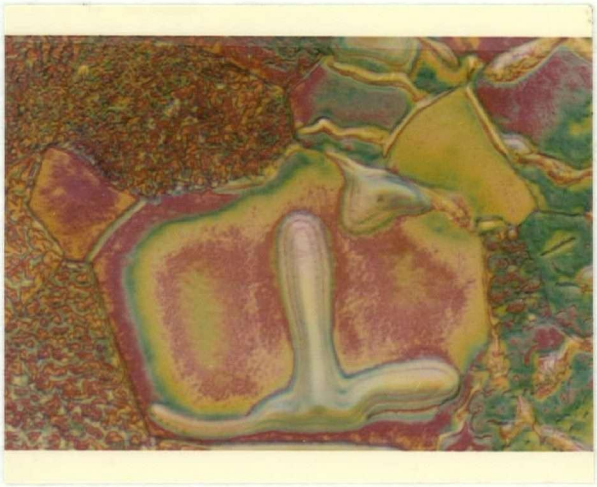

[c] same as [a], different area

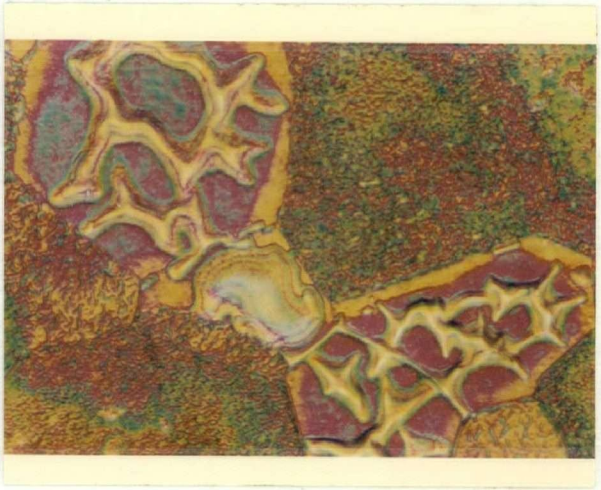

[d] same as [a], different area

[e] 500°C, 1 mm, 1200 min. X800

[f] same as [e], different area

Figure 24. Colour photomicrographs of oxide networks in various growth stages

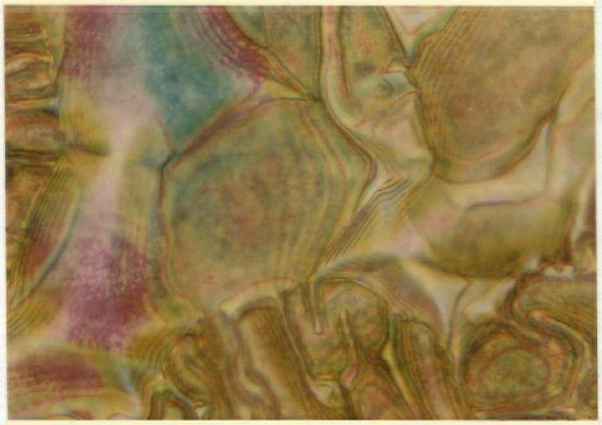

[a] $10^{-3}$ mm, 1200 min. X800

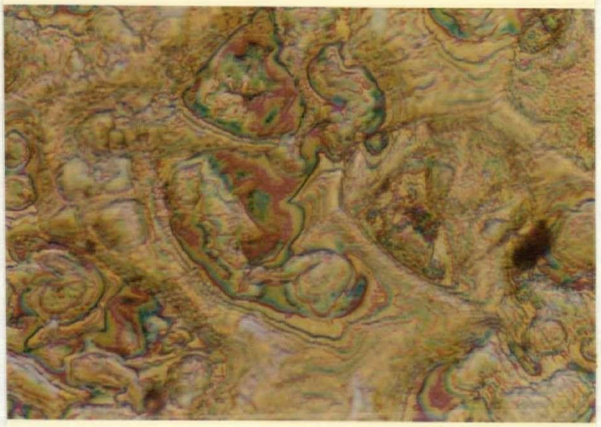

[b] $10^{-4}$ mm, 1200 min. X800

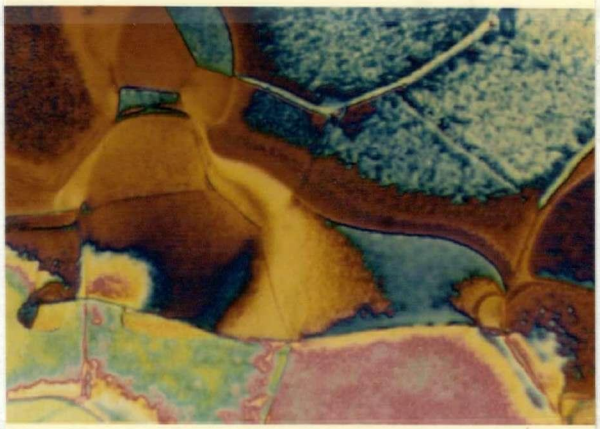

[c] $5 \times 10^{-5}$ mm, 1200 min. X800

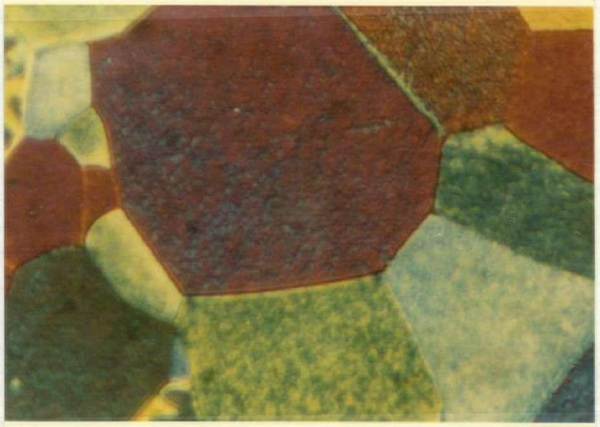

[d] $10^{-5}$ mm, 1200 min. X800

[e] $10^{-3}$ mm, 10 min. X800

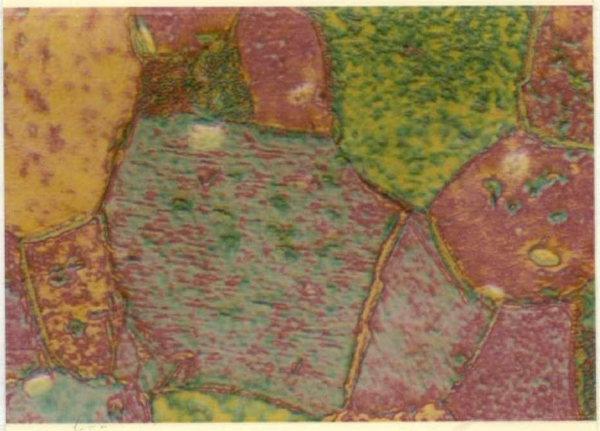

[f] $10^{-5}$ mm, 1200 min. X800
as-annealed

Figure 25. Oxide networks formed under low pressure at 500°C [in colour]

for electron microscope study will be presented from left to right beginning with specimen 99.

1. Specimen 99: 500°C, 760 mm, 5 minutes

Figure 26a shows a general view of the stripped oxide film as viewed with transmission electron microscopy. The overall structure replicates the underlying metal grain completely in the sense that metal grain boundaries are clearly delineated in the photograph. Hereafter the layer of oxide lying within these boundaries and covering one metal grain will be referred to as an oxide pseudograin, which usually consists of many small crystals arranged in a complex network of suppressed and accelerated growth regions as shown in Figure 26a. Note that comparison with the optical view of this same oxide attached to the metal (Figure 21a) reveals that the colour tones are reversed (i.e. black regions of thicker oxide in Figure 26a correspond to the white networks in Figure 21a). A magnified inclined view of the network region shows many small spikes (sometimes called whiskers, a special form thereof) protruding from the surface (Figure 26b). These spikes are thin oxide membranes of three general profiles: dagger-shaped, candle-flame shaped, and perfectly circular. The high magnification view of specimen 99 in Figure 26c shows predominant dagger shapes with the occasional circle as outlined in the box.

2. Specimen 93: 500°C, 10 mm, 10 minutes

Specimen 93, unlike all others, was stripped in a dilute HF solution which caused severe fragmentation of the film. However a general view of the oxide appears in Figure 27a. The optical view of this specimen (Figure 18b) reveals a pseudograin with no network. A similar pseudograin was discovered in the electron microscope (Figure 27b) and a diffraction pattern of its structure obtained (Figure 27d). A magnified view of the network is shown in Figure 27c with accompanying diffraction patterns from the light (Figure 27e)

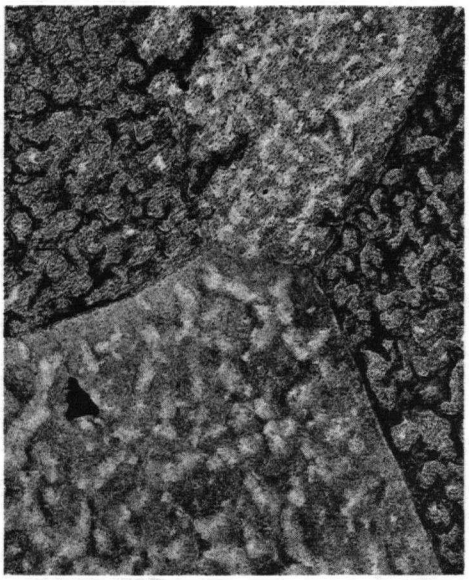

[a] 1100X

[b] 6800X

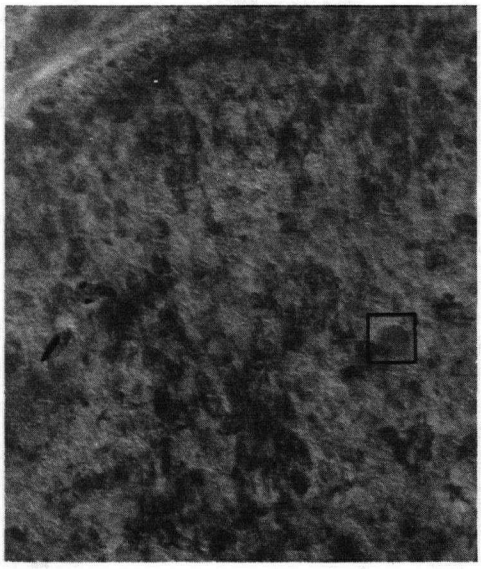

[c] 38,000X

Figure 26. Transmission electron micrographs of specimen 99: 500°, 760 mm, 5 minutes

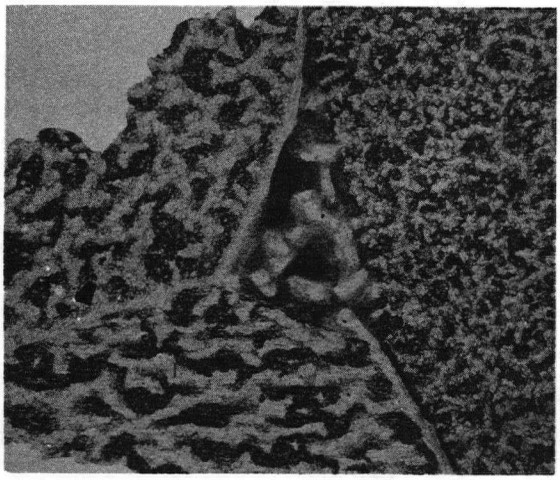

[a] X2000

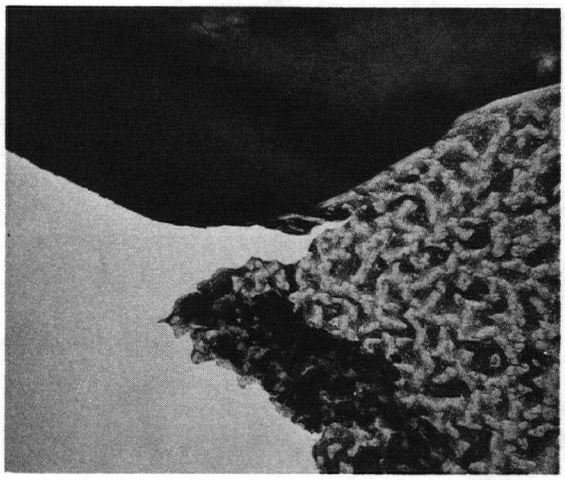

[b] X1500

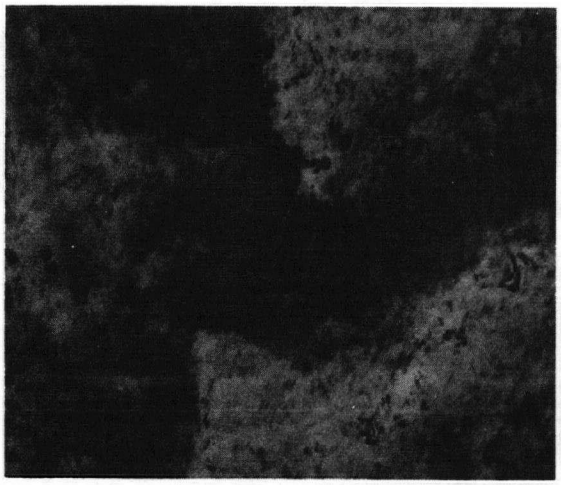

[c] X30,000

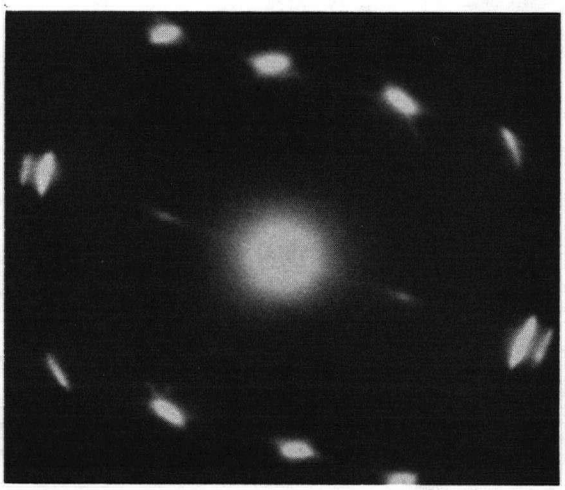

[d]

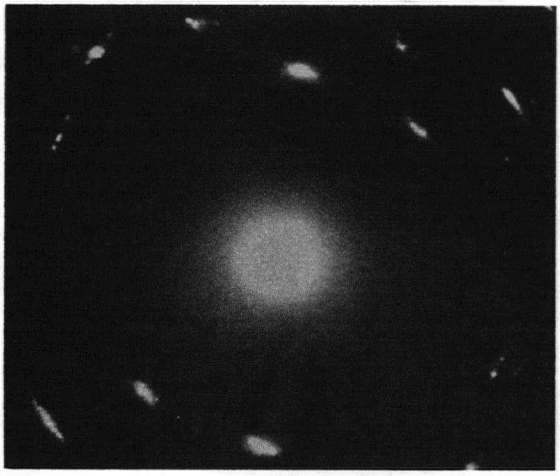

[e]

[f]

Figure 27. Specimen 93: 500°C, 10 mm, 10 minutes

and dark (Figure 27f) area as shown.

3. Specimen 95: 500°C, $10^{-3}$ mm, 10 minutes

As lower pressures are employed there is a tendency towards network suppression in the early stages as shown in Figure 28a. In those pseudograins where a network forms, the network may have a random pattern as in Figure 28a, or a preferred growth direction (Figure 28b). A magnified inclined view of a random network adjacent to a pseudograin without network is shown in Figure 28c. Note the accelerated whisker growth in the dense network. Figure 28d shows a magnified view of an oriented network together with its diffraction pattern. In addition to pseudograins with and without networks, some had a rather mottled appearance similar to the one at the left of Figure 28b. In these grains the light-coloured regions correspond to white areas in the optical view (Figure 18d). At higher magnification these light and dark regions were found to be areas of suppressed and accelerated whisker growth as shown in Figure 28e. Some of these areas contained clusters of peculiar plate-like whiskers with a thicker core similar to a candle flame as in Figure 28f.

4. Specimen 94: 500°C, 5 x $10^{-5}$ mm, 10 minutes

The stripped film from this specimen revealed only two types of pseudograin as shown in Figure 31d; those without a network (A) and those with a faint semblance of an oriented network (B). The network-free pseudograin gives a finely polycrystalline diffraction pattern (Figure 31e) in contrast to the single crystal pattern of a similar grain in 27b. The network diffraction pattern of grain B (Figure 31f) shows a high degree of preferred orientation with a weaker random background pattern.

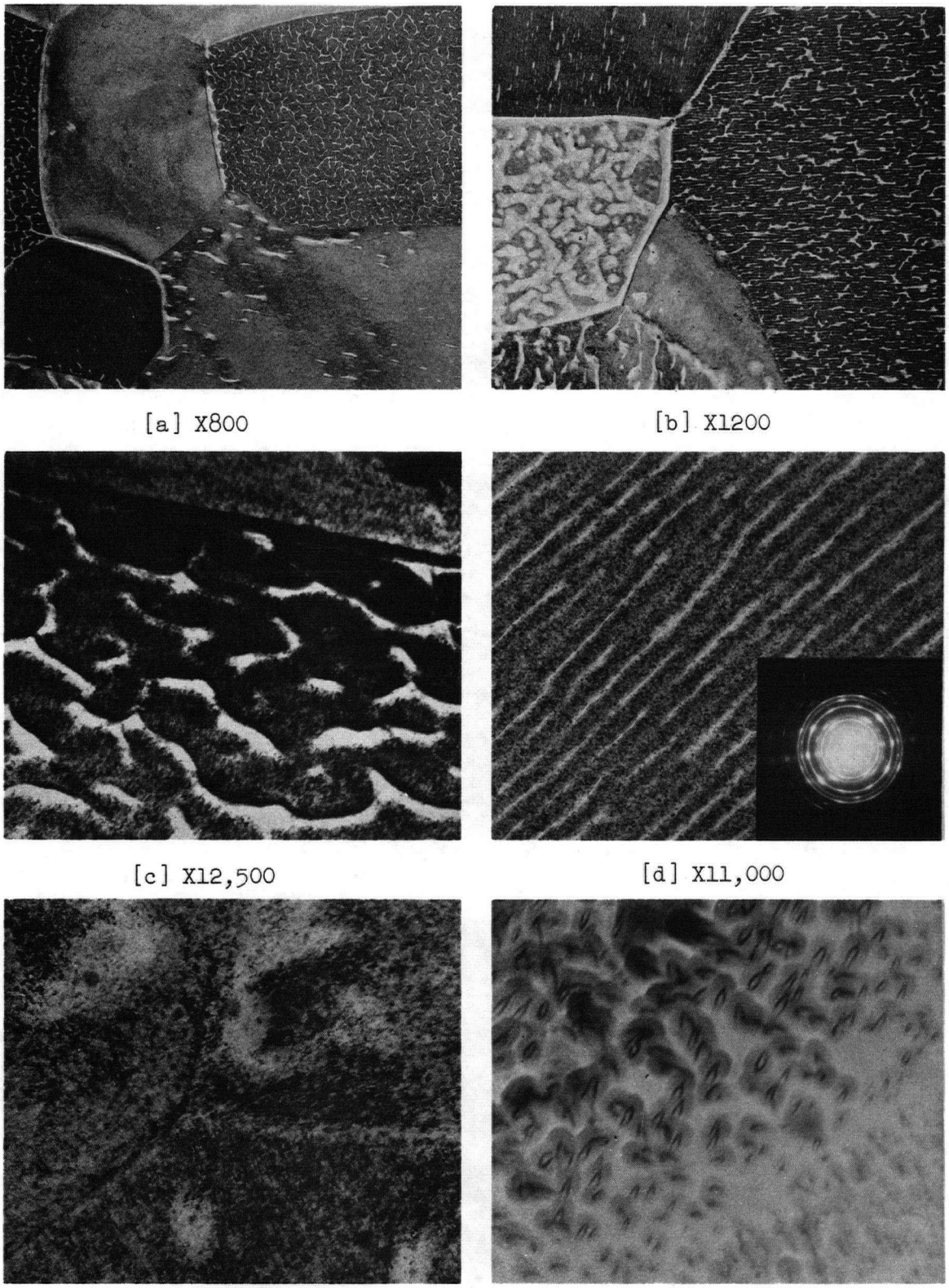

[a] X800 [b] X1200

[c] X12,500 [d] X11,000

[e] X15,000 [f] X58,000

Figure 28. Specimen 95: 500°C, $10^{-3}$ mm, 10 minutes

5. Specimen 123: 500°C, 760 mm, 100 minutes

After 100 minutes at this pressure the network has developed on all pseudograins in degrees ranging from very fine to coarse as shown in Figure 29a. A magnified view of the fine network reveals regions of suppressed and very pronounced whisker growth (Figure 29b). An unusually well-defined coarse network is shown in Figure 29c. Closer examination of the dark area reveals the existence of many small dark oxide crystals interspersed with whiskers of candle-flame shape (Figure 29d). Tangential views of curled film edges also revealed the presence of the circular whiskers (Figure 29e).

6. Specimen 125: 500°C, 760 mm, 100 minutes

This specimen was very heavily gold shadowed at an angle of 30° with the surface and then both shadow and oxide were simultaneously stripped from the metal. In some cases the oxide broke away from the gold shadow leaving a perfect replica of the surface as shown in Figure 30a. A magnified view of a similar region appears in Figure 30b. The exceptional degree of preferred orientation of the oxide crystals suggested by the surface morphology is confirmed by the diffraction pattern of the adjacent rutile (Figure 30c).

A shadowed pseudograin with well-defined coarse network is shown in Figure 30d. Figures 30e and 30f are magnified views of the interface between the dark and light area in 30d. The light area contains sparsely distributed oxide crystals of well-defined symmetry similar to that in 30a. An electron diffraction pattern of the light and dark area is shown in Figure 31a and 31b respectively. Whiskers were also observed in profusion on pseudograins with fine networks.

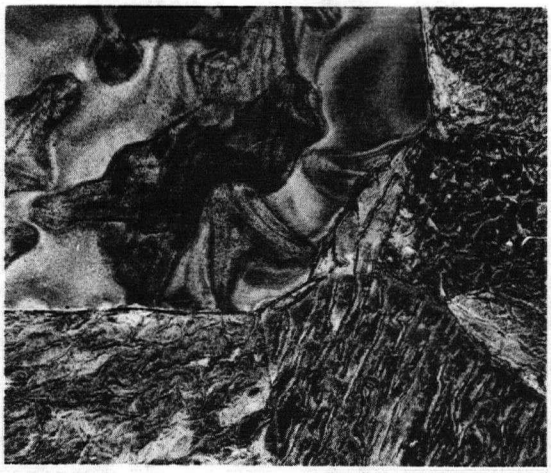

[a] X1000

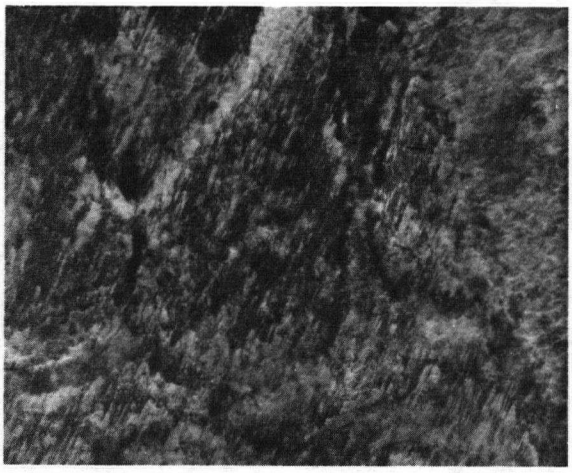

[b] X17,000

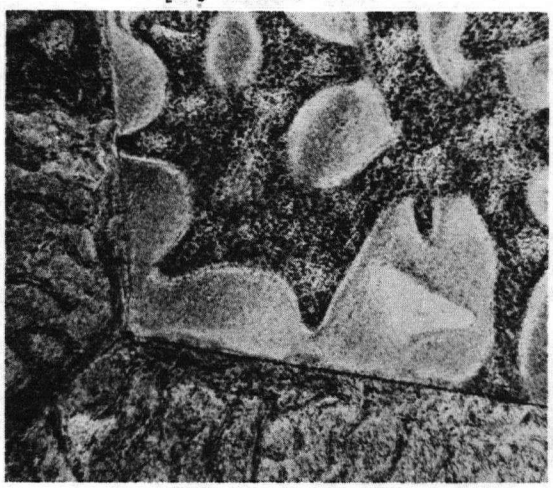

[c] X2000

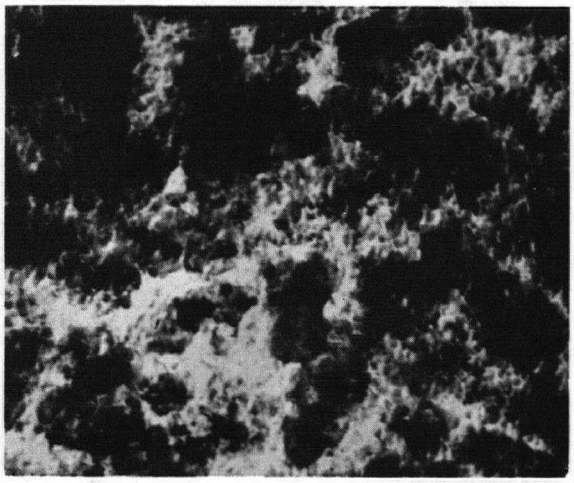

[d] X40,000

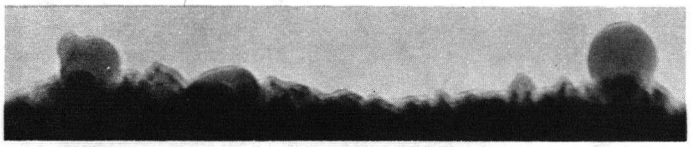

[e] X58,000

Figure 29. Specimen 123: 500°C, 760 mm, 100 minutes

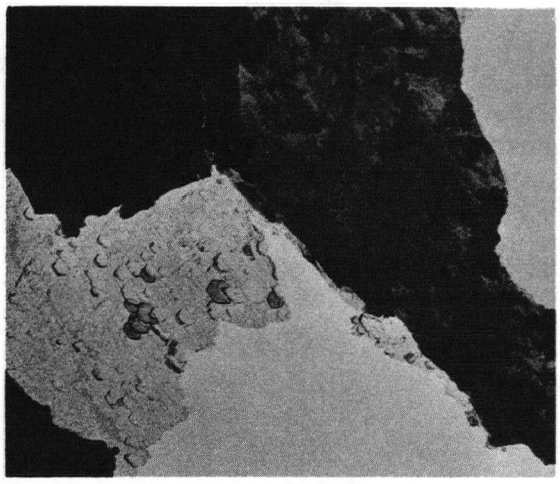

[a] X9000

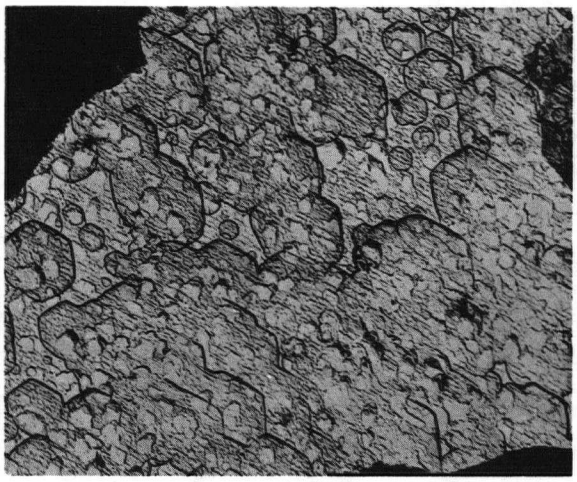

[b] X34,000

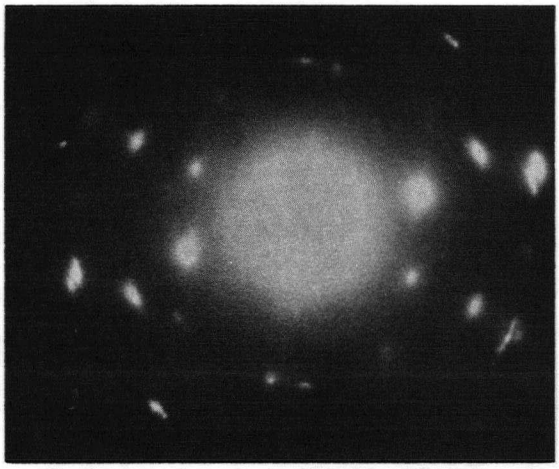

[c]

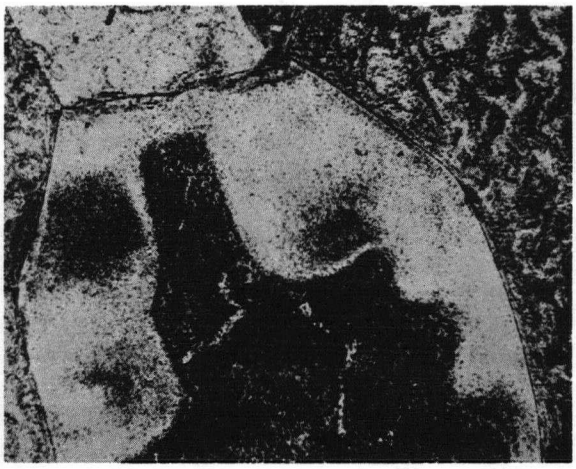

[d] X1600

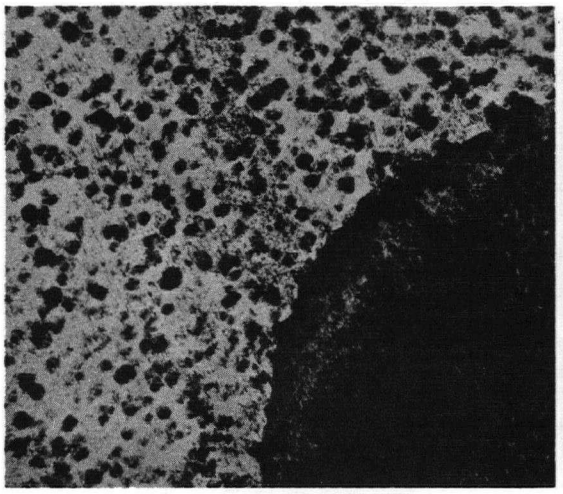

[e] X8000

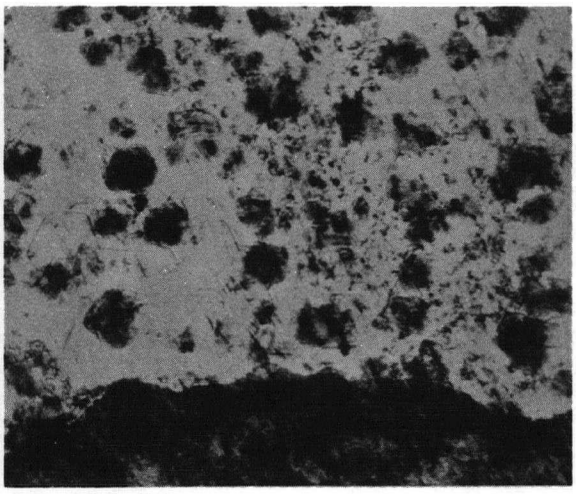

[f] X25,000

Figure 30. Specimen 125: 500°C, 760 mm, 100 minutes [gold-shadowed]

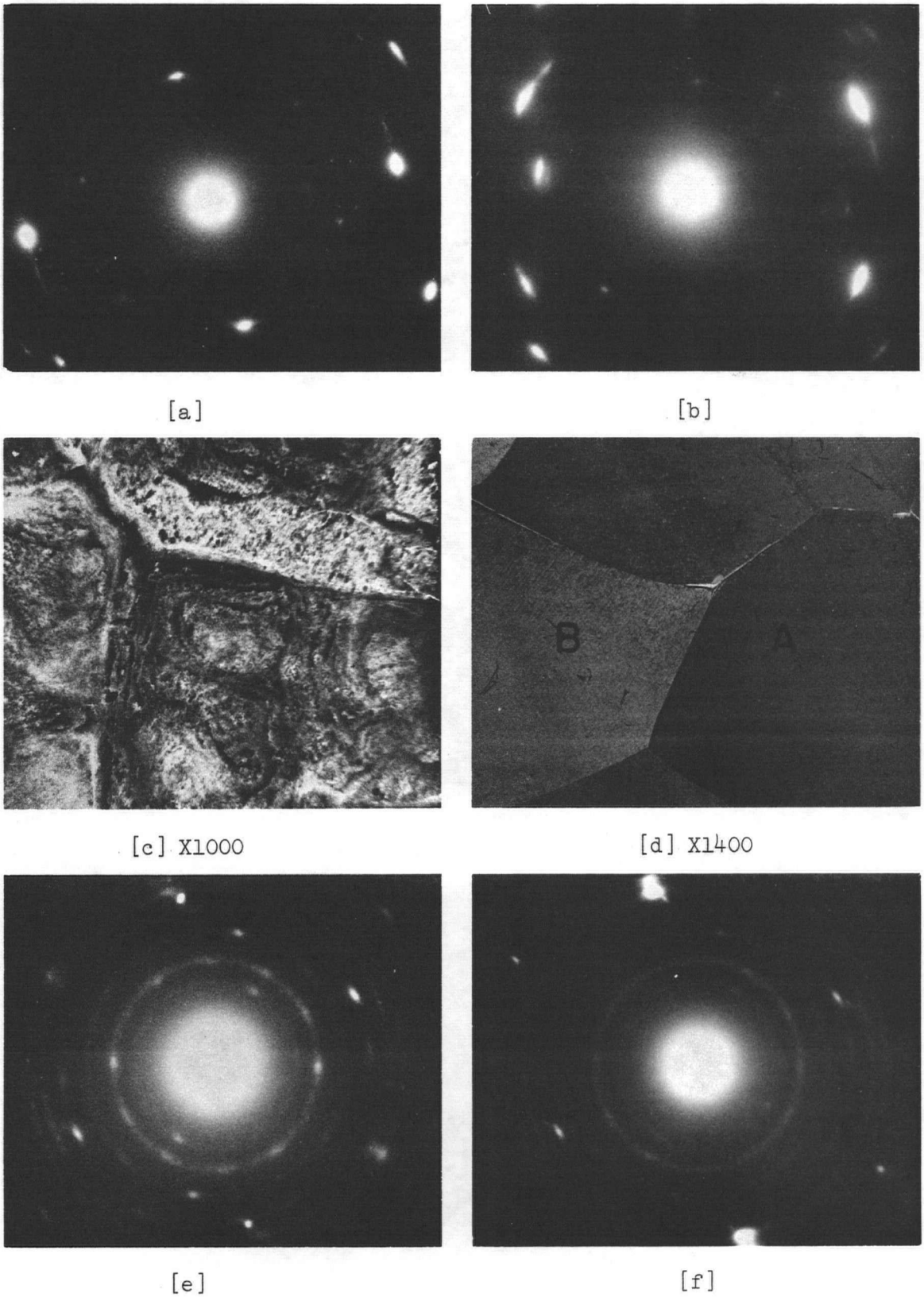


Figure 31. Miscellaneous electron micrographs of stripped films

7. Specimen 87: 500°C, 760 mm, 1200 minutes

The thickness of oxide film after 1200 minutes exceeded that required for complete absorption of 100 KV electrons in most cases. Consequently only a few thinner regions were penetrable and these lacked definition as shown in Figure 31c. However the presence of spikes and a thick oxide network is evident.

8. Specimen 114: 500°C, 10 mm, 1200 minutes

General views of the oxide are shown in Figures 32a and 32b. The unusual configuration in Figure 32c shows two oxide pseudograins containing small crystals aligned in rows similar to Figure 28d. However a coarse growth network has evolved out of the original structure in both cases. Closer inspection in Figure 32d indicates that some of these small aligned crystals have undergone rapid growth relative to others in the same row. The random structure of Figure 32e once again shows the profusion of whisker outcroppings.

9. Specimen 98: 500°C, $10^{-3}$ mm, 1200 minutes

The unusual feature of specimen 98, as seen in the optical view (Figure 19d) is the exceptionally coarse network on all grains. This network takes the form of great wandering regions of thick oxide as shown in Figure 33a. A magnified view of the interface between light and dark regions (Figure 33b) shows very pronounced whisker growth. The edge of curled films confirmed this observation with greater clarity (Figures 33c, 33d, and 33e).

10. Specimen 116: 500°C, $5 \times 10^{-5}$ mm, 1200 minutes

The general view of specimen 116 (Figure 33f) is similar to that of specimen 94. In other words, the growth morphology has not altered significantly from the original few minutes of oxidation. Small black spots

[a] X1000

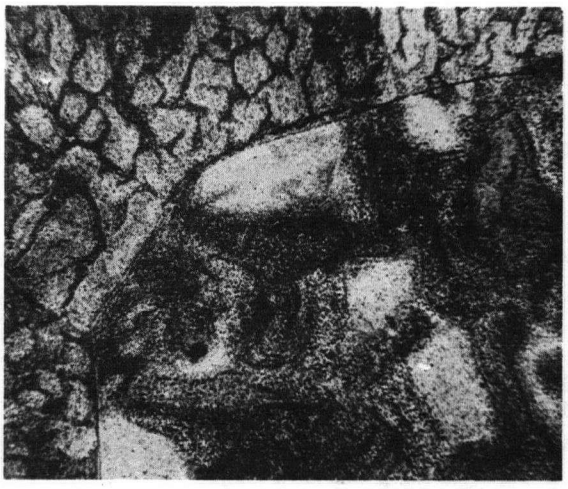

[b] X1000

[c] X1000

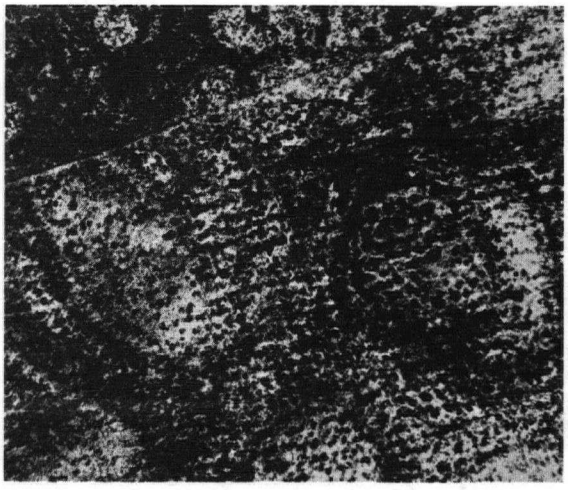

[d] X2400

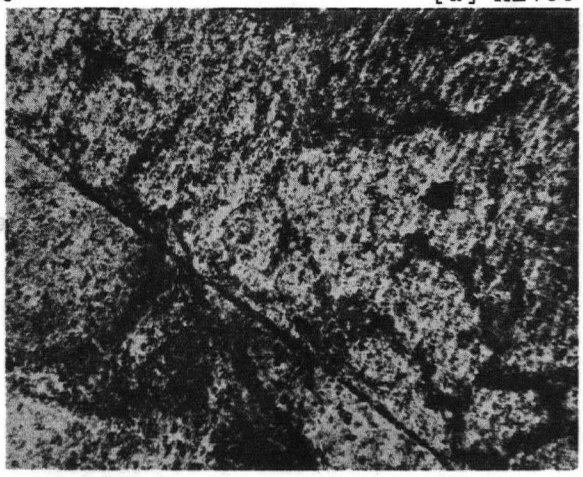

[e] X2800

Figure 32. Specimen 114: 500°C, 10 mm, 1200 minutes

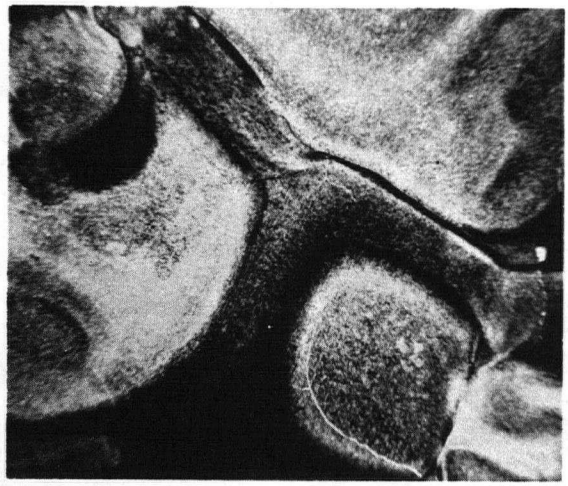

[a] X800

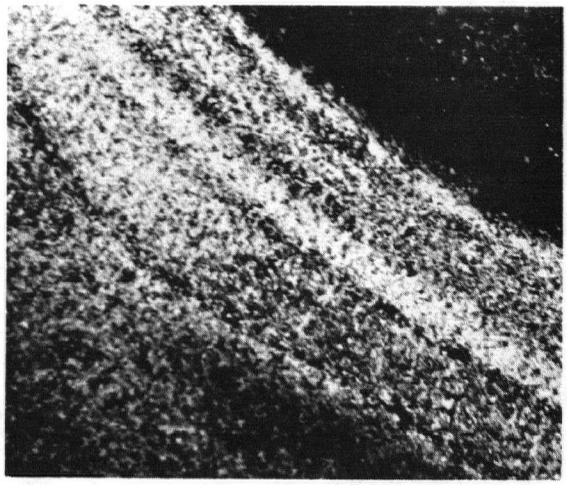

[b] X5500

[c] X71,000

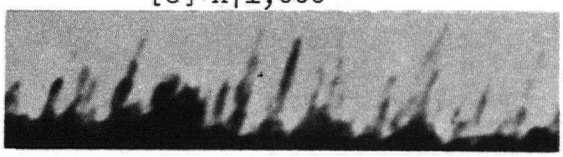

[d] X125,000

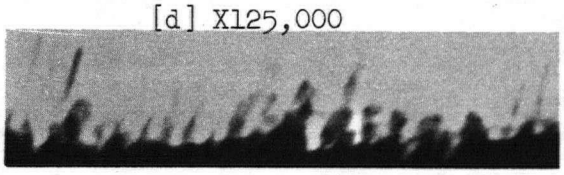

[e] X125,000

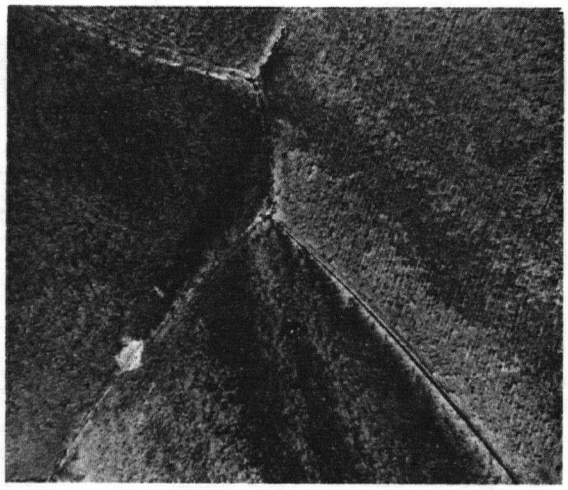

[f] X1000

[g] X5500

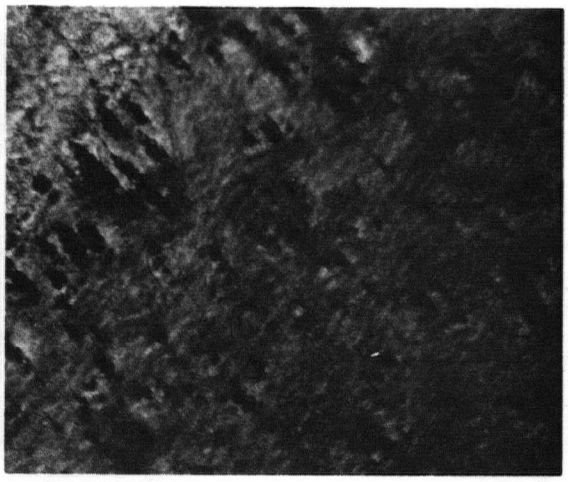

[h] X9400

Figure 33. Specimens 98 and 116

appear on all types of pseudograin. Higher magnification reveals that these spots are well-defined oxide spikes lying in rows of preferred orientation (Figure 33g) on some pseudograins and randomly dispersed (Figure 33h) on others.

11. Specimen 124: 400°C, 760 mm, 1700 minutes

The striped appearance of the pseudograins in the optical view (Figure 22b) becomes even more pronounced in the electron microscope (Figure 34a). The dark stripes are rows of accelerated whisker growth (Figure 34b) whereas the same stripes on the adjacent grain (medium shade) are rows of suppressed whisker growth delineated by regions of enhanced growth (Figure 34c). The mottled appearance of other pseudograins (Figure 34d) also arises from light areas of suppressed growth (Figure 34e) surrounded by rings of accelerated growth. An edge view of dagger-shaped and circular whiskers appears in Figure 34f.

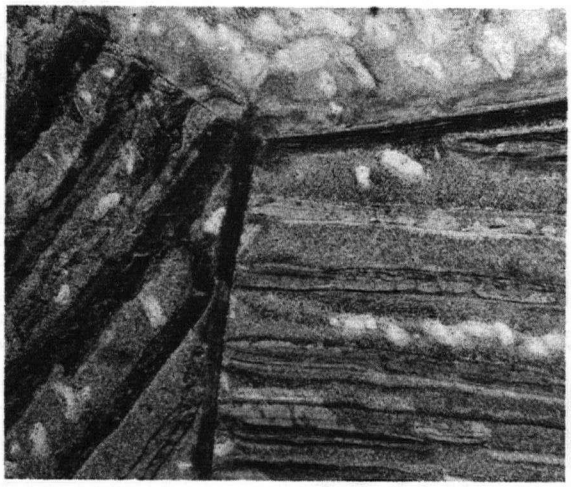

[a] X1400

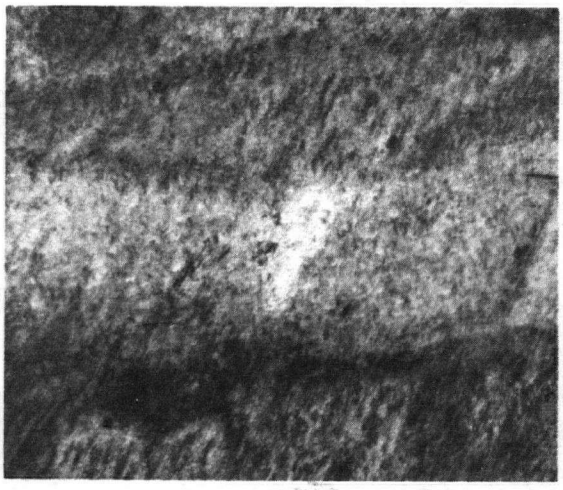

[b] X12,000

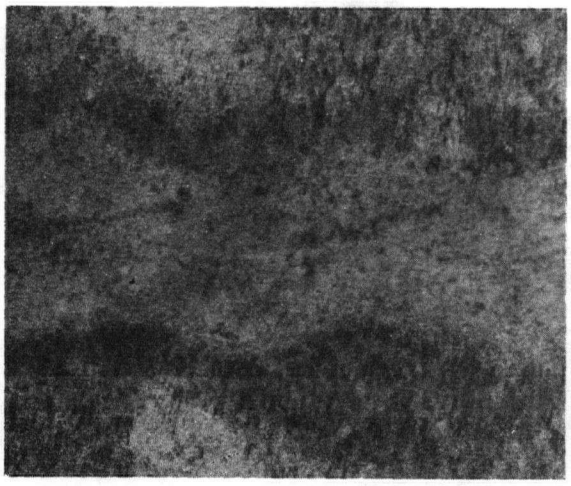

[c] X17,000

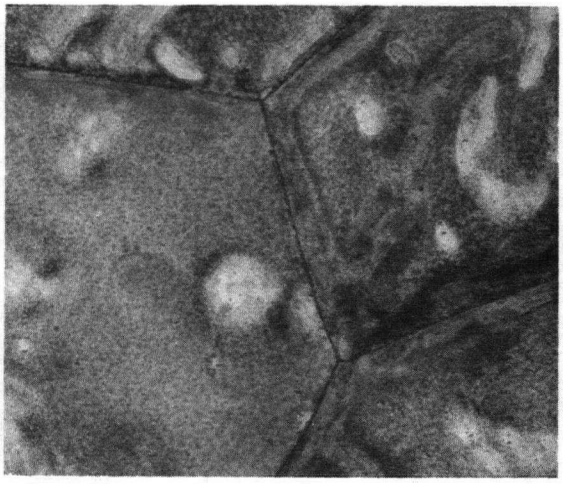

[d] X2000

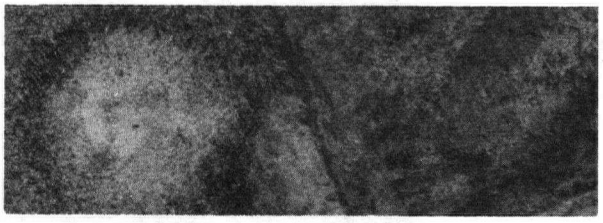

[e] X6000

[f] X 250,000

Figure 34. Specimen 124: 400°C, 760 mm, 1700 minutes

# IV. DISCUSSION

## A. General

The experimental evidence indicates that the oxidation of titanium is even more complicated than originally thought by previous investigators. In spite of this complexity, definite trends and patterns emerge from the kinetic data which are obviously related to the irregular growth morphology. The rate curves obtained with improved and sophisticated techniques using a recording electrobalance eliminate the necessity of having to draw a line of best fit through a series of scattered points. This latter step has contributed to the multitude of different rate laws observed between 400 and 600°C by other authors.

Another factor causing confusion in this region is the number of rate transitions occurring at various time intervals under a fixed temperature and pressure. As can be seen from the kinetic data of this work, the log-log plots rarely show a region of prolonged linearity that could be associated with some simple rate law currently applicable to other oxidation systems (parabolic, linear, etc). And yet the complex shape of the rate curve obtained under a specific set of conditions is completely reproducible. One must conclude, under these circumstances, that the kinetic data associated with these periods of transition cannot be explained by conventional kinetic theories without taking the complex growth morphology into account. This probably explains the failure of other authors to attach a simple label to titanium oxidation kinetics under these conditions.

For those curves exhibiting some linearity, data up to 10,000 minutes would be desirable to confirm the observations but this becomes impractical because of prolonged equipment immobilization. Hence one is forced to assume a particular rate law applies to a short linear region

of the curve when in fact this may be only a period of transition.

The shifting preferential oxide-growth areas observed in some instances, both on a microscopic (whiskers) and macroscopic (networks) scale, discount any explanation of the weight gain data in terms of the transport theories based upon constant area and uniform thickness assumptions.

Unfortunately geometry-insensitive techniques such as weight-gain or gas absorption do not provide information regarding the distribution of oxygen consumed and hence local variations, although significant, are not detected. The exceptional oxidation anisotropy and network formation illustrated in the colour photographs (Figure 23 to 25) also confirms that interference colour and polarized light methods only provide very crude approximations of oxide thickness unless performed on single crystals, and even these would not eliminate network effects. In fact the general concept of oxide thickness, as related to current theories, becomes meaningless in periods of network growth and development unless one considers the thickness of individual oxide crystallites which usually vary from a hundred to a thousand Angstroms in diameter.

Oxidation anisotropy has been observed on most other polycrystalline metals but fortunately the film has been reasonably uniform in thickness across an oxide pseudograin. In the absence of network formation, oxidation anisotropy does not influence kinetic measurements because the weight gain of a single pseudograin can still be represented by an individual relation of the type

$$\Delta W_i = A_i x_i$$

$$\text{where} \quad x_i = k_i t^n$$

$A_i$ = area of a pseudograin
$x_i$ = average thickness of a pseudograin
$k_i$ = rate constant for a particular orientation of pseudograin
$n$ = constant

The measured weight gain is then a sum of several pseudograins in various states of oxide growth, as described by the equation, but this still yields a meaningful relationship with time because

$$\Delta W = \Sigma \Delta W_i = \Sigma A_i k_i t^n$$

$$= Kt^n$$

providing $A_i$ and $k_i$ do not vary with time. However during network formation a variation of this type occurs and the relation is no longer valid.

B. Kinetics

Figure 11 confirms the suspicion that significant oxidation occurs during the high vacuum warmup if the specimen is heated within the furnace. For example, after ten minutes at 500°C, 1 mm of $O_2$, the heated specimen showed a weight gain of 3 $\mu g/cm^2$ while the remote-lowered specimen showed a weight gain of 13 $\mu g/cm^2$. This discrepancy of 10 $\mu g$ alters the shape of the kinetic curve significantly up to approximately 100 minutes, whereupon both procedures give the same shape of curve. Note that the sudden acceleration of oxidation at 100 minutes on the curves using procedure A may have gone unobserved had procedure B been employed.

The oxidation rates measured by Hurlen[1] are in surprisingly good agreement with the results of this work when procedure B is used (Figure 12). In fact the agreement is probably better than any other two independent studies of oxidation in this region. The chemically polished specimens are closer to Hurlen's results than the as-annealed specimen, which is unexpected. However the shorter annealing time ($\frac{1}{2}$ hour) and lower temperature (800°C) used by Hurlen may have had less effect on subsequent oxidation and this would

bring his results in line with the polished specimens of this work. Of course other minor variations in metal purity, technique, etc. could also be contributing to the discrepancy.

The effect of different preparations in Figure 13 does not grossly alter the shape of the curve but shifts the curve upward to greater oxidation. The mechanically polished specimens always exhibited a greater weight gain than the chemically polished specimens, probably as a result of increased surface roughness over the same apparent area. The as-annealed specimen (97) oxidized much more slowly than all others at 500°C, 10 mm, which is in agreement with the behaviour of specimen 118 at 500°C, 1 mm (Figure 12).

The existence of inflections in the 500°C rate curves between 10 and 1000 minutes was first observed by Hurlen and confirmed in this work. The two cold-worked specimens and the 550°C annealed specimen however fail to show the inflection observed at approximately 20 minutes in the three 850°C annealed specimens (Figure 13) with different surface finishes. This inflection, as will later be shown, seems to be related to the rapid formation of coarse oxide networks. The high temperature (850°C) anneal appears to delay this growth process. The suppressed network formation on all as-annealed specimens oxidized under identical conditions to chemically polished specimens suggests that surface oxygen enrichment during annealing may retard network formation. In this regard note that the inflection in the curve of specimen 118 (Figure 12) occurs at approximately 100 minutes whereas the other curves for polished specimens show inflections at 20 to 30 minutes. Rapid network growth on a cold-worked surface probably occurs in the first few minutes so that no inflection is observed.

With the exception of Hurlen, previous authors have claimed no observed pressure effects on oxidation below 800°C. This work shows a

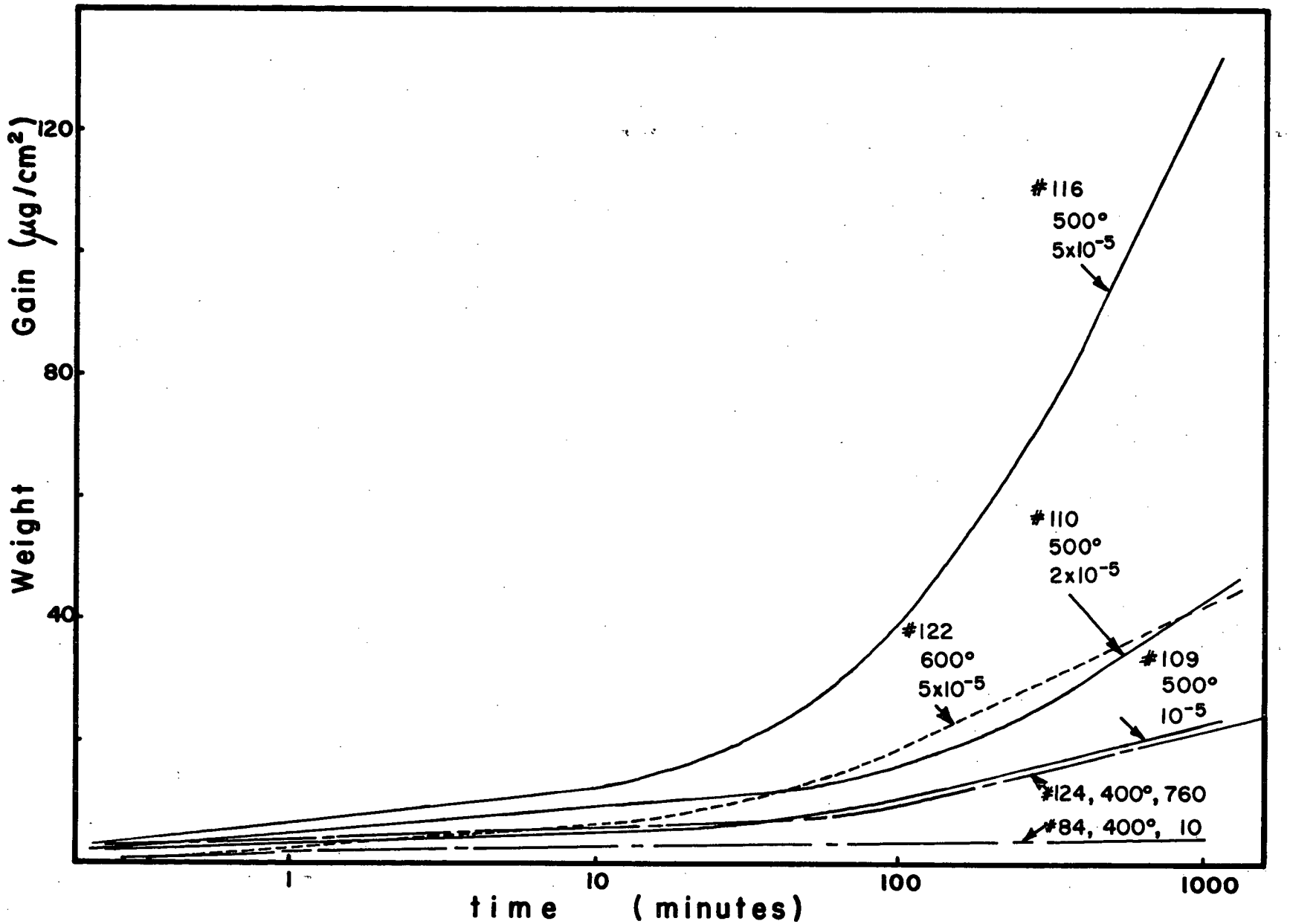


Figure 35. Semi-log plots of kinetic data

reproducible pressure effect at all temperatures. The effect is usually subtle in the pressure region from 10 to 760 mm and becomes pronounced at pressures less than 10 mm. Although previous work has been confined to studies above $10^{-2}$ mm, the present results indicate that significant oxidation takes place down to $10^{-5}$ mm and probably lower.

The pressure relations at 500°C are most complex. Hurlen had difficulty deciding whether his results could best be represented by a number of direct logarithmic equations or by a cubic plot at this temperature. This work shows that both relations are applicable, depending upon the pressure of oxidation. At very low pressures ($\leq 5 \times 10^{-5}$ mm) the rate curves can be represented by two regions of logarithmic growth as shown in Figure 35. As the pressure is increased to $10^{-4}$ mm, oxide growth follows a cubic relation after a few minutes and remains in cubic growth up to 1200 minutes. Oxidation still follows a cubic relation at pressures from one to 760 mm but in all cases the cubic period is preceded by an incubation period as shown in Figure 14. This incubation period is one of very rapid growth in the first minute followed by almost complete cessation for the next twenty (760 mm, 10 mm) to sixty (1 mm) minutes. In some cases the rate curve associated with this incubation period approximates a logarithmic relation whereas in others there is no simple approximation.

After this pause, oxidation suddenly increases, in accord with the observations of Hurlen, and eventually a cubic relation is established (after 300 minutes at 760 mm, 10 mm, and after 2500 minutes at 1 mm). It can be seen from Figure 14 that the kinetic behaviour of titanium oxidation at 760 mm and 10 mm is almost identical whereas the 1 mm curve shows a longer incubation period. The curve for $10^{-5}$ mm (Figure 15) is quite similar to the curve for 760 mm up to 1200 minutes, which is the extent of Hurlen's experiments. One can therefore appreciate his interpretation of the 760 mm

curve in terms of the same double logarithmic law that he observed at lower pressures. However the 4000 minute experiment of this work (Figure 14) confirms the establishment of a cubic relation from 400 to 4000 minutes.

Another classic example of the pitfalls of interpreting kinetic data is illustrated in Figure 14, curve 112 and 113. On the basis of curve 112 one would be tempted to interpret the establishment of a parabolic rate between 600 and 1000 minutes because of the slope equal to one half. However a repeated experiment lasting 2500 minutes reveals this quasi-parabolic region to be one of transition to a probable cubic relation after 2500 minutes as shown.

The effect of increasing temperature on trends in the rate relations is shown in Table IV. At the lowest pressure examined at 400°C, the rate followed a single logarithmic relation after 20,000 minutes. This degenerated into a double logarithmic relation at 760 mm. A transition to a cubic relation, which may or may not be preceded by an incubation period, occurs with increasing temperature. At 600°C the first appearance of a parabolic relation after 1000 minutes at 760 mm is observed. The time to first appearance of this parabolic relation decreases to 30 minutes at 700°, 760 mm and is less than a minute at 800°C, 760 mm. After 200 to 300 minutes at 800°C the observed rate becomes linear. Of course the arbitrary assignment of a simple rate relation to those regions of network growth is only a crude approximation.

Most authors of previous titanium oxidation papers have attempted to treat their rate data in terms of an idealized oxide film, neglecting possible morphological effects. This technique can also be applied to the kinetic results of this work, as shown in Appendix D and E, but the treatment is inadequate in view of the time transitions

TABLE IV.

Table of Rate Transitions

| | 400 | 500 | 600 | 700 | 800°C |
|---|---|---|---|---|---|
| parabolic linear | | | | | 760 mm<br>10 mm |
| cubic parabolic | | | 760 mm | 760 mm<br>10 mm | |
| cubic | | 760 mm<br>$10^{-4}$ mm | 10 mm<br>$10^{-3}$ mm | | |
| dual logarithmic | 760mm | $5 \times 10^{-5}$mm<br>$10^{-5}$ mm | $10^{-4}$ mm<br>$10^{-5}$ mm | | |
| single logarithmic | 10 mm | | | | |

associated with the morphology. As can be seen from the activation energy calculation in Appendix D, the approximations involved are questionable, although they provide a value in agreement with other authors. Similarly, the pressure dependence relations calculated in Appendix E and summarized in Figure 39 could be interpreted as follows: first order dependence between $10^{-5}$ and $10^{-4}$ mm; pressure-independent oxidation between $10^{-4}$ and 760 mm as suggested by Kubaschewski and Hopkins[7]. But here again the extremely crude approximations and large scatter of points in Figure 39 makes such a conclusion doubtful in view of the related morphological effects.

## C. Structures

### 1. Networks

At temperatures from 400 to 600°C oxidation proceeds by preferential growth patterns which seem to be related to the underlying metal. However since it was not possible to prepare transmission thin-film oxide specimens with small amounts of metal attached for epitaxial studies this relationship could not be positively established.

The growth morphology is most complicated at 500°C. Oxide growth occurs in two stages: primary and secondary network formation. The primary network, consisting of areas of suppressed and accelerated oxide growth within each pseudograin as shown in Figure 28a, can be considered as a network of thick oxide surrounding isolated areas of thinner oxide or vice-versa, depending on the pseudograin.

Primary networks may be either randomly distributed (Figure 28a) or oriented in a single direction (Figure 28b) on an oxide pseudograin. Each pseudograin is in a different state of network development at any fixed time and the growth and shape of the network is a function of pressure and temperature as well as time. As a result of the optical views shown in

Figure 18d and 25e it was initially thought that the primary network formed by nucleation on pseudograins without networks. However stripped films examined in the electron microscope revealed that the apparent white nuclei were in fact regions of suppressed rather than accelerated oxide growth as shown in Figures 28b and 28e. Not one of the multitude of electron microscope samples stripped from short-time oxidation specimens indicated any dark nuclei comparable to the white patches in Figure 18d. In fact no dark nuclei were observed on any of the pseudograins that could be interpreted as the beginning of a network overgrowth similar to that observed by Douglass. The first appearance of primary network formation is shown by the fine structure of Figure 28a (random case) and Figure 31d (oriented case). At higher pressures (760 mm, 5 minutes) a coarser structure is formed as in Figure 26a. This micrograph also shows four pseudograins in various stages of network growth. Note that the primary network develops uniformly across an entire pseudograin and seems to undergo very little change in lateral configuration with time. The network only grows in the direction perpendicular to the metal surface and its growth merely increases the contrast between thin and thick areas.

Pseudograins that are slow to develop networks, such as those in Figure 18b, seem to develop a very coarse one eventually as shown in Figure 29c. These coarse random secondary networks may form not only from a network-free grain, but also from a fine oriented primary network as shown in Figure 32c and 32d or a fine random primary network although the latter is not obvious from the electron micrographs and must be deduced, i.e. none of the pseudograins examined after 1200 minutes at $10^{-3}$ mm (Figure 19d and 33a) displayed evidence of a random network as fine as those observed after ten minutes oxidation (Figure 28a). All were exceptionally coarse and must represent secondary networks.

As in the case of primary network formation, the secondary networks do not appear to form by nucleation and lateral growth. They form rather as a result of preferential growth of small crystallites within a particular pseudograin.

Random primary network formation does not seem to be related to underlying metal structure although some relation between metal sub-grain structure and network configuration may exist. Oriented primary network formation does seem to be related to metal substrate orientation as shown in Figure 28b.

The formation of both types of primary network is suppressed at lower oxygen pressures (Figure 18) although a comparable weight gain (i.e. average oxide thickness) is observed. The formation of secondary networks is completely suppressed even after 1200 minutes at $10^{-5}$ mm as shown in Figure 22c.

The complete absorption of 100KV electrons by the stripped film in Figure 31c, which, from weight gain conversion, averages 4800 to 5400 Angstroms in thickness, agrees with Douglass's observation of complete absorption by 4000 Angstrom films.

2. Crystallites

A review of all of the high magnification electron micrographs indicates the presence of many small dark spots within each pseudograin. It is the increased density and size of these spots that give rise to the overall network pattern observed at lower magnifications. As both Markali[9] and Douglass[44] point out, the difference in contrast between these dark areas and the light background can arise from

(a) thickness difference alone, or

(b) diffraction contrast resulting from crystallites in favorable

orientations for Bragg reflections. The work of both authors indicates that a large contribution from (b) is causing much of the contrast.

Although Douglass makes no mention of whisker growth (possibly because his experiments were conducted in air) Markali observed whisker growth on the darker "islands" of oxide similar to those in Figure 28c. The replica work of Hurlen[1] also shows regions of whisker growth which probably correspond to networks observed in the transmission studies.

A most important observation arises from previous investigations and the results of this work as summarized in Table V. The average oxide crystallite size at 500°C under all conditions varies from 50 to 5000 Angstroms. An average oxide pseudograin would contain between 10,000 and 100 million crystallites. In terms of density considerations, the crystallites average between $4 \times 10^8$ and $4 \times 10^{12}$ per square centimeter, which is rather high to be related to the dislocation density of the fully annealed underlying metal.

The orientation distribution of these crystallites in any one pseudograin varies from random (with slight preferred orientation) as in Figure 28d and 31e to highly preferred arrangements as indicated by the diffraction patterns in Figures 27a, 30c, and 31a,b, and f. The random configurations must give rise to an enormous high-angle grain-boundary region, comprising between one and twenty percent of the total area undergoing oxidation. The preferred configurations can be considered as single crystal oxide with large volumes of subgrain boundary, or a large number of individual crystallites connected by low angle grain boundaries. However if these crystallites have similar orientations as indicated by the diffraction pattern of Figure 30c, then the difference in contrast of oxide crystallites in 30a must arise from thickness differences, which is confirmed by

TABLE V.

Table of Crystallite Sizes

(as measured from transmission electron micrographs)

| Foreign particles (Figure 8) ------ 250 to 1000 Å | | | | | | |
|---|---|---|---|---|---|---|
| Temp. °C | Time min. | Press. mm | Circular Whiskers dia. Å | Dagger whiskers Width Å | Dagger whiskers Height Å | Crystallite size Å |
| 500 | 5 | 760 | 1000 | 100-250 | to 1000 | |
| | 10 | 10 | 500 | 100-300 | 500 | 100- 700 |
| | 10 | $10^{-3}$ | 700 | 100-300 | 800 | 100- 800 |
| | 10 | $5x10^{-5}$ | | | | 50- 300 |
| | 100 | 760 | 1500 | 100-400 | 3000 | 250-2000 |
| | 1200 | 760 | | | | to 10000 |
| | 1200 | 10 | | | | 500-5000 |
| | 1200 | $10^{-3}$ | 1200 | 80-300 | 1000 | 200-3000 |
| | 1200 | $5x10^{-5}$ | | to400 | 3000 | 200-3000 |
| 400 | 1700 | 760 | 800 | 100-600 | 2000 | 100- 600 |

the shadowed replica pattern of Figures 30a and 30b. It is difficult to understand how such well-formed growth facets can exist on the outer surface of an oxide which presumably grows at the inner (metal-oxide) surface.

It was originally thought that perhaps the foreign particles observed in the annealed metal (Figure 8) could be associated with crystallites of accelerated growth in view of their comparable size (250 to 1000 Angstroms). However stripped films from cold-worked oxidation specimens, which contained no foreign particles, also showed crystallites of accelerated growth comparable in size and distribution to the annealed specimens.

Areas of accelerated crystallite growth also seem to be areas of profuse whisker growth (see Figure 28c). The existence of the circular type (Figure 33c) was rare in most cases compared to the dagger-shaped whiskers. Although no attempt was made to establish their growth direction in this study, previous work[9] indicates preferential whisker growth along the tetragonal axis. The results of Table V show that whiskers increase only in height, not width, with time.

Perhaps the most significant relationship arising from diffraction studies is the existence of a slight difference in crystallite orientation across a network interface as shown in Figures 27e, 27f, 31a, and 31b. This difference may give rise to preferred growth directions and favorable epitaxial relations with the metal substrate for rapid growth.

All of the electron diffraction patterns indexed in this study revealed the exclusive presence of the rutile modification of titanium dioxide, which is in agreement with other studies.

D. Relation Between Kinetics and Growth Morphology

The most pronounced cubic growth relations (curve 90, 98, and 107,

Figure 15, and curve 82, Figure 16) are associated with the most coarse secondary networks in which whole pseudograins become mounds of accelerated growth (Figures 19d, 19e, and 20b). Less coarse networks, such as Figures 19a,b, and c, form only after an incubation period but eventually exhibit a cubic growth relationship. At the moment the network disappears (Figure 20a) a parabolic growth pattern is observed and the structure remains similar to Figure 21f which represents 4000 minutes at 600°C, 760 mm.

The cubic-parabolic transition at 760 mm, as shown in Figure 17, occurs at 1000 minutes, 30 minutes, and one minute at 600, 700, and 800°C respectively. If these times are plotted versus the reciprocal of temperature as in Figure 36, some linear relation may exist but more points are needed to establish this effect. Although this suggests that the onset of the parabolic region is thermally activated, it is difficult to interpret the significance of the activation energy in terms of the mechanism involved.

The relation between the double logarithmic kinetic data and the growth morphology is less obvious. The only apparent change in structure at the very low pressures is the formation of whiskers after a time interval in excess of ten minutes. Normally whisker growth does not affect the kinetic data in other systems because the weight gain from whisker formation is negligible with respect to the oxide film formation. However on a thin film approximately 300 to 400 Angstroms thick, the dense growth of whiskers, similar to those in Figures 33g and 33h, to a height of 2000 Angstroms may superimpose an additional weight gain on the primary logarithmic relation. The profuse whisker growth at 400°C, 760 mm (Figure 34) which is also associated with a double logarithmic relation, is further evidence in support of this observation.

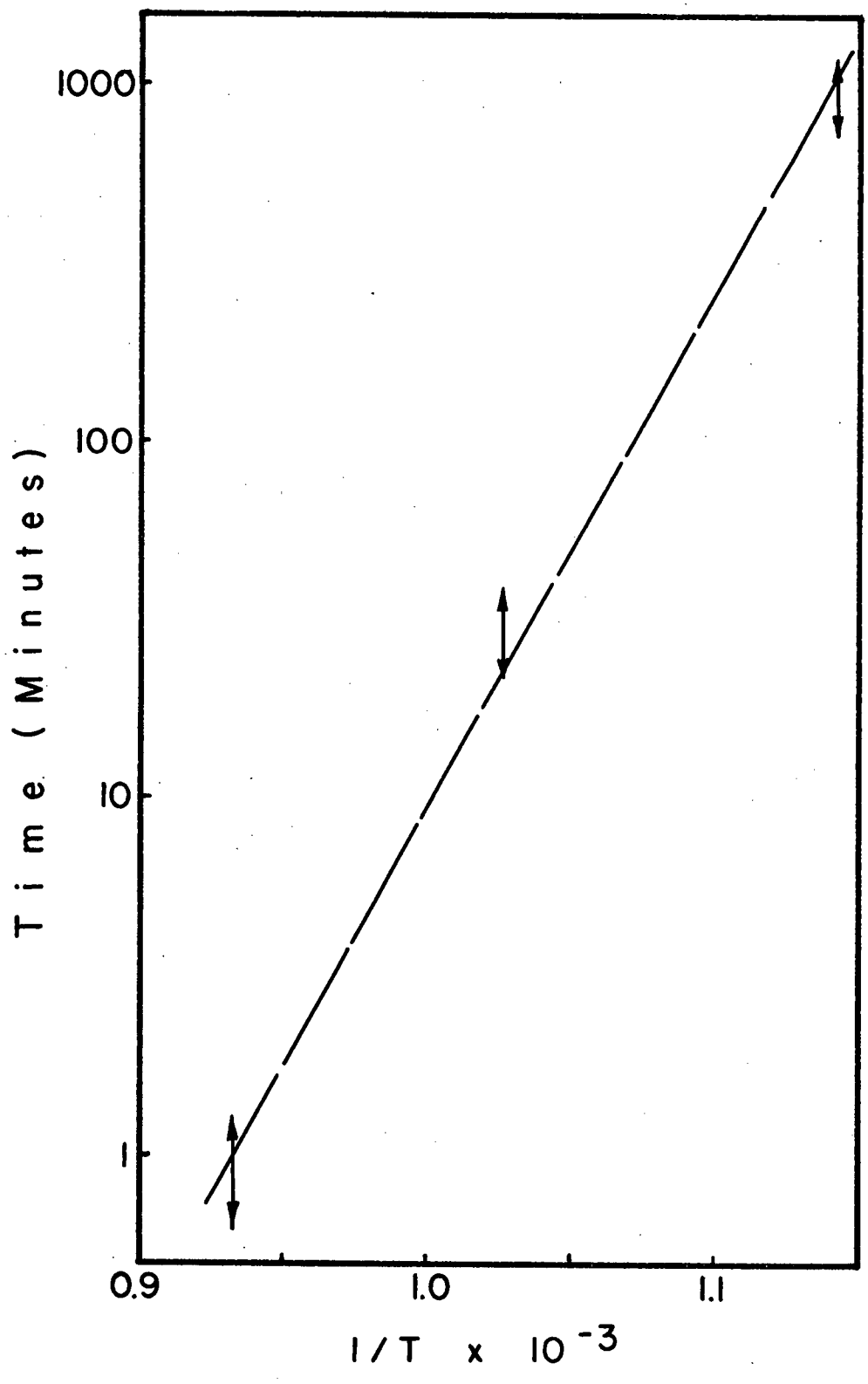


Figure 36. Plot of reciprocal temperature vs. time to onset of parabolic rate

E. Mechanisms

Explanations of the complicated kinetics of titanium oxidation generally can be considered as atomistic, phenomenological, or geometric. The currently popular atomistic explanation of the cubic phenomenon lies in a consideration of the simultaneous metallic solution of oxygen and diffusion through the oxide as proposed by Kofstad et al[2]. Elaborating on this hypothesis, Smith[42] has derived a theory which indicates that the cubic region is a period of transition between two parabolic regions. A phenomenological theory developed by Smeltzer and coworkers[43] supposes that grain boundary and dislocation pipe diffusion is the principal mechanism of oxide formation in the early stages. This suggestion was also presented by Markali[9] in his electron microscope study.

Although there has been some suggestion that the complicated growth morphology may affect the kinetic data, no one has attempted to derive a cubic rate relation in terms of strictly geometrical effects, i.e. shifting areas of preferred oxide growth. Such a theory would necessarily have to relate oxidation effects on a crystallite scale (approximately 1000 Angstroms) to the overall weight gain observed on specimens in the centimeter dimension range. At present the complexities of network growth and whisker formation would seem to make such a theory difficult to postulate, even with simplifications.

The implication of Kofstad's theory that the thickness of oxide scale remains constant during the cubic period of oxidation does not find support in the optical or electron microscope studies of this work. It becomes quite obvious, for example, that the scale thickness at 1200 minutes, 500°C, $10^{-3}$ mm (Figures 19d and 25a) is much greater than that after ten minutes under the same conditions (Figures 18d and 25e) although a cubic relation is observed during the interim. A comparison of the electron

microscope results for these two specimens also supports this observation (Figures 28a and 33a). A similar argument applies to the scale formation at 500°C, $10^{-4}$ mm.

The theory of Smith[42], which introduces the assumption that the diffusion coefficient of oxygen in metallic titanium is concentration-dependent in order to account for the cubic period, applies to one of Kofstad's experiments after some approximations are made. However the absence of preceding and successive parabolic regions in the cubic curves of this work at 500°C cannot be accounted for by Smith's theory. The transition from cubic to parabolic with increasing temperature is in qualitative agreement with his theory although the numerical values do not coincide with Smith's predictions.

The phenomenological theory developed by Smeltzer et al[43] is based upon the same concept of decreasing low-resistance diffusion paths as the logarithmic theory of Davies et al[53]. With the incorporation of a weighted diffusion coefficient accounting for diffusion along unspecified disordered paths Smeltzer arrives at an exponential oxidation equation which he fits to the results of Kofstad and coworkers. Unfortunately the theory does not account for inflections in the rate curves nor does it explain the pressure dependence of oxidation observed by the author and also by Hurlen.

Hence none of the current theories adequately explains the complex kinetic data of this work. The striking relationship between the kinetic curves and growth morphology appears to hold the key to the explanation. If the cause of network formation and a better atomistic understanding of its growth could be obtained from further electron microscopy and diffusion studies perhaps some hypothesis could be developed. Although the results of

tracer studies by Haul and Dumbgen[40] have provided conclusive information about the bulk diffusion rates of oxygen in rutile, more information is needed on the surface and grain boundary diffusion rates of both oxygen and titanium ions in rutile. Although oxygen ions take preference in bulk diffusion, titanium ions may diffuse more rapidly by grain boundary diffusion. If the total grain boundary area is between one and twenty percent as the results suggest, and if the oxide forms principally by grain boundary diffusion, growth may take place at the oxide-gas interface and this could possibly account for observed pressure effects and growth facets. The slight shift in orientation between crystallites located on either side of a network interface also suggests that some preferred growth direction, possibly associated with epitaxial relations, may be dictating the network formation.

# V. CONCLUSION

The oxidation kinetics of titanium are an exceptionally complicated function of temperature, pressure, and time. While maintaining two of these three variables constant, a general sequence of kinetic relations is observed with increasing temperature, pressure, or time: single logarithmic → dual logarithmic → cubic → parabolic → linear. These relations are only crude approximations of more complex rate curves that are inadequately described by the simple bulk transport theories proposed by previous investigators.

The kinetics are intimately related to the growth morphology, which is also complex. Between 400 and 600°C the oxide forms a network of suppressed and accelerated growth areas, the form of which is also a function of temperature, pressure, and time. These networks consist of thousands of small crystallites arranged in random or preferred configurations and exhibiting well-defined growth facets. A cubic growth relation is related to the development of coarse oxide networks which eventually disappear giving rise to a parabolic relation. The mechanism of network growth is not understood although surface and grain boundary diffusion appears to play a prominant role in view of the extremely small rutile crystallite size [50 to 5000 Angstroms]. Orientation effects in the network also suggest preferred growth directions with possible epitaxial effects. The dual logarithmic growth rate is associated with the growth of a thin film in the first stage followed by profuse whisker growth in the second stage. Whiskers generally have a dagger-shaped profile but occasionally grow as thin circular discs.

# VI. RECOMMENDATIONS FOR FURTHER WORK

Before a better understanding of the oxide growth mechanism can be obtained, tracer studies using oxygen and titanium isotopes must be performed on bicrystals of rutile containing low and high angle grain boundaries so that grain boundary and surface diffusion rates can be compared with bulk diffusion in single crystals. The solution of oxygen in metallic titanium between 200 and 700°C could be determined with $O^{18}$ or neutron irradiation to produce unstable isotopes. This would provide definite conclusions regarding current theories based upon concentration dependence of interstitial diffusion coefficients. The relation of oxide growth rate to epitaxy with the underlying metal, determined by preparation of metal-oxide transmission specimens, would also be useful. This could possibly be studied by vacuum deposition of thick films onto heated metal substrates, inert with respect to oxidation at temperatures less than 600°C. Oxidation of the titanium film and substrate could be measured with a microbalance and the substrate could be subsequently dissolved for electron microscope examination. Continuous monitoring of the network growth with specimens on an electron microscope hot stage would certainly provide a clearer understanding of the development.

# VII. APPENDICES

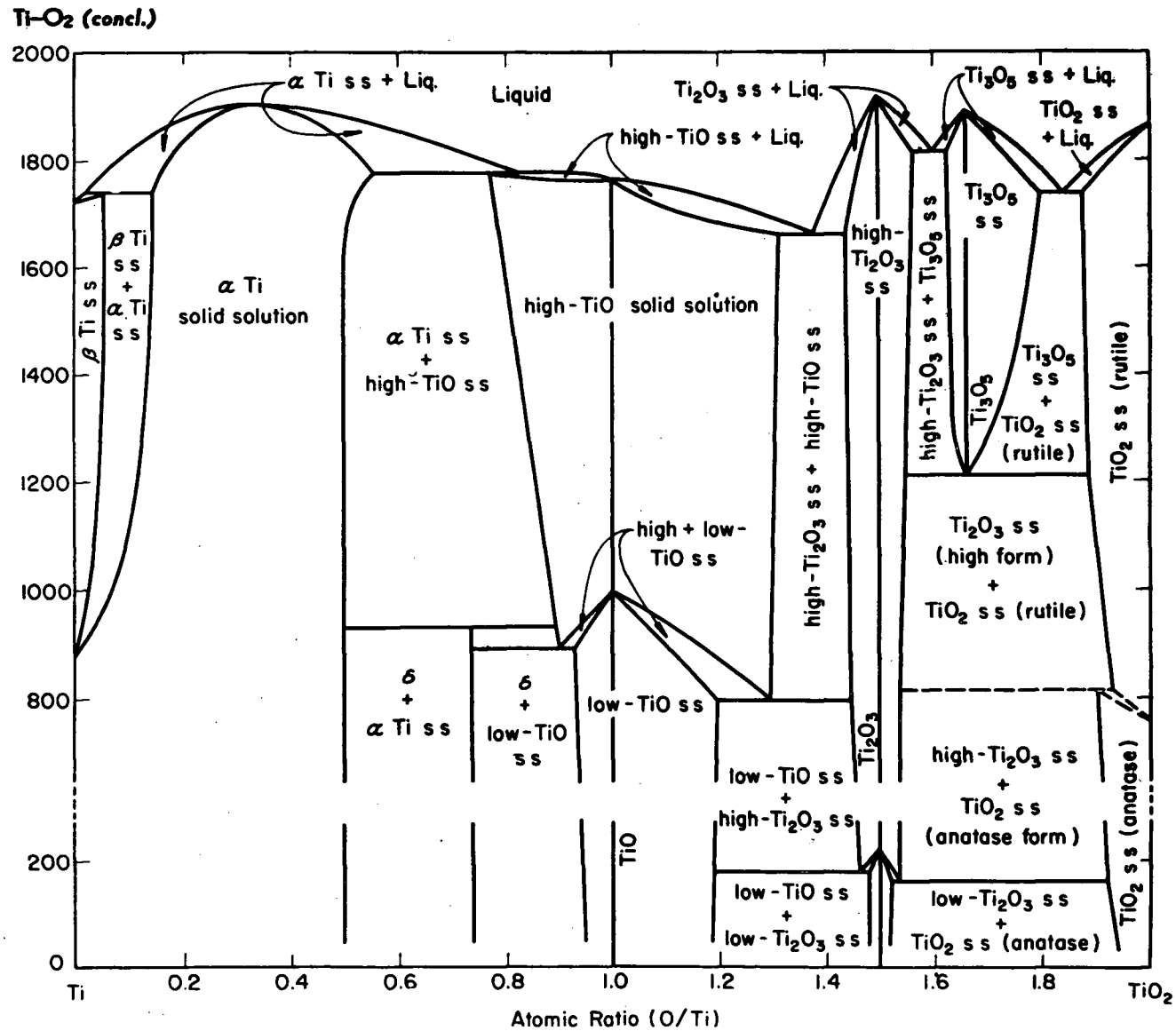


Figure 37. Phase diagram of the titanium-oxygen system[28]

# APPENDIX B

## TITANIUM ANALYSES

| (All concentrations in parts per million) | | | | | | | | | | | | | | | | | Type |
|---|---|---|---|---|---|---|---|---|---|---|---|---|---|---|---|---|---|
| | W | Al | Fe | Mn | Si | C | $N_2$ | Ca | Cr | Cu | V | Sr | Ni | $O_2$ | Mg | Sn | |
| This work | - | 10 | 70 | 200 | 300 | - | - | 20 | 30 | 20 | 50 | 10 | 10 | 300 | ND | 3 | EP |
| Author | | | | | | | | | | | | | | | | | |
| Hurlen[1] | - | - | 70 | 30 | 600 | - | - | - | - | tr | - | - | - | - | 300 | tr | KR |
| Kofstad[2] | - | 100 | 100 | 100 | - | - | - | - | 100 | 10 | - | - | - | - | 100 | 100 | VA |
| | - | - | 1000 | 10 | 100 | - | - | 10 | - | 10 | - | - | - | - | 1000 | 10 | KR |
| Stringer[23] | 1000 | - | 500 | - | - | 400 | 120 | - | - | - | - | - | - | 400 | - | - | KR |
| Waber[19] | - | 500 | 10 | - | 10 | - | - | - | - | - | - | - | - | - | 10 | - | VA |
| Alexander[13] | - | - | - | - | - | - | 500 | - | - | - | - | - | - | 1200 | - | - | KR |
| Davies[16] | - | - | 800 | - | - | 1800 | 940 | - | - | - | - | - | - | - | - | - | KR |

Notations:

- \- not reported
- ND not detected
- tr trace detected
- EP titanium produced by fused salt electrolysis
- KR Kroll titanium
- VA Van Arkel titanium

Other works:

Hass[15] evaporated 99.9% iodide titanium

Menard[26] used 99.5% commercial titanium

Lainer[24] detected 400 ppm Si and twelve other elements $<$100 ppm

Analyses not given:

Gulbransen[12], Kieffer[14], Waber[17], and Revyakin[25]

# APPENDIX C

## METAL HISTORY PRIOR TO OXIDATION

1. Hurlen[1]:

   Vacuum arc melt ($10^{-4}$ mm)
   Cold Roll
   Mechanical polish
   Anneal 30 minutes at 800°C, $10^{-4}$ mm
   .....oxidized as-annealed sheet

2. Kofstad[2]:

   Arc melt under argon
   Remelt and cast
   Cold roll
   Anneal at 800°C
   Cold roll again (in some cases only)
   Mechanical polish
   .....oxidized mechanical-polished sheet

3. Markali[9]:

   Cold roll
   Mechanical polish
   Anneal 30 minutes at 800°C under high vacuum
   .....oxidized as-annealed sheet

4. Lainer[24]:

   Arc melt
   Cold roll
   Anneal 30 minutes at 800°C, $10^{-4}$ mm.
   .....oxidized as-annealed sheet

# APPENDIX D

## KINETIC ANALYSIS OF TEMPERATURE DATA

If one assumes the oxide growth rate is some function of pressure and time at constant temperature, then an average thickness can be defined by the general equation:

$$x = kp_{O_2}^{m}t^{n} \qquad \ldots.(1D)$$

where
$k$ = rate constant
$m, n$ = constants
$t$ = time
$p_{O_2}$ = oxygen partial pressure

It is evident from Figure 17 that neither m nor n is constant, however assuming they are and taking logs of equation (1D):

$$\log x = \log k + m \log p_{O_2} + n \log t \ldots(2D)$$

Since activation energies are obtained from the slope of graphs of log k versus 1/T, it is necessary to simplify equation (2D) by holding one of the variables constant. For ultimate simplification consider only those kinetic curves at 10 mm and 760 mm (Figure 17) where a small pressure effect is observed (except at 600°C). Assume these pressure effects are negligible and in fact oxidation is pressure-independent in these regions so that the m log $p_{O_2}$ term disappears. Then it is necessary to evaluate

$$\log x = \log k + n \log t \qquad \ldots.(3D)$$

Assuming a uniform oxide distribution across the surface of known area so that the weight gain measured,

$$\Delta W = Ax\rho \qquad \ldots.(4D)$$

where
$A$ = surface area
$x$ = average oxide thickness
$\rho$ = oxide density

Assuming the area undergoing oxidation equals the apparent area, the weight gain per square centimeter of surface is

$$\Delta W = x\rho \qquad \ldots.(5D)$$

The kinetic curves in this work (Figures 11 to 17) are plotted in terms of the weight gain per square centimeter and since $\rho$ is constant, equation (3D) can be written:

$$\log \Delta W = \log k + n \log t \qquad \ldots.(6D)$$

In order to solve this equation for log k, it is necessary to evaluate n, which is the slope of the curves of log $\Delta W$ versus log t (Figure 17). For the ideal case, only linear regions of each curve should be chosen where n is constant for a short period (or hopefully longer periods). It would also be desirable to have linear regions on three temperature curves at some fixed time. However no three curves satisfy this requirement completely. In Figure 17, the 760 mm pressure curves (curves 126, 89, and 115) will be considered to approximate this requirement. The 700°C curve shows a linear region of constant parabolic slope (equal to one half) from 50 to 1000 minutes. The 800°C curve displays a cubic slope going through a transition to linear between 10 and 300 minutes. However the changing slope approximates one half at 100 minutes and this will be considered a valid point. The slope of the 600°C curve at one hundred minutes is also changing and is not a simple integer but again assume it is one half and constant. Now it is possible to evaluate log k at 100 minutes assuming $n=\frac{1}{2}$ by reading off $\Delta W$ values from the curves and substituting into equation (6D), which becomes

$$\log k = \log \Delta W - 1 \qquad \ldots.(7D)$$

It is more common practice in oxidation studies to define parabolic rate equations, according to Kubaschewski et al[7], by the equation

$$\Delta W^2 = kt \qquad \text{....(8D)}$$

which, after taking logs, becomes

$$2 \log \Delta W = \log k + \log t \qquad \text{....(9D)}$$

When t = 100, $$\tfrac{1}{2} \log k = \log \Delta W - 1 \qquad \text{....(10D)}$$

Hence a factor of two must be introduced into equation (7D) so that calculated activation energies can be compared to other published values. The following table summarizes the calculations:

| $T^oC$ | $1/T^oK$ | $\Delta W$ | $\log \Delta W$ | $\log k$ |
|---|---|---|---|---|
| 600 | $1.145 \times 10^{-3}$ | 142 | 2.152 | 1.152 |
| 700 | $1.027 \times 10^{-3}$ | 375 | 2.574 | 1.574 |
| 800 | $0.929 \times 10^{-3}$ | 1650 | 3.218 | 2.218 |

Assuming a straight line relation exists when these three values of log k are plotted versus 1/T as in Figure 38, which is doubtful, one obtains an activation energy varying from 37 to 70 Kcal/mole. Other kinetic studies at higher temperatures (above 800°C) in which parabolic regions were observed report activation energies of 62 Kcal/mole[23] and 51 Kcal/mole[33].

A similar analysis to this for cubic slopes on the 10 mm curves (83, 82, and 92, Figure 17) at 100 minutes was performed. Based upon a similar three-point analysis, activation energies varied from 40 to 80 Kcal/mole.

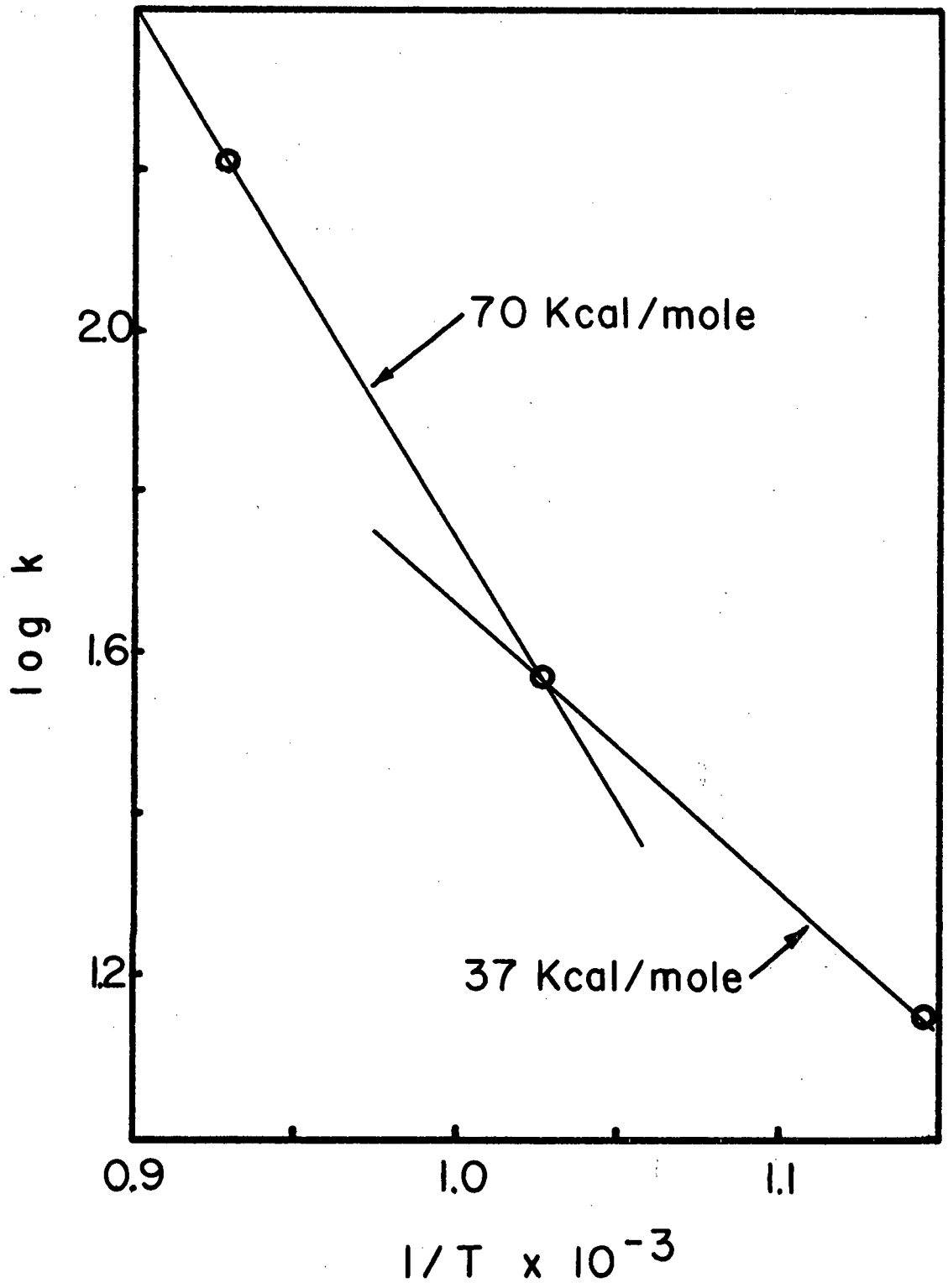


Figure 38. Graphical Determination of Activation Energy

# APPENDIX E

## KINETIC ANALYSIS OF PRESSURE DATA

Consider the effect of pressure at 500°C, for which the kinetic data are most complete. Assume the rate of oxidation is some function of pressure of the type

$$\frac{dW}{dt} = k \; p_{O_2}^{x} \qquad \text{....(1E)}$$

where
$W$ = weight
$t$ = time
$k$ = constant
$x$ = order of dependence upon pressure
$p_{O_2}$ = oxygen partial pressure

$$\log \frac{dW}{dt} = \log k + x \log p_{O_2} \qquad \text{....(2E)}$$

Hence the slope of a plot of $\log \frac{dW}{dt}$ versus $\log p_{O_2}$ should establish the pressure dependence.

### Evaluation of equation (2E)

$\frac{dW}{dt}$ is obtained from the log-log plots (Figures 14 and 15) by the following method: assume the curve obeys an equation of the type

$$W = kt^{n} \qquad \text{....(3E)}$$

then

$$\frac{dW}{dt} = nkt^{n-1} \qquad \text{....(4E)}$$

from (3E)

$$\log W = \log k + n \log t \qquad \text{....(5E)}$$

from (4E)

$$\log \frac{dW}{dt} = \log n + \log k + (n-1)\log t \qquad \text{...(6E)}$$

combining (5E) & (6E),

$$= \log n + \log W - \log t \qquad \text{....(7E)}$$

Equation (7E) will be used to evaluate $\log \frac{dW}{dt}$ for all pressures at fixed times of 1, 10, 100, and 1000 minutes at 500°C. Since at a fixed time the log t term is the same for each pressure evaluation, it does not influence a determination of x (equation 2E) and will be neglected for calculation simplicity. The slope of the log-log plots is n (equation 5E) which is assumed to be constant. Since it clearly is not constant, it

will be evaluated for each curve by placing a rule tangent to the curve at the time indicated.

$$\text{Since} \qquad n \approx \frac{\log W_1 - \log W_2}{\log t_1 - \log t_2} \qquad \ldots.(8E)$$

choosing an abscissa length of one time cycle reduces equation (8E) to

$$n \approx \log W_1 - \log W_2 \qquad \ldots.(9E)$$

Figure 39 shows a plot of log $\frac{dW}{dt}$ versus log $p_{O_2}$ after equation (7E) was evaluated for all pressures at the time intervals indicated.

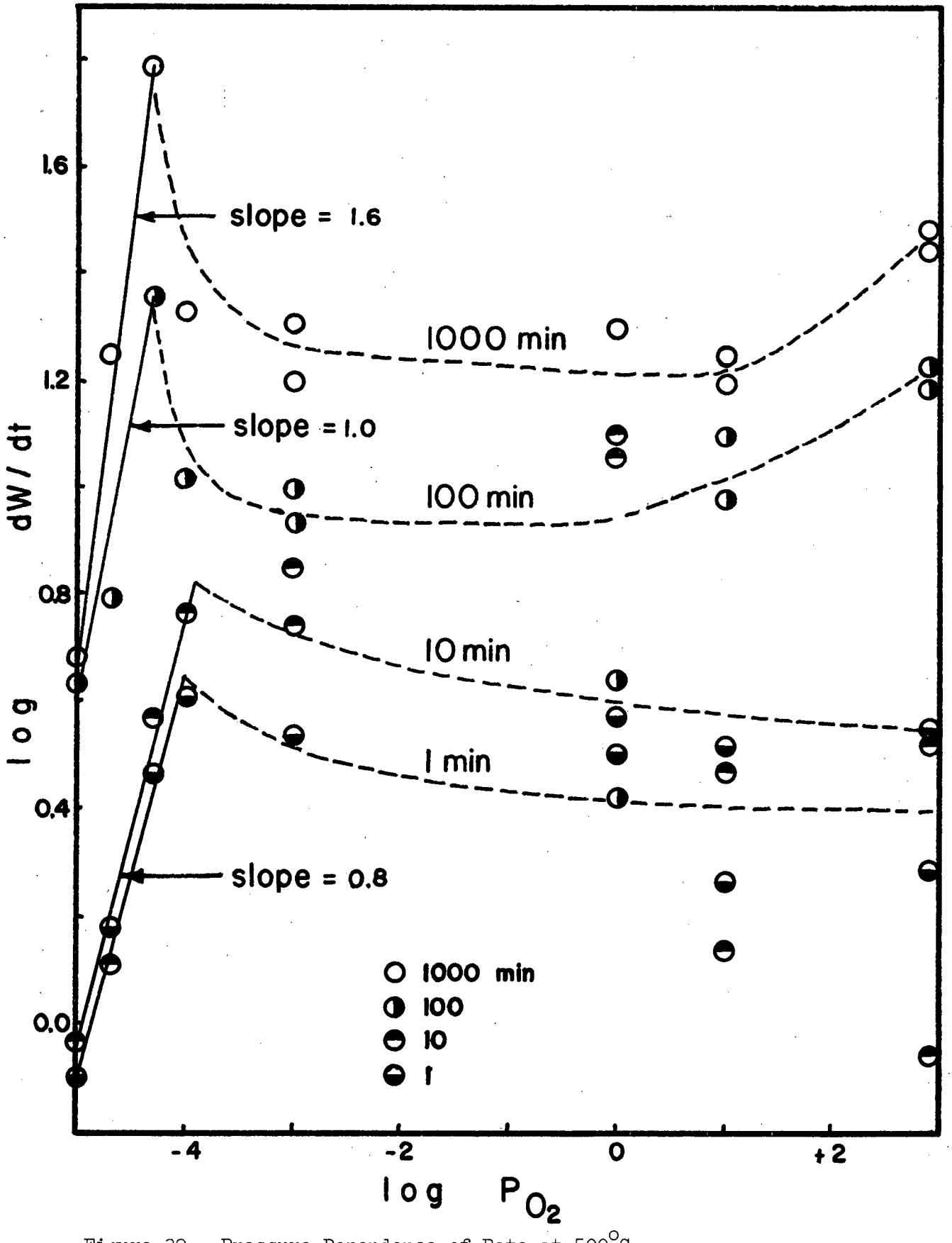


Figure 39. Pressure Dependence of Rate at 500°C.

# VIII. BIBLIOGRAPHY


1. Hurlen, T., J. Inst. Met. 89, 128 (1960).

2. Kofstad, P., Hauffe, K., and Kjollesdal, H., Acta Chem. Scand. 12, 239 (1958).

3. Lawless, K. R., "Energetics in Metallurgical Phenomena, Vol. I," ed. W. M. Mueller, Gordon and Breach, N. Y., 1965.

4. Young, F. W., Cathcart, J. V., and Gwathmey, A. T., Acta Met. 4, 145 (1956).

5. Otter, M., Z. Naturf., 14a, 355 (1959).

6. Mehl, R. F., and McCandless, E. L., Trans. AIME 125, 531 (1937).

7. Kubaschewski, O., and Hopkins, B. E., "The Oxidation of Metals and Alloys," second edition, Butterworths, London, 1962.

8. Hauffe, K., "Oxidation of Metals," Plenum Press, N. Y., 1965.

9. Markali, J., Proceedings, Fifth International Congress for Electron Microscopy, Academic Press, N. Y., 1962.

10. Douglass, D. L., and Van Landuyt, J., Acta Met. 13, 1069 (1965).

11. Benard, J., "Oxydation des Metaux," Gauthier-Villars, Paris, 1962.

12. Gulbransen, E. A., and Andrew, K. F., J. Metals 1, 741 (1949).

13. Alexander, W. A., and Pidgeon, L. M., Can. J. Res. 28, 60 (1950).

14. Kieffer, R. and Kolbl, F., Z. Anorg. Chem. 262, 229 (1950).

15. Hass, G. and Bradford, A. P., J. Opt. Soc. Am. 47, 125 (1957).

16. Davies, M. H. and Birchenall, C. E., J. Metals 3, 877 (1951).

17. Waber, J. T., J. Chem. Phys. 20, 734 (1952).

18. Pfeiffer, H., and Hauffe, K., Z. Metallk. 43, 364 (1952).

19. Waber, J. T., Sturdy, G. E., and Wise, E. N., J. Am. Chem. Soc. 75, 2269 (1953).

20. Richardson, L. S., and Grant, N. J., J. Met. 6, 69 (1954).

21. Jenkins, A. E., J. Inst. Met. 84, 1 (1955).

22. Wallwork, G. R., and Jenkins, A. E., J. Electrochem. Soc. 106, 10 (1959).

23. Stringer, J., Acta Met. 8, 758 (1960).

24. Lainer, D. I., and Tsypin, M. I., Izvest. Akad. Nauk. SSSR, Otdel. Tekh. Nauk., Met. I Toplivo, 1, 146 (1961).

25. Revyakin, A. V., Titan i ego Splavy, Akad. Nauk. SSSR, Inst. Met. 8, 175 (1962).

26. Menard, R. C., J. Opt. Soc. Am. 52, 427 (1962).

27. Engell, H. J., Hauffe, K., and Ilschner, B., Z. Elektrochem. 58, 478 (1954).

28. DeVries, R. C., and Roy, R., Am. Cer. Soc. Bull. 33, 370 (1954).

29. Morton, P. H, and Baldwin, W. M., Trans. ASM, 44, 1004 (1952).

30. Ehrlich, P., Z. Elektrochem. 45, 362 (1939).

31. Andersson, S., Collen, B., Kuylenstierna, V., and Magneli, A., Acta Chem. Scand. 11, 1641 (1957).

32. Graves, P. W., Ph.D. Thesis, University of Birmingham, 1963.

33. Kofstad, P., Anderson, P. B., and Krudtaa, O. J., J. Less Common Metals, 3, 89 (1961).

34. Jenkins, A. E., J. Inst. Met. 82, 213 (1953).

35. Arkharov, V. I. and Blankova, Ye B., Fiz. Metal. i Metalloved. 10, 63 (1960).

36. Lainer, D. I., and Bai, A. S., Fiz. Metal. i Metalloved. 14, 283 (1962).

37. Hurlen, T., Acta Chem. Scand. 13, 365 (1959).

38. Hauffe, K., Grunewald, H., and Trankler-Greese, R., Zeit. Elektrochem. 56, 937 (1952).

39. Hauffe, K., "Reaktionen in und an Festen Stoffen," Springer Verlag, Berlin, 1955.

40. Haul, R., and Dumbgen, G., Z. Electrochem. 66, 636 (1962).

41. Kofstad, P., and Hauffe, K., Werkstoffe und Korrosion, 7, 642 (1956).

42. Smith, T., J. Electrochem. Soc. 112, 39 (1965).

43. Smeltzer, W. W., Haering, R. R., and Kirkaldy, J. S., Acta Met. 9, 880 (1961).

44. Douglass, D. L., and Van Landuyt, J., Paper presented at 1965 Gordon Corrosion Research Conference, New London, New Hampshire, 1965.

45. Gulbransen, E. A., Trans. Electrochem. Soc. 81, 327 (1942).

46. Cahn, L., and Schultz, H. R., Vacuum Microbalance Techniques, 2, 7 (1962).

47. Private Communication, C. S. Goodloe, Chicago Research and Development Corporation, 5810 47th Avenue, Riverdale, Maryland, Dec. 17, 1964.

48. Clark, H. T., Trans. AIME, 188, 1154 (1950).

49. Gilman, J. J., "The Art and Science of Growing Crystals," J. Wiley and Sons, N. Y., 1963.

50. Churchman, A. T., Proc. Roy. Soc. 226, 216 (1954).

51. Arntz, F., and Chernow, F., J. Vac. Sci. & Techn. 2, 20 (1965).

52. Private Communication, D. L. Douglass, G. E. Vallecitos Atomic Laboratory, Pleasanton, California, October 15, 1965.

53. Davies, D. E., Evans, U. R., and Agar, J. N., Proc. Roy. Soc. A225, 443 (1954).

54. Cabrera, N., and Mott, N. F., Rept. Progr. in Physics, 12, 163 (1949).